University of South Bohemia in České Budějovice

Faculty of Science

Time-resolved spectroscopy of light-induced processes

Ph.D. Thesis

M. Sc. Valentyna Kuznetsova

Supervisor: **Mgr. Marcel Fuciman, Ph.D.**

Faculty of Science, University of South Bohemia, České Budějovice

České Budějovice 2017

This thesis should be cited as:

Annotation

This Ph.D. thesis is devoted to the study of the photophysical properties of photosynthetic pigments. The brief introduction to the field is given in Chapter 1. In studies presented in the thesis, femtosecond pump-probe spectroscopy was used to determine the relation between the molecular structure of carotenoids and its spectroscopic properties. The experimental and data analysis methods are described in Chapter 2. Chapter 3 addresses the investigation of the effect of isomerization on excited-state dynamics of the carbonyl carotenoid fucoxanthin. In Chapter 4, the different response of carbonyl carotenoids to solvent proticity is used to estimate the structure of an unknown carotenoid from *Chromera velia*. In Chapter 5, spectroscopic properties of the S_1 state of three linear carotenoids were studied after excess energy excitation in the S_2 state. Chapter 6 presents a femtosecond spectroscopic comparison study of Orange and Red Carotenoid Proteins binding different carotenoids.

Declaration [in Czech]

Prohlašuji, že svoji disertační práci jsem vypracoval samostatně pouze s použitím pramenů a literatury uvedených v seznamu citované literatury.

Prohlašuji, že v souladu s § 47b zákona č. 111/1998 Sb. v platném znění souhlasím se zveřejněním své disertační práce, a to v úpravě vzniklé vypuštěním vyznačených částí archivovaných Přírodovědeckou fakultou elektronickou cestou ve veřejně přístupné části databáze STAG provozované Jihočeskou univerzitou v Českých Budějovicích na jejích internetových stránkách, a to se zachováním mého autorského práva k odevzdanému textu této kvalifikační práce. Souhlasím dále s tím, aby toutéž elektronickou cestou byly v souladu s uvedeným ustanovením zákona č. 111/1998 Sb. zveřejněny posudky školitele a oponentů práce i záznam o průběhu a výsledku obhajoby kvalifikační práce. Rovněž souhlasím s porovnáním textu mé kvalifikační práce s databází kvalifikačních prací Theses.cz provozovanou Národním registrem vysokoškolských kvalifikačních prací a systémem na odhalování plagiátů.

České Budějovice, 25. července 2017   ....

Valentyna Kuznetsova

Financial Support

To my Mom

Acknowledgements

> *If you have an apple and I have an apple and we exchange apples, then you and I will still each have one apple. But if you have an idea and I have an idea and we exchange these ideas, then each of us will have two ideas.*
>
> George Bernard Shaw

It is a pleasure to thank the many people who contributed in some way to the work described in this thesis and made this thesis possible.

It is difficult to overstate my gratitude to *Tomáš*, who had accepted me into the lab about 4 years ago, and who believed in me when I almost did not. I am grateful for your trust, support, and for giving me the opportunity to work on many interesting projects and be part of such an amazing team.

I am indebted to my supervisor *Marcel*, who has introduced me to the world of optical spectroscopy and has taught me everything that I needed. It was an outstanding experience to build our setup, thank you for sharing your knowledge with me. Thank you for the right questions that always led to the fruitful discussions, and for the clear answers when I was struggling with some problems.

I am thankful to my colleagues *Robert, Gurkan, Hristina, Milan, Vašek I, and Vašek II* for sharing our working time, your help in the lab, and all the fun we had together during our productive and curious discussions. *Robert* and *Gurkan*, without you guys every day would be just another working day, thank you for becoming my friends. *Hristina*, thank you for sharing with me your insightful and constructive ideas, and experience. *Vašek I,* thank you for collaboration in the OCP project and a great time in Amsterdam. I also want to thank *Pavel*, who I will always consider as a part of our great team. It was a pleasure to work with you in Lund and during your stay here.

Finally, I must express my very profound gratitude to my Mom, my sister *Ksusha*, and my soulmate *Ivan* for their constant love and support. This accomplishment would not have been possible without them. *Ivan*, thank you for providing me with unfailing support and continuous encouragement throughout my years of study, research, and writing this thesis. Thank you.

List of papers and author's contribution

The thesis is based on the following papers (listed in the order of their presentation in the Research Section):

I.   **V. Kuznetsova**, P. Chábera, R. Litvín, T. Polívka, M. Fuciman. Effect of isomerization on excited-state dynamics of the carotenoid fucoxanthin. Journal of Physical Chemistry B, 2017, 121 (17), 4438–4447.

VK separated the carotenoid isomers by the HPLC method, conducted the time-resolved transient absorption measurements in the visible spectral region and the single-wavelength anisotropy measurements, analyzed the data, and participated in writing and revision of the manuscript.

II.   G. Keşan, M. Durchan, J. Tichý, B. Minofar, **V. Kuznetsova**, M. Fuciman, V. Šlouf, C. Parlak and T. Polívka. Different response of carbonyl carotenoids to solvent proticity helps to estimate structure of the unknown carotenoid from Chromera velia. Journal of Physical Chemistry B, 2015, 119 (39), 12653–12663.

VK participated in time-resolved transient absorption measurements.

III.   **V. Kuznetsova**, J. Southall, R. J. Cogdell, M. Fuciman, T. Polívka. Spectroscopic properties of the S_1 state of linear carotenoids after excess energy excitation. Chemical Physics Letters, 2017 (*In Press*).

VK conducted the time-resolved transient absorption measurements, analyzed the data, and participated in writing and revision of the manuscript.

IV.   V. Šlouf, **V. Kuznetsova**, M. Fuciman, C. B. de Carbon, A. Wilson, D. Kirilovsky, T. Polívka. Ultrafast spectroscopy tracks carotenoid configurations in the Orange and Red Carotenoid Proteins from cyanobacteria. Photosynthesis Research, 2017, 131 (1), 105-117.

VK participated in the time-resolved transient absorption measurements in the visible spectral region, analyzed the data, and participated in writing and revision of the manuscript.

Contents

List of abbreviations

ATP - adenosine triphosphate

BChl – bacteriochlorophyll

Chl – chlorophyll

DADS – decay-associated difference spectra

DFT – density functional theory

EADS – evolution-associated difference spectra

ESA – excited-state absorption

FCP – fucoxanthin-Chl-a-Chl-c-protein

FWHM – full width at half maximum

GSB – ground-state bleaching

HPLC - high-performance liquid chromatography

ICT – intramolecular charge-transfer

IRF – instrument response function

LH1/LH2 – integral membrane antennas of bacteria

LHC – light-harvesting complexes

LHCI/LHCII – integral membrane antenna of cyanobacteria, algae and higher plants

NADP – nicotinamide adenine dinucleotide phosphate

NIR – near-infrared

NPQ – non-photochemical quenching

OCP – orange carotenoid protein

OPA – optical parametric amplifier

PCP – peridinin-chlorophyll-a protein

PSI/PHII – photosystem I/II

RC1/2 – reaction center 1/2

RCP – red carotenoid protein

SADS – species- associated difference spectra

SE – stimulated emission

TA – transient absorption

WLC – white-light continuum

1. Introduction

1.1. Preface

Through the 20th century, the world energy consumption increased approximately ten times, with energy consumption rising primarily due to increased industrial growth; one of the major challenges that our society is going to face in the near future is the depletion of the accessible fossil fuel sources. The importance of the adoption of new renewable energy sources is not a subject to debate anymore, but it is rather a matter of increase of their efficiency and economic viability. By far, one of the most abundant renewable energy sources is sunlight. The overall amount of sunlight reaching the Earth's surface is enough to provide us with the energy to eliminate our dependency on fossil fuel, however, today only a small part of it is being converted to electricity or heat. Photosynthetic organisms such as plants and algae were the first to develop the ability to capture, convert and store solar energy in the form of simple sugars. The significance of photosynthesis as one of the most fundamental life processes has recently encouraged a significant research effort dedicated to the improvement of photosynthetic efficiency in various living organisms as well as the development of efficient artificial systems that mimic photosynthesis for energy production. Both research directions would be impossible without a complete understanding of the crucial role played by the process of light harvesting and its regulation during naturally occurring photosynthesis.

1.2. Photosynthesis

Initially, the word *photosynthesis* was proposed by Charles Reid Barnes for the first time in 1893, and summarized the prevalent comprehension of this process as "the synthesis of complex carbon compounds out of carbonic acid, in the presence of chlorophyll, under the action of light".[1,2] Although the modern definition differs from the one proposed by Barnes and generalizes the series of

the processes from capturing the light to its conversion to chemical energy, it took about 100 years to generalize this term.[3] One can believe that more than a century should be enough to fully understand something that is happening on such a small scale. Though there are many great reviews of photosynthesis studies,[4–8] they all to some extent reflect the author's personal research interests and expertise. A truly comprehensive review is beyond the scope of this thesis; therefore this section will be devoted to a brief summary of all the steps of the photosynthesis but mainly focused on the primary photosynthetic light reactions.

Photosynthesis is a biological process in which the captured light energy is stored by the organism and then is used to drive the cellular processes. The photosynthesis can be both oxygenic and non-oxygenic. Oxygenic photosynthesis is carried out by higher plants, algae, and cyanobacteria and involves chlorophyll-type pigments as light-harvesters, and water as a source of electrons which eventually reduce carbon dioxide to sugars, starch and other metabolites. Non-oxygenic organisms, such as photosynthetic bacteria, use bacteriochlorophylls as a light harvesting pigment and other electron donors such as sulfide, hydrogen or organic substrates. Despite the fact that definition of photosynthesis includes different forms of photosynthesis, such as photosynthesis occurring in some bacteria using the protein bacteriorhodopsin,[7,9] this thesis is focused on the (bacterio-) chlorophyll-based photosynthesis.

Chlorophyll is not the only pigment that takes part in the light-harvesting. All photosynthetic organisms contain carotenoids, which also function as accessory pigments. Different pigments are assembled in the antenna complexes and absorb solar energy in the visible spectrum range. Although several types of *photosynthetic antenna* exist (LH1[10] and LH2[11,12] in bacteria, LHCI[13] and LHCII[14] in cyanobacteria, algae and higher plants, phycobilisomes,[15,16] peridinin-chlorophyll-protein[17] etc.), they use similar principles for light harvesting: an array of highly ordered pigments organized in an energy hierarchy and optimized for maximal photon capture efficiency at relatively low light intensities. The antenna system works by an energy transfer process that involves the migration of

electronic excited states from one molecule to another, and efficiently transfers the energy to the reaction centers.

The *reaction centers*, found in photosystems I (PSI) and II (PSII), are multi-subunit protein complexes.[18–23] There are two types of reaction centers (RCs), called type 1 and type 2. The RC types differ in the early electron acceptor cofactors: iron-sulfur (RC1) and pheophytin-quinone (RC2). While non-oxygenic organisms have just one type, oxygenic organisms have one of each type. The RCs capture energy by either exciton transfer from antenna complexes, or by direct absorption of light by chlorophyll-type pigments. The pigment (P) is promoted to an electronic excited state (P*) and rapidly loses an electron to a nearby acceptor molecule, generating an ion-pair state P^+A^-. This is the primary reaction of photosynthesis.[24]

There are two ways to return an excited pigment to its original state: by converting the received energy into heat (or emitting a photon) or by converting the excitation energy into chemical energy by cyclic or non-cyclic electron transfer. The *cyclic electron transfer chain* uses PSI and produces only ATP. Essentially, the electron transfer process returns the electron to the primary donor. The electron transfer is coupled to proton transport across the membrane, and the resulting electrochemical gradient is used to drive the synthesis of ATP. The *non-cyclic electron transfer chain* utilizes two photosystems reaction centers that are interconnected and work in series. PSII utilizes water as electron donor; it splits two water molecules into oxygen and four protons (H^+) and four electrons. The electrons from water are transferred from PSII to PSI reaction centers. The PSI transfers the received electrons from PSII to a final electron acceptor $NADP^+$ (nicotinamide adenine dinucleotide phosphate) along with the H^+, thereby reducing it to NADPH. Protons are also transported across the membrane, creating an electrochemical proton gradient that is used to make ATP; the latter is used for the conversion of carbon dioxide to carbohydrates.[24]

1.3. Carotenoid Structure and its Role in Photosynthesis

As it was mentioned in the previous section photosynthesis starts from the absorption of light by pigments. There are many pigments that are present in

different photosynthetic organisms, and they have various functions. The research focus of the current thesis is the study of one type of photosynthetic pigment, namely the carotenoids, and their spectroscopic properties. Carotenoids are naturally abundant pigments and can be found in almost all organisms, although they can only be synthesized by plants, microorganisms, and fungi. In photosynthetic organisms, carotenoids absorb in the blue-green region of the visible spectrum expanding the absorption range of the antenna complexes, and transfer the energy to the (bacterio-) chlorophylls to drive photosynthesis.

Carotenoids form complexes with other pigments and proteins, and their chemical and physical properties are strongly influenced by other molecules in their vicinity. For example, different carotenoid isomers can be either a part of the light-harvesting complexes (the all-*trans* form) or reaction centers (*cis*-conformation).[25] In relation to natural selection, it is believed that all-*trans* carotenoids are responsible for light-harvesting, while *cis*-carotenoids serve for a photoprotection function in the RCs. The other example of this influence is the photoactive Orange Carotenoid Protein (OCP) which is responsible for quenching of phycobilisome fluorescence when, upon its activation, it significantly changes the carotenoid configuration. In turn, the binding carotenoid also influences the properties of the OCP, and only carotenoids having a carbonyl group induce a photoprotective mechanism (**Chapter 6** in the Research Section). Carotenoids can also act as quenchers of reactive chlorophyll and singlet oxygen species under excess light conditions.[26–28] Due to their structure they react easily with free radicals, thus serving antioxidant role in non-photosynthetic organisms.

Many chemically distinct carotenoids exist in nature, but all of them share similar structural features: they consist of conjugated polyene chain with alternating single and double carbon bonds. The chemical structures of carotenoids being the subject of this thesis research are shown in the Figure 1-1. Carotenoids may contain ring structures at each end of the chain, as well as inorganic atoms and functional groups incorporated in their polyene chain. Depending on their structure they can characterized as carotenes or xanthophylls. Carotenoids consisting only of carbon and hydrogen atoms are called *carotenes*.

Carotenoids containing an oxygen atom, usually as part of hydroxyl or epoxide groups, are called *xanthophylls*.

The carotenoid special functions and spectroscopic properties are determined by their structural features such as length of the conjugation chain (**Chapter 5** in the Research Section), conformation (**Chapter 3** in the Research Section), and carotenoid environment (**Chapter 3, 4** and **6** in the Research Section).
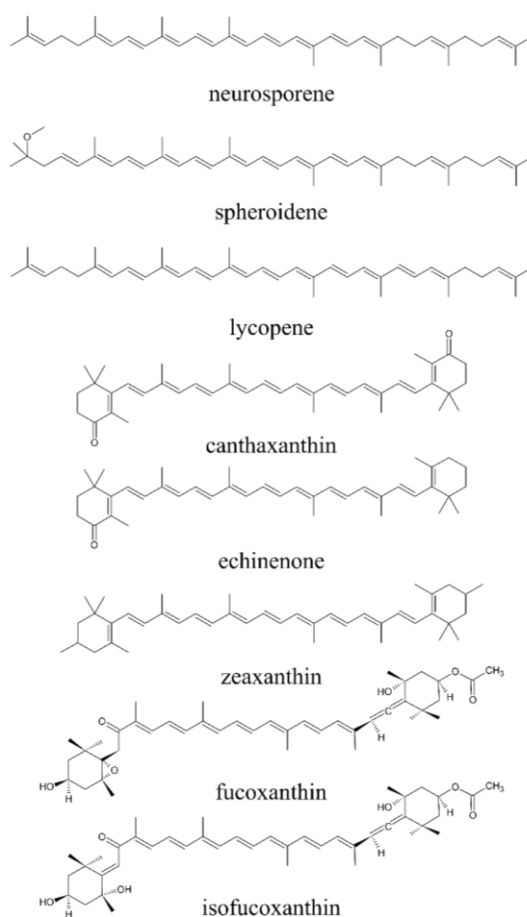
Figure 1-1. Chemical structures of carotenoids presented in this study.

1.4. The Electronic Properties of Carotenoids

The carotenoids' photophysics and electronic structure are crucial for understanding their role and functions in photosynthesis. Carotenoids are characterized by a long polyene chain consisting of C–C single and C=C double bonds, with a delocalized π electron system. The number of conjugated double bonds N (the so-called π-electron conjugation length) and functional groups attached to the chain alter the electronic excited states of carotenoids.[29–31]
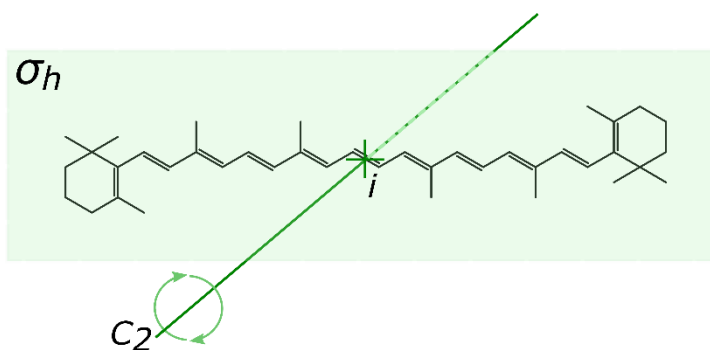
Figure 1-2. Chemical structure of the all-*trans* β-carotene and the symmetry operations of the C_{2h} symmetry group: identity, two-fold rotation axis **C_2**, combined with horizontal plane of reflection symmetry **σ_h**, and inversion center **i**.

Traditionally, the selection rules for photon absorption, derived from linear polyenes with idealized C_{2h} symmetry (Figure 1-2), are applied to describe carotenoids vibrational and excited state manifold. Symmetry elements are geometric entities, such as: axes, planes or points with respect to which various symmetry operations can be carried out, leaving the molecules in an undistinguishable spatial orientation form the original. The symmetry operations of the C_{2h} symmetry group include: the C_2 axis of rotational symmetry (rotation by π radians about this axis generates the identical of the original structure), the plane of reflection symmetry designated as **σ_h** (reflection about this plane leaves the object in the same orientation), inversion i (the change of the position of each atom in a straight line through the point to the opposite side of the molecule gives an identical structure), and the identity (essential operator to group theory). The

assignment of molecules to the C_{2h} group defines the symmetry properties of its wavefunctions, from which all the states and transitions can be derived. The excited states are classified as having either nA_g or nB_u symmetry, where n increases with the energy of the excited state with particular symmetry type. A and B refer to the states that are, respectively, symmetric and asymmetric with respect to rotation about the $\mathbf{C_2}$ axis. The signs g and u classify the states by even (g) or odd (u) symmetry with respect to inversion $\boldsymbol{i}$ through molecular center.[32] In addition to the symmetry the states are labeled by the Pariser pseudoparity signs that denote covalent "-" and ionic "+" states.[33]

According to these rules a scheme of the carotenoid electronic states are shown in the Figure 1-3 whereby the horizontal thick lines represent the electronic states, and within each state are multiple vibronic energy states (thinner lines). The ground state S_0 is labeled as $1A_g^-$, and the first excited singlet state S_1 in carotenoids has the same symmetry as the ground state and is labeled $2A_g^-$; whereas, the second singlet excited state is $1B_u^+$. In order to determine if the transition is allowed, we have to define its transition dipole moment:

$$\mu_{ba} = \int \psi_a \, \hat{\mu} \psi_b \, dV$$

where ψ_a and ψ_b are wavefunctions of the initial and final states, respectively, and $\hat{\mu}$ is electric dipole moment operator. The transition dipole moment has a nonzero value, when the product under integral has a component that is totally symmetric (A_g) with respect to all the symmetry operations that apply to the molecule. Thus the selection rules determine the electronic transition between two states with the same symmetry as forbidden. According to this rule, one-photon transition between $S_0(1A_g^-) \rightarrow S_1(2A_g^-)$ states is forbidden (two states have the same parity g), while that between $S_0(1A_g^-) \rightarrow S_2(1B_u^+)$ is allowed.[32] The pseudoparity signs introduced earlier are used to take into account the interaction between electrons in the molecule, and fulfil the optical selection rules. The optical transition is allowed between a pair of states having different Pariser's signs, contrary to internal conversion, which is allowed between two states having the same Pariser's signs.[34,35] However, not all the molecules are totally symmetric, twisting

and bending distortions may break the symmetry, thus allowing some of the transition.[36]
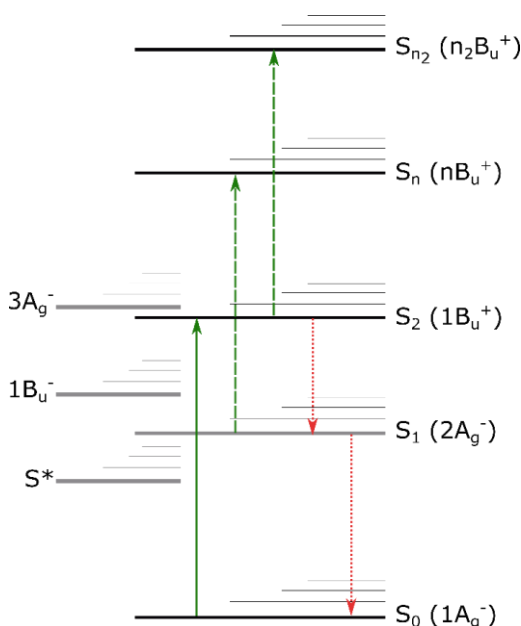
Figure 1-3. Typical energy level scheme of a carotenoid molecule. The green solid arrow – ground state absorption transition, dashed green arrows – excited-state absorption, dotted red arrows – internal conversion and energy dissipation. Grey levels – electronic "dark" states.

The dark states $1B_u^-$ and $3A_g^-$ were predicted by theoretical studies of long polyenes.[34,35] The $1B_u^-$ state approaches the energy of the $1B_u^+$ state for $N \approx 9$, while for long carotenoids $N > 10$ it should be located between the $2A_g^-$ and $1B_u^+$ states.[37–39] The $3A_g^-$ state was predicted to be in the vicinity of the $1B_u^+$ for carotenoids $N \approx 13$, but above the second excited state for most of the carotenoids.[39] The S* state was identified from the transient absorption experiments and is generally accepted to be associated with specific carotenoid conformations either in the ground $1A_g^-$ or first excited $2A_g^-$ states. [30,40]

1.5. Excited States of Carotenoids in Solution

Knowledge of the properties of the carotenoids' excited states in solution is essential to fully understand their functions in more complex natural and artificial systems. A number of different techniques and quantum chemical calculations were applied to naturally occurring and synthesized carotenoids to describe the properties of their electronic states. This section will summarize the main properties of the excited states of carotenoids that will be discussed in the Research Section.

The strong absorption of carotenoids in the blue-green spectral range is solely due to the S_0-S_2 transition (Figure 1-4, a). The S_0-S_2 absorption band usually exhibits a characteristic three-peak structure that reflects the first three vibrational levels of the S_0-S_2 transition. The energy separation between the vibrational peaks is due to a combination of two vibrational stretching modes: C–C (~1150 cm^{-1}) and C=C (~1600 cm^{-1}). A loss of a vibrational structure is observed for carotenoids having conjugation extended to the various end groups, due to the broader distribution of carotenoid conformers.[41] An absorption band shift to higher energy is observed with a decrease of the number of the conjugated double bonds N. The dependence of the S_2 state energy on conjugation length (N) can be described by E=A+B/N, where E – energy of the S_0-S_2 transition, N – number of the conjugated double bonds, A and B are parameters.[42,43] The energy of the S_0-S_2 transition also depends on the refractive index of the solvent; consequently, the spectral shift to lower energies is observed in solvents with high polarizability.[44,45] Last but not least, carotenoids with a carbonyl group (e.g. fucoxanthin) exhibit solvent polarity effect (Figure1-4, b), while in non-polar solvents the vibrational peaks of the S_0-S_2 absorption are still resolved, in a polar solvent the vibrational structure is lost.

The relaxation from the S_2 state to the S_1 state which takes place in a few hundred femtoseconds due to the fast internal conversion depends on both conjugation length of carotenoid and solvent properties. The S_2 state lifetime can be obtained from the global analysis of the transient absorption data, but usually suffers from error as other states contribute to the signal and resolution is limited by the instrument response function of the experimental setup (typically around 100 fs). Fluorescence up-conversion techniques enable the study of the relaxation

dynamics of the S_2 state by direct measurements of the S_2 fluorescence. The energy gap law predicts that the S_2 lifetimes should increase with the conjugation length, however, up-conversion experiments revealed that internal conversion rates are not proportional to the energy gap,[46,47] showing that the dependence of the S_2 state lifetime on the conjugation length is not straightforward.
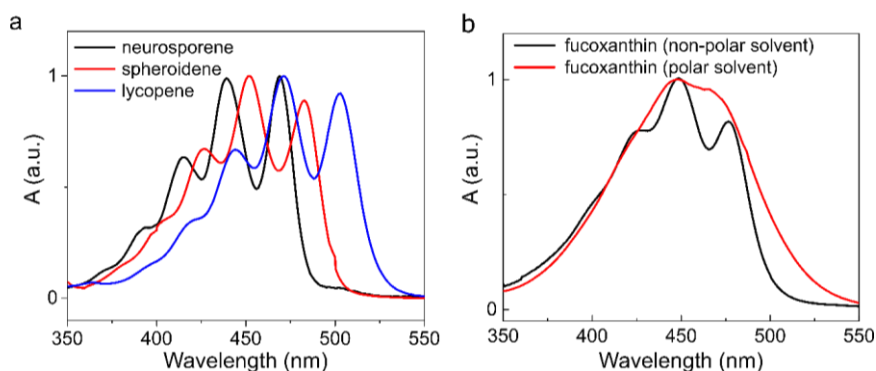
Figure 1-4. Absorption spectra of: a) linear carotenoids with different conjugation length: neurosporene (N=9), spheroidene (N=10), lycopene (N=11) and b) carbonyl carotenoid fucoxanthin in non-polar (*n*-hexane) and polar (methanol) solvents.

The S_0-S_1 transition is one-photon forbidden due to the symmetry rules; therefore, a number of different techniques were applied to determine the S_1 state energy, such as, fluorescence,[43,48,49] or resonance Raman[50–52] spectroscopic techniques. The S_1 energy also can be inferred by the spectra of the symmetry allowed S_1-S_2 transition in the near-infrared region by transient absorption spectroscopy. The location of the carotenoid S_1 state can then be calculated from the spectral origins of S_0-S_2 and S_1-S_2 transitions.[53] The energy of the S_1 excited state also depends on the number of the conjugated C=C bonds, it differs between 11000 cm^{-1} (N>13) and 16000 cm^{-1} (N<9) and decreases with the conjugation length, thus making the S_2-S_1 gap larger for longer carotenoids.[41,44,54]

The S_1 state properties are characterized by transient absorption spectroscopy via its strong S_1-S_n excited state absorption (ESA) in the 500-600 nm spectral region. The internal conversion from the S_2 state populates a hot S_1

state which relaxes on the subpicosecond timescale,[55,56] and is characterized by a broad, red-shifted spectrum compared to the relaxed S_1-S_n ESA spectrum. After vibrational relaxation, the lifetime of the S_1 state is extracted from the global analysis. The dynamics of the S_1 state are dependent on the carotenoid's conjugation length, structure, and environment. The S_1 state lifetime varies from 1 ps for spirilloxanthin (N=13) to several hundred picoseconds for shorter carotenoid analogs, with regard to the S_0-S_1 energy gap.

The polarity effect on the S_1 state lifetime is observed exclusively in carbonyl carotenoids: in polar solvents the S_1 state lifetime is more than an order of magnitude shorter than in non-polar solvents. For example, the S_1 state lifetime of fucoxanthin is 20 ps in polar (methanol) versus 56 ps in non-polar solvents (*n*-hexane) (see Research Section, **Chapter 3**). The unique polarity-dependent behavior of carbonyl carotenoids is associated with an intramolecular charge transfer (ICT) state which is stabilized in polar solvents. The ICT state is identified by ESA in the 550-700 nm spectral region, which is more pronounced in the polar solvent, and a negative feature associated with the stimulated emission in the NIR region.[57,58] The ICT state is of highly polar nature and, as a result, can be stabilized by the polar environment of the solvent.[59,60] It does not relax directly to S_0, but does so through an intermediate state on the ground state potential surface.[61–63] The ICT and S_1 states co-exist in an excited state equilibrium, as was shown by the recent pump-dump-probe spectroscopy.[61] The study on the carbonyl carotenoids and the properties of the ICT state in solution can be found in **Chapters 3** and **4**, and in the carotenoid-protein complexes in **Chapter 6** in the Research Section.

Another dark state, designated as S*, can be observed in carotenoids with long (N>10) conjugation length by transient absorption spectroscopy. The presence of the S* is evidenced by the ESA band which is blue-shifted from the S_1-S_n ESA band, and by usually longer lifetime than the S_1 state. Its origin remains a matter of debate,[62,64–66] but there is accumulating evidence that for carotenoids with N<12 the S* has its origin in the S_1 excited state,[67,68] while for very long conjugated systems the S* signal corresponds to a hot ground state.[65,69] In the

Chapter 5 (Research Section), we have shown the formation of the S* state after excess energy excitation due to the generation of the different conformations of the molecule in the S_1 state.

1.6. Orange and Red Carotenoid Proteins

It should be noted that not all pigments bound in protein are involved in light-harvesting and energy transfer. One such example, is the Orange Carotenoid Protein (OCP) found in cyanobacteria. In cyanobacteria, which are prokaryotes performing oxygenic photosynthesis, solar energy is absorbed by the large extramembrane complex called the phycobillisome. The phycobillisome is composed of several types of chromophorylated phycobiliproteins and of linker peptides.[70] Harvested energy is then transferred to photosystem II (PSII) and photosystem I (PSI). However, exposure of organisms to strong light can damage their photosynthetic apparatus, due to oxidative damage induced by excessive excitation.[71] Cyanobacteria have developed a mechanism known as non-photochemical quenching (NPQ), protecting the PSII reaction centers by conversion of excess energy absorbed by phycobillisome to heat.[72]
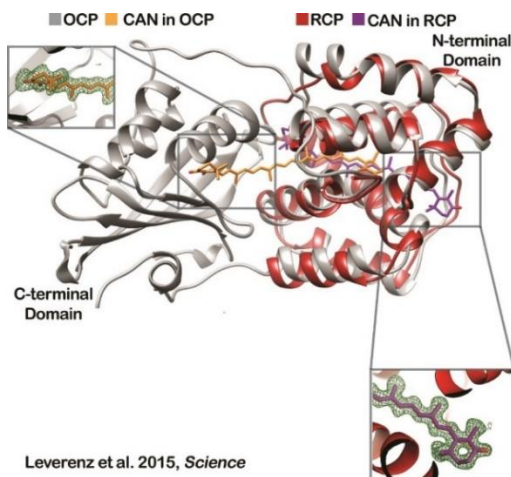

Figure 1-5. Structure of the OCP (grey) and RCP (red) binding carotenoid canthaxanthin (orange in OCP, purple in RCP). (The figure is reprinted from Ref. 75 Leverenz et al. 2015).

This energy dissipation mechanism involves OCP, a water soluble 35 kD protein containing a single non-covalently bound carotenoid. OCP consists of two domains: an α-helix/β-sheet C-terminal domain (the regulator of the quenching activity)[73,74] and an α-helical N-terminal domain (the active part responsible for quenching, which binds phycobillisomes).[73,75] The Red Carotenoid Protein (RCP) represents an isolated, activated N-terminal domain of OCP. The absorbance of blue-green light by the OCP induces structural changes in the carotenoid and the protein, switching its dark stable form into a relatively unstable red form.[76,77] The recently published X-ray structures[75] of OCP and RCP confirmed that after photo-activation of OCP carotenoid translocation within the protein takes place (Figure 1-5). **Chapter 6** aims to associate molecular structure with spectroscopic measurements for the OCP-RCP pair with the carotenoid canthaxanthin. The most important marker of changes in carotenoid configuration after OCP activation was the magnitude of the transient signal associated with the carotenoid ICT state.

1.7. Application of Spectroscopy Techniques for the Study of Carotenoid Properties

Over the past decades, the development of state-of-the-art laser technologies has provided a range of innovative ultrafast spectroscopic techniques, which can be applied to the study of photosynthetic pigments and their complexes. Both the energy transfer as well as the excited state dynamics of carotenoids take place in picosecond and subpicosecond timescale; thus ultrafast time-resolved spectroscopic techniques are the most suitable to analyze these processes. In this section, I would like to elaborate more on some of these techniques which I had experienced during my Ph.D. study. Although I would like to shortly introduce four ultrafast techniques and their capabilities, all studies presented in the Research Section were performed on the pump-probe setup. Three of the techniques belong to the transient absorption spectroscopy (pump-probe, multi-pulse, and two-photon absorption spectroscopic methods); the other belongs to the vibrational spectroscopy (femtosecond stimulated Raman spectroscopy).

Pump-probe spectroscopy is a technique widely used for the study of the photochemical and photophysical properties of photosynthetic pigments and their

complexes. The pump pulse promotes the molecules to their excited states, while the probe pulse, sent with the time delay after the pump, monitors the evolution of the excited states (described in details in the **Chapter 2**). Over the past decades, many naturally occurring and synthetic carotenoids were characterized by the pump-probe technique in solution,[31,41,78–80] proteins,[81–84] reaction centers,[85–87] and light-harvesting complexes.[88–90] These studies reveal that carotenoids have various functions: light-harvesting, energy transfer, and photoprotection. Pump-probe spectroscopic studies of carotenoid properties and their functions are the subject of this thesis and are presented in the Research Section.

Multi-pulse transient absorption spectroscopy, which is also used in our laboratory, utilizes three laser pulses: pump and probe pulses (as used in the pump-probe setup) and an additional pulse with a certain delay after the pump pulse, which further perturbs the system. Depending on the chosen energy of the third pulse, it selectively re-excites some of the molecules to higher-lying excited states (called *repump*) or it depopulates the excited state to ground state (called *dump*). The multi-pulse technique has already shown great potential in applications related to photosynthetic pigments. A recent multi-pulse transient absorption study of the carbonyl carotenoids[61,62] has provided the evidence that the S_1 and ICT states are two distinct excited states, and a subsequent target analysis of the multi-pulse data has shown that both states rapidly equilibrate.

Two-photon absorption spectroscopy is a powerful tool for the study of one-photon forbidden, but two-photon allowed, excited states due to the different symmetry-selection rules for one- versus two-photon excitation. Two-photon absorption occurs when two laser pulses are temporarily overlapped and their combined energy is resonant with a higher electronic state. The method requires short pulses with a high photon density in the excitation volume. This allows the observation of non-linear processes, such as a direct population of the states, which are optically forbidden for one-photon absorption. One of the applications of the two-photon absorption spectroscopy is verification of the involvement of the carotenoids S_1 state in the energy transfer to chlorophyll or bacteriochlorophyll molecules.[91–93] While the one-photon excitation pump-probe experiments are generally designed to excite the second excited S_2 state, the two-photon absorption

spectroscopy excludes the possible contribution of the S_2 and vibrationally unrelaxed S_1 states in the energy transfer to acceptor molecules.

Femtosecond Stimulated Raman Spectroscopy (FSRS) allows monitoring the changes of the molecular conformations and bond structure in the excited states on an ultrafast time scale. In this method, the molecules are promoted to the excited states by a resonant actinic pulse (pump), while Raman transitions are probed by a narrowband Raman pump pulse and ultrashort probe pulse after a certain delay time. The experimental setup is often designed in a way to obtain not only time-resolved excited-state vibrational Raman spectra, but electronic ground state vibrational spectra and transient absorption spectra as well in a single experiment. The FSRS technique has been applied to study many carotenoids in both solutions[94–96] and light-harvesting complexes,[97] and has provided unique information about vibrational cooling processes. Recently, Redeckas et al.[61] have performed an FSRS study of carbonyl carotenoid fucoxanthin using different Raman pump wavelength. The results have shown that the S_1 state and ICT are two distinct vibronic species in the fucoxanthin excited-state manifold. In a different experiment, another research group has aimed to resolve an issue regarding the nature of the S* state.[98] Their results showed that the S* state has an origin in the S_1 state in certain carotenoid conformations with a shorter effective conjugation length.

1.8. Goals and Structure of the Thesis

In spite of the fact that in the past decades there were many studies which focused on the excited states of carotenoids, many questions still remain unanswered. The main goal of the work presented here was to examine the relationship between the structure and spectroscopic properties of carotenoids both in solution and as part of proteins.

The main questions raised in the thesis are as follows:

- What is the effect of the isomerization on the excited states in the carbonyl carotenoid fucoxanthin? How does isomerization affect the ICT state?

-        What is the possible structure of the unknown carbonyl carotenoid from *Chromera velia*? Can we use transient absorption spectroscopic techniques to estimate it?

-        How are the S_1 state relaxation processes affected by excess energy excitation of the S_2 state in linear carotenoids?

-        What is the role of carotenoids bound to photoactive proteins? How does their configuration change upon activation?

In order to answer these questions we have performed a number of femtosecond transient absorption spectroscopy experiments for a number of carotenoids in solution and in proteins. The results were analyzed using a variety of different methods in order to gain an insight into the carotenoids excited states dynamics.

Chapter 1 provides a short introduction into photosynthesis, the carotenoids photophysics, with a focus on their excited states. Furthermore, it includes an overview of spectroscopy techniques that can be applied to the study of carotenoids and their properties.

In **Chapter 2** spectroscopy techniques are presented together with the analytical tools that were used for these studies.

Research Section is devoted to the results of different experiments performed to answer the questions raised in the beginning of this section. **Chapter 3** addresses the investigation of the effect of isomerization on excited-state dynamics of the carotenoid fucoxanthin. Different response of carbonyl carotenoids to solvent proticity is used to estimate the structure of an unknown carotenoid from *Chromera velia*, and the results are discussed in detail in **Chapter 4**. In **Chapter 5**, spectroscopic properties of the S_1 state of three linear carotenoids were studied after excess energy excitation in the S_2 state. **Chapter 6** presents a femtosecond spectroscopic comparison study of Orange and Red Carotenoid Proteins binding different carotenoids.

References

(1)   Barnes, C. R. On the Food of Green Plants. *Bot. Gaz.* **1893**, *18* (11), 403–411.

(2)   Gest, H. History of the Word Photosynthesis and Evolution of Its Definition. *Photosynth. Res.* **2002**, *73* (1–3), 7–10.

(3)   Gest, H. Photosynthetic and Quasi-Photosynthetic Bacteria. *FEMS Microbiol. Lett.* **1993**, *112* (1), 1–5.

(4)   Cogdell, R. J.; Gardiner, A. T.; Molina, P. I.; Cronin, L. The Use and Misuse of Photosynthesis in the Quest for Novel Methods to Harness Solar Energy to Make Fuel. *Philos. Trans. A. Math. Phys. Eng. Sci.* **2013**, *371* (1996), 20110603.

(5)   Cogdell, R. J.; Gardiner, A. T.; Cronin, L. Learning from Photosynthesis: How to Use Solar Energy to Make Fuels. *Philos. Trans. R. Soc. A Math. Phys. Eng. Sci.* **2012**, *370* (1972), 3819–3826.

(6)   Hohmann-Marriott, M. F.; Blankenship, R. E. Evolution of Photosynthesis. *Annu. Rev. Plant Biol.* **2011**, *62* (1), 515–548.

(7)   Bryant, D. A.; Frigaard, N. U. Prokaryotic Photosynthesis and Phototrophy Illuminated. *Trends Microbiol.* **2006**, *14* (11), 488–496.

(8)   Ort, D. R.; Merchant, S. S.; Alric, J.; Barkan, A.; Blankenship, R. E.; Bock, R.; Croce, R.; Hanson, M. R.; Hibberd, J. M.; Long, S. P.; et al. Redesigning Photosynthesis to Sustainably Meet Global Food and Bioenergy Demand. *Proc. Natl. Acad. Sci.* **2015**, *112* (28), 8529–8536.

(9)   Mathies, R. A.; Lin, S. W.; Ames, J. B.; Pollard, W. T. From Femtoseconds to Biology : Mechanism of Bacteriorhodopsin's Light-Driven Proton Pump. *Annu. Rev. Biophys. Biophys. Chem.* **1991**, No. 20, 491–518.

(10)   Karraschl, S.; Bulloughl, P. A.; Ghosh, R. The 8.5 A Projection Map of the Light-Harvesting Complex I from Rhodospirillum Rubrum Reveals a Ring Composed of 16 Subunits. *EMBO J.* **1995**, *14* (4), 631–638.

(11)   McDermott, G.; Prince, S. M.; Freer, A. A.; Hawthornthwaite-Lawless, A. M.; Papiz, M. Z.; Cogdell, R. J.; Isaacs, N. W. Crystal Structure of an Integral Membrane Light-Harvesting Complex from Photosynthetic Bacteria.

Nature. 1995, pp 517–521.

(12)   Koepke, J.; Hu, X.; Muenke, C.; Schulten, K.; Michel, H. The Crystal Structure of the Light-Harvesting Complex II (B800–850) from Rhodospirillum Molischianum. *Structure* **1996**, *4* (5), 581–597.

(13)   Klimmek, F.; Ganeteg, U.; Ihalainen, J. A.; Roon, H. van; Jensen, P. E.; Scheller, H. V.; Jan P. Dekker, A.; Jansson, S. Structure of the Higher Plant Light Harvesting Complex I: In Vivo Characterization and Structural Interdependence of the Lhca Proteins. *Biochenistry.* **2005,** *44* (8), 3065-3073.

(14)   Drop, B.; Webber-Birungi, M.; Yadav, S. K. N.; Filipowicz-Szymanska, A.; Fusetti, F.; Boekema, E. J.; Croce, R. Light-Harvesting Complex II (LHCII) and Its Supramolecular Organization in Chlamydomonas Reinhardtii. *Biochim. Biophys. Acta - Bioenerg.* **2014**, *1837* (1), 63–72.

(15)   Fan, M.; Li, M.; Liu, Z.; Cao, P.; Pan, X.; Zhang, H.; Zhao, X.; Zhang, J.; Chang, W. Crystal Structures of the PsbS Protein Essential for Photoprotection in Plants. *Nat. Struct. Mol. Biol.* **2015**, *22* (9), 729–735.

(16)   Watanabe, M.; Semchonok, D. A.; Webber-Birungi, M. T.; Ehira, S.; Kondo, K.; Narikawa, R.; Ohmori, M.; Boekema, E. J.; Ikeuchi, M. Attachment of Phycobilisomes in an Antenna-Photosystem I Supercomplex of Cyanobacteria. *Proc. Natl. Acad. Sci.* **2014**, *111* (7), 2512–2517.

(17)   Schulte, T.; Hiller, R. G.; Hofmann, E. X-Ray Structures of the Peridinin-Chlorophyll-Protein Reconstituted with Different Chlorophylls. *FEBS Lett.* **2010**, *584* (5), 973–978.

(18)   Amunts, A.; Drory, O.; Nelson, N. The Structure of a Plant Photosystem I Supercomplex at 3.4 Å Resolution. *Nature* **2007**, *447* (7140), 58–63.

(19)   Ben-Shem, A.; Frolow, F.; Nelson, N. Crystal Structure of Plant Photosystem I. *Nature* **2003**, *426* (6967), 630–635.

(20)   Rhee, K. H.; Morris, E. P.; Zheleva, D.; Hankamer, B.; Kuehlbrant, W.; Barber, J. Two-Dimensional Structure of Plant Photosystem II at 8-Å Resolution. *Nature* **1997**, *389*, 522–526.

(21)   Rhee, K.-H.; Morris, E. P.; Barber, J.; Kuhlbrandt, W. Three-Dimensional Structure of the Plant Photosystem II Reaction Centre at 8 A

Resolution. *Nature* **1998**, *396*, 283–286.

(22)   Zouni, A.; Witt, H. T.; Kern, J.; Fromme, P.; Krauss, N.; Saenger, W.; Orth, P. Crystal Structure of Photosystem II from Synechococcus Elongatus at 3.8 A Resolution. *Nature* **2001**, *409* (1988), 739–743.

(23)   Kamiya, N.; Shen, J.-R. Crystal Structure of Oxygen-Evolving Photosystem II from Thermosynechococcus Vulcanus at 3.7-A Resolution. *Proc. Natl. Acad. Sci.* **2003**, *100* (1), 98–103.

(24)   Blankenship, R. E. *Molecular Mechanisms of Photosynthesis*; Blackwell Science: Oxford, UK, 2002.

(25)   Koyama, Y.; Fujii, R. Cis-Trans Carotenoids in Photosynthesis: Configurations, Excited-State Properties and Physiological Functions. In *The Photochemistry of Carotenoids*; Frank, H. A., Young, A. J., Britton, G., Gogdell, R. J., Eds.; Kluwer Academic Publishers: Dordrecht, The Neterlands, 1999; pp 161–188.

(26)   Cogdell, R. J. Carotenoids in Photosynthesis. *Pure Appl Chem* **1985**, *57* (5), 723–728.

(27)   Ramel, F.; Birtic, S.; Cuiné, S.; Triantaphylidès, C.; Ravanat, J.-L.; Havaux, M. Chemical Quenching of Singlet Oxygen by Carotenoids in Plants. *Plant Physiol.* **2012**, *158* (3), 1267–1278.

(28)   Young, A. J. The Photoprotective Role of Carotenoids in Higher Plants. *Physiol. Plant.* **1991**, *83* (4), 702–708.

(29)   Zigmantas, D.; Hiller, R. G.; Sharples, F. P.; Frank, H. A. Effect of a Conjugated Carbonyl Group on the Photophysical Properties of Carotenoids. **2004**, 3009–3016.

(30)   Chábera, P.; Fuciman, M.; Hríbek, P.; Polívka, T. Effect of Carotenoid Structure on Excited-State Dynamics of Carbonyl Carotenoids. *Phys. Chem. Chem. Phys.* **2009**, *11* (39), 8795–8803.

(31)   Niedzwiedzki, D.; Koscielecki, J. F.; Cong, H.; Sullivan, J. O.; Gibson, G. N.; Birge, R. R.; Frank, H. a. Ultrafast Dynamics and Excited State Spectra of Open-Chain Carotenoids at Room and Low Temperatures. *J. Phys. Chem. B* **2007**, *111* (21), 5984–5998.

(32)   Parson, W. W. *Modern Optical Spectroscopy : With Exercises and*

Examples from Biophysics and Biochemistry, Student Edition.; Springer, 2007.

(33)   Pariser, R.; Parr, R. G. A Semi-Empirical Theory of the Electronic Spectra and Electronic Structure of Complex Unsaturated Molecules. II. *J. Chem. Phys.* **1953**, *21* (5), 767–776.

(34)   Tavan, P.; Schulten, K. Electronic Excitations in Finite and Infinite Polyenes. *Physical Review B*. **1987**, *36* (8), 4337–4358.

(35)   Tavan, P.; Schulten, K. The Low-Lying Electronic Excitations in Long Polyenes: A PPP-MRD-CI Study. *J.Chem.Phys.* **1986**, *85* (11), 6602–6609.

(36)   Fiedor, L.; Heriyanto; Fiedor, J.; Pilch, M. Effects of Molecular Symmetry on the Electronic Transitions in Carotenoids. *J. Phys. Chem. Lett.* **2016**, *7* (10), 1821–1829.

(37)   Kosumi, D.; Fujiwara, M.; Fujii, R.; Cogdell, R. J.; Hashimoto, H.; Yoshizawa, M. The Dependence of the Ultrafast Relaxation Kinetics of the S2 and S1 States in β -Carotene Homologs and Lycopene on Conjugation Length Studied by Femtosecond Time-Resolved Absorption and Kerr-Gate Fluorescence Spectroscopies. *J. Chem. Phys.* **2009**, *130* (21).

(38)   Nakamura, R.; Fujii, R.; Nagae, H.; Koyama, Y.; Kanematsu, Y. Vibrational Relaxation in the State of Carotenoids as Determined by Kerr-Gate Fluorescence Spectroscopy. *Chem. Phys. Lett.* **2004**, *400* (1–3), 7–14.

(39)   Koyama, Y.; Rondonuwu, F. S.; Fujii, R.; Watanabe, Y. Light-Harvesting Function of Carotenoids in Photo-Synthesis: The Roles of the Newly Found 11Bu- State. *Biopolymers* **2004**, *74* (1–2), 2–18.

(40)   Gradinaru, C. C.; Kennis, J. T.; Papagiannakis, E.; van Stokkum, I. H.; Cogdell, R. J.; Fleming, G. R.; Niederman, R. a; van Grondelle, R. An Unusual Pathway of Excitation Energy Deactivation in Carotenoids: Singlet-to-Triplet Conversion on an Ultrafast Timescale in a Photosynthetic Antenna. *Proc. Natl. Acad. Sci. U. S. A.* **2001**, *98* (5), 2364–2369.

(41)   Polívka, T.; Sundstrom, V. Ultrafast Dynamics of Carotenoid Excited States-from Solution to Natural and Artificial Systems. *Chem. Rev.* **2004**, *104* (4), 2021–2071.

(42)   Frank, H. A.; Desamero, R. Z. B.; Chynwat, V.; Gebhard, R.; Van Der Hoef, I.; Jansen, F. J.; Lugtenburg, J.; Gosztola, D.; Wasielewski, M. R.

Spectroscopic Properties of Spheroidene Analogs Having Different Extents of π - Electron Conjugation. *J. Phys. Chem. A* **1997**, *101*, 149–157.

(43)   Andersson, P. O.; Gillbro, T. Photophysics and Dynamics of the Lowest Excited Singlet State in Long Substituted Polyenes with Implications to the Very Long-Chain Limit. *J. Chem. Phys.* **1995**, *103* (7), 2509–2519.

(44)   Christensen, R. L. The Electronic States of Carotenoids. In *The Photochemistry of Carotenoids*; Frank, H. A., Young, A. J., Britton, G., Gogdell, R. J., Eds.; Kluwer Academic Publishers: Dordrecht, The Netherlands, 1999; pp 137–159.

(45)   Andersson, P. O.; Gillbro, T.; Ferguson, L.; Cogdell, R. J. Absorption Spectral Shifts of Carotenoids Related To Medium Polarizability. *Photochem. Photobiol.* **1991**, *54* (3), 353–360.

(46)   Akimoto, S.; Yamazaki, I.; Takaichi, S.; Mimuro, M. Excitation Relaxation of Carotenoids within the S2 State Probed by the Femtosecond Fluorescence up-Conversion Method. *Chem. Phys. Lett.* **1999**, *313* (1–2), 63–68.

(47)   Akimoto, S.; Yamazaki, I.; Takaichi, S.; Mimuro, M. Excitation Relaxation Dynamics of Linear Carotenoids. *J. Lumin.* **2000**, *87*, 797–799.

(48)   Bondarev, S. L.; Knyukshto, V. N. Fluorescence from the S1(2 1Ag) State of All-Trans-β-Carotene. *Chem. Phys. Lett.* **1994**, *225* (4–6), 346–350.

(49)   Fujii, R.; Onaka, K.; Kuki, M.; Koyama, Y.; Watanabe, Y. The 2Ag− Energies of All-Trans-Neurosporene and Spheroidene as Determined by Fluorescence Spectroscopy. *Chem. Phys. Lett.* **1998**, *288* (5–6), 847–853.

(50)   Gaier, K.; Angerhofer, A.; Wolf, H. C. The Lowest Excited Electronic Singlet States of All-Trans β-Carotene Single Crystals. *Chem. Phys. Lett.* **1991**, *187* (1–2), 103–109.

(51)   Hashimoto, H.; Koyama, Y.; Mori, Y. Mechanism Activating the 21Ag State in All-Trans-β-Carotene Crystal to Resonance Raman Scattering. *Jpn. J. Appl. Phys.* **1997**, *36* (Part 2, No. 7B), L916–L918.

(52)   Sashima, T.; Nagae, H.; Kuki, M.; Koyama, Y. A New Singlet-Excited State of All-Trans-Spheroidene as Detected by Resonance-Raman Excitation Profiles. *Chem. Phys. Lett.* **1999**, *299* (2), 187–194.

(53)   Polívka, T.; Herek, J. L.; Zigmantas, D.; Akerlund, H. E.;

Sundström, V. Direct Observation of the (Forbidden) S1 State in Carotenoids. *Proc. Natl. Acad. Sci. U. S. A.* **1999**, *96* (9), 4914–4917.

(54)   Christensen, R. L.; Galinato, M. G. I.; Chu, E. F.; Howard, J. N.; Broene, R. D.; Frank, H. A. Energies of Low-Lying Excited States of Linear Polyenes. *J. Phys. Chem. A* **2008**, *112* (49), 12629–12636.

(55)   Weerd, F. L. De; Stokkum, I. H. M. Van; Grondelle, R. Van. Subpicosecond Dynamics in the Excited State Absorption of All- Trans-β - Carotene. *Chem. Phys. Lett.* **2002**, *354*, 38–43.

(56)   Hörvin Billsten, H.; Zigmantas, D.; Sundström, V.; Polívka, T. Dynamics of Vibrational Relaxation in the S1 State of Carotenoids Having 11 Conjugated C=C Bonds. *Chem. Phys. Lett.* **2002**, *355* (5–6), 465–470.

(57)   Kosumi, D.; Fujii, R.; Sugisaki, M.; Oka, N.; Iha, M.; Hashimoto, H. Characterization of the Intramolecular Transfer State of Marine Carotenoid Fucoxanthin by Femtosecond Pump-Probe Spectroscopy. *Photosynth. Res.* **2014**, *121* (1), 61–68.

(58)   Zigmantas, D.; Polívka, T.; Hiller, R. G.; Yartsev, A.; Sundström, V. Spectroscopic and Dynamic Properties of the Peridinin Lowest Singlet Excited States. *J. Phys. Chem. A* **2001**, *105* (45), 10296–10306.

(59)   Bautista, J. A.; Connors, R. E.; Raju, B. B.; Hiller, R. G.; Sharples, F. P.; Gosztola, D.; Wasielewski, M. R.; Frank, H. A. Excited State Properties of Peridinin: Observation of a Solvent Dependence of the Lowest Excited Singlet State Lifetime and Spectral Behavior Unique among Carotenoids. *J. Phys. Chem. B* **1999**, *103* (41), 8751–8758.

(60)   Enriquez, M. M.; Fuciman, M.; Lafountain, A. M.; Wagner, N. L.; Birge, R. R.; Frank, H. A. The Intramolecular Charge Transfer State in Carbonyl-Containing Polyenes and Carotenoids. **2011**, *114* (38), 12416–12426.

(61)   Redeckas, K.; Voiciuk, V.; Vengris, M. Investigation of the S1/ICT Equilibrium in Fucoxanthin by Ultrafast Pump–dump–probe and Femtosecond Stimulated Raman Scattering Spectroscopy. *Photosynth. Res.* **2016**, *128* (2), 169–181.

(62)   Papagiannakis, E.; Vengris, M.; Larsen, D. S.; Stokkum, I. H. M. Van; Hiller, R. G.; Grondelle, R. Van. Use of Ultrafast Dispersed Pump − Dump

− Probe and Pump − Repump − Probe Spectroscopies to Explore the Light-Induced Dynamics of Peridinin in Solution Use of Ultrafast Dispersed Pump - Dump - Probe and Pump - Repump - Probe Spectroscopies to Explore the L. *J. Phys. Chem. B.* **2006**, *110,* 512–521.

(63)   Papagiannakis, E.; Larsen, D. S.; Stokkum, I. H. M. Van;; Vengris, M.; Hiller, R. G.; Grondelle, R. Van. Resolving the Excited State Equilibrium of Peridinin in Solution. *Biochemistry.* **2004**, *43* (49), 15303-15309.

(64)   Hauer, J.; Maiuri, M.; Viola, D.; Lukes, V.; Henry, S.; Carey, A. M.; Cogdell, R. J.; Cerullo, G.; Polli, D. Explaining the Temperature Dependence of Spirilloxanthin's S* Signal by an Inhomogeneous Ground State Model. *J. Phys. Chem. A* **2013**, *117* (29), 6303–6310.

(65)   Ehlers, F.; Scholz, M.; Schimpfhauser, J.; Bienert, J.; Oum, K.; Lenzer, T. Collisional Relaxation of Apocarotenals: Identifying the S* State with Vibrationally Excited Molecules in the Ground Electronic State S(0)*. *Phys. Chem. Chem. Phys.* **2015**, *17* (16), 10478–10488.

(66)   Larsen, D. S.; Papagiannakis, E.; Van Stokkum, I. H. M.; Vengris, M.; Kennis, J. T. M.; Van Grondelle, R. Excited State Dynamics of β-Carotene Explored with Dispersed Multi-Pulse Transient Absorption. *Chem. Phys. Lett.* **2003**, *381* (5–6), 733–742.

(67)   Ostroumov, E. E.; Reus, M. G. M. M.; Holzwarth, A. R.; Holzwarth, A. R. On the Nature of the "Dark S*" Excited State of β-Carotene. *J. Phys. Chem. A* **2011**, *115* (16), 3698–3712.

(68)   Balevičius, V.; Pour, A. G.; Savolainen, J.; Lincoln, C. N.; Lukes, V.; Riedle, E.; Valkunas, L.; Abramavicius, D.; Hauer, J. J. Vibronic Energy Relaxation Approach Highlighting Deactivation Pathways in Carotenoids. *Phys. Chem. Chem. Phys.* **2015**, *4* (8), 1166–1169.

(69)   Balevičius, V.; Abramavicius, D.; Polívka, T.; Galestian Pour, A.; Hauer, J. A Unified Picture of S* in Carotenoids. *J. Phys. Chem. Lett.* **2016**, *1* (August), 3347–3352.

(70)   Kirilovsky, D.; Kerfeld, C. a. The Orange Carotenoid Protein in Photoprotection of Photosystem II in Cyanobacteria. *Biochim. Biophys. Acta - Bioenerg.* **2012**, *1817* (1), 158–166.

(71)   Boulay, C.; Abasova, L.; Six, C.; Vass, I.; Kirilovsky, D. Occurrence and Function of the Orange Carotenoid Protein in Photoprotective Mechanisms in Various Cyanobacteria. *Biochim. Biophys. Acta - Bioenerg.* **2008**, *1777* (10), 1344–1354.

(72)   Wilson, A.; Punginelli, C.; Gall, A.; Bonetti, C.; Alexandre, M.; Routaboul, J.-M.; Kerfeld, C. A.; van Grondelle, R.; Robert, B.; Kennis, J. T. M.; et al. A Photoactive Carotenoid Protein Acting as Light Intensity Sensor. *Proc. Natl. Acad. Sci. U. S. A.* **2008**, *105* (33), 12075–12080.

(73)   Leverenz, R. L.; Jallet, D.; Li, M.-D.; Mathies, R. a.; Kirilovsky, D.; Kerfeld, C. A. Structural and Functional Modularity of the Orange Carotenoid Protein: Distinct Roles for the N- and C-Terminal Domains in Cyanobacterial Photoprotection. *Plant Cell* **2014**, *26*, 1–13.

(74)   Sutter, M.; Wilson, A; Leverenz, R. L.; Lopez-Igual, R.; Thurotte, A; Salmeen, A. E.; Kirilovsky, D.; Kerfeld, C. A. Crystal Structure of the FRP and Identification of the Active Site for Modulation of OCP-Mediated Photoprotection in Cyanobacteria. *Proc Natl Acad Sci USA* **2013**, *110* (24), 10022–10027.

(75)   Leverenz, R. L.; Sutter, M.; Wilson, A.; Gupta, S.; Thurotte, A.; Bourcier de Carbon, C.; Petzold, C. J.; Ralston, C.; Perreau, F.; Kirilovsky, D.; et al. A 12 A Carotenoid Translocation in a Photoswitch Associated with Cyanobacterial Photoprotection. *Science* **2015**, *348* (6242), 1463–1466.

(76)   Berera, R.; Van Stokkum, I. H. M.; Gwizdala, M.; Wilson, A.; Kirilovsky, D.; Van Grondelle, R. The Photophysics of the Orange Carotenoid Protein, a Light-Powered Molecular Switch. *J. Phys. Chem. B* **2012**, *116* (8), 2568–2574.

(77)   Niedzwiedzki, D. M.; Liu, H.; Blankenship, R. E. Excited State Properties of 3'-Hydroxyechinenone in Solvents and in the Orange Carotenoid Protein from Synechocystis Sp. PCC 6803. *J. Phys. Chem. B* **2014**, *118* (23), 6141–6149.

(78)   Niedzwiedzki, D. M.; Sullivan, J. O.; Polívka, T.; Birge, R. R.; Frank, H. A. Femtosecond Time-Resolved Transient Absorption Spectroscopy of Xanthophylls. *J. Phys. Chem. B* **2006**, *110* (45), 22872–22885.

(79)   Polli, D.; Cerullo, G.; Lanzani, G.; De Silvestri, S.; Hashimoto, H.; Cogdell, R. J. Excited-State Dynamics of Carotenoids with Different Conjugation Length. *Synth. Met.* **2003**, *139* (3), 893–896.

(80)   Magdaong, N. M.; Niedzwiedzki, D. M.; Greco, J. A; Liu, H.; Yano, K.; Kajikawa, T.; Sakaguchi, K.; Katsumura, S.; Birge, R. R.; Frank, H. A. Excited State Properties of a Short π-Electron Conjugated Peridinin Analogue. *Chem. Phys. Lett.* **2014**, *593*, 132–139.

(81)   Durchan, M.; Tichý, J.; Litvín, R.; Šlouf, V.; Gardian, Z.; Hříbek, P.; Vácha, F.; Polívka, T. Role of Carotenoids in Light-Harvesting Processes in an Antenna Protein from the Chromophyte Xanthonema Debile. *J. Phys. Chem. B* **2012**, *116* (30), 8880–8889.

(82)   Polívka, T.; Chábera, P.; Kerfeld, C. a. Carotenoid-Protein Interaction Alters the S(1) Energy of Hydroxyechinenone in the Orange Carotenoid Protein. *Biochim. Biophys. Acta* **2013**, *1827* (3), 248–254.

(83)   Polívka, T.; Hiller, R. G.; Frank, H. A. Spectroscopy of the Peridinin-Chlorophyll-a Protein: Insight into Light-Harvesting Strategy of Marine Algae. *Arch. Biochem. Biophys.* **2007**, *458* (2), 111–120.

(84)   Papagiannakis, E.; H M van Stokkum, I.; Fey, H.; Büchel, C.; van Grondelle, R. Spectroscopic Characterization of the Excitation Energy Transfer in the Fucoxanthin-Chlorophyll Protein of Diatoms. *Photosynth. Res.* **2005**, *86* (1–2), 241–250.

(85)   Bautista, J. A.; Chynwat, V.; Cua, A.; Jansen, F. J.; Lugtenburg, J.; Gosztola, D.; Wasielewski, M. R.; Frank, H. A. The Spectroscopic and Photochemical Properties of Locked-15,15'-cis-Spheroidene in Solution and Incorporated into the Reaction Center of Rhodobacter Sphaeroides R-26.1. *Photosynth. Res.* **1998**, *55* (1), 49–65.

(86)   Lin, S.; Katilius, E.; Taguchi, A. K. W.; Woodbury, N. W. Excitation Energy Transfer from Carotenoid to Bacteriochlorophyll in the Photosynthetic Purple Bacterial Reaction Center of Rhodobacter Sphaeroides. *J. Phys. Chem. B.* **2003**, *107* (50), 14103-14108.

(87)   Šlouf, V.; Chábera, P.; Olsen, J. D.; Martin, E. C.; Qian, P.; Hunter, C. N.; Polívka, T. Photoprotection in a Purple Phototrophic Bacterium Mediated

by Oxygen-Dependent Alteration of Carotenoid Excited-State Properties. *Proc. Natl. Acad. Sci. U. S. A.* **2012**, *109* (22), 8570–8575.

(88)   Slouf, V.; Fuciman, M.; Johanning, S.; Hofmann, E.; Frank, H. A.; Polívka, T. Low-Temperature Time-Resolved Spectroscopic Study of the Major Light-Harvesting Complex of Amphidinium Carterae. *Photosynth. Res.* **2013**, *117* (1–3), 257–265.

(89)   Di Donato, M.; van Grondelle, R.; van Stokkum, I. H. M. and; Groot, M. L. Excitation Energy Transfer in the Photosystem II Core Antenna Complex CP43 Studied by Femtosecond Visible/Visible and Visible/Mid-Infrared Pump Probe Spectroscopy. *J. Phys. Chem. B.* **2007**, *111* (25), 7345-7352.

(90)   Kwa, S. L. S.; van Amerongen, H.; Lin, S.; Dekker, J. P.; van Grondelle, R.; Struve, W. S. Ultrafast Energy Transfer in LHC-II Trimers from the Chl A/b Light-Harvesting Antenna of Photosystem II. *Biochim. Biophys. Acta - Bioenerg.* **1992**, *1102* (2), 202–212.

(91)   Linden, P. A.; Zimmermann, J.; Brixner, T.; Holt, N. E.; Vaswani, H. M.; Hiller, R. G.; Fleming, G. R. Transient Absorption Study of Peridinin and Peridinin-Chlorophyll a-Protein after Two-Photon Excitation. *J. Phys. Chem. B* **2004**, *108*, 10340–10345.

(92)   Walla, P. J.; Linden, P. A.; Ohta, K.; Fleming, G. R. Excited-State Kinetics of the Carotenoid S1 State in LHC II and Two-Photon Excitation Spectra of Lutein and β-Carotene in Solution: Efficient Car S1-Chl Electronic Energy Transfer via Hot S1 States? *J. Phys. Chem. A* **2002**, *106*, 1909–1916.

(93)   Jian-Ping Zhang; Ritsuko Fujii; Pu Qian; Toru Inaba; Tadashi Mizoguchi; Yasushi Koyama; Kengo Onaka, A.; Yasutaka Watanabe; Nagae, H. Mechanism of the Carotenoid-to-Bacteriochlorophyll Energy Transfer via the S1 State in the LH2 Complexes from Purple Bacteria. *J. Phys. Chem. B* **2000**, *104*, 3683–3691.

(94)   McCamant, D. W.; Kukura, P.; Mathies, R. A. Femtosecond Time-Resolved Stimulated Raman Spectroscopy: Application to the Ultrafast Internal Conversion in β-Carotene. *J. Phys. Chem. A* **2003**, *107* (40), 8208–8214.

(95)   Kukura, P.; McCamant, D. W. and; Mathies, R. A. Femtosecond Time-Resolved Stimulated Raman Spectroscopy of the S2 (1Bu+) Excited State

of β-Carotene. *J. Phys. Chem. A.* **2004**, *108* (28), 5921-5925.

(96)   Kardas, T. M.; Ratajska-Gadomska, B.; Lapini, a.; Ragnoni, E.; Righini, R.; Di Donato, M.; Foggi, P.; Gadomski, W. Dynamics of the Time-Resolved Stimulated Raman Scattering Spectrum in Presence of Transient Vibronic Inversion of Population on the Example of Optically Excited Trans-β-Apo-8'-Carotenal. *J. Chem. Phys.* **2014**, *140* (20), 204312.

(97)   Yoshizawa, M.; Nakamura, R.; Yoshimatsu, O.; Abe, K.; Sakai, S.; Nakagawa, K.; Fujii, R.; Nango, M.; Hashimoto, H. Femtosecond Stimulated Raman Spectroscopy of the Dark S1 Excited State of Carotenoid in Photosynthetic Light Harvesting Complex. *Acta Biochim. Pol.* **2012**, *59* (1), 49–52.

(98)   Kloz, M.; Weissenborn, J.; Polívka, T.; Frank, H. A.; Kennis, J. T. M. Spectral Watermarking in Femtosecond Stimulated Raman Spectroscopy: Resolving the Nature of the Carotenoid S* State. *Phys. Chem. Chem. Phys.* **2016**, *18* (21), 14619–14628.

2. Experimental methods and data analysis

2.1. High-Performance Liquid Chromatography

High-Performance Liquid Chromatography (HPLC) is a versatile method that is used to separate a mixture of compounds in analytical chemistry, biochemistry, pharmacy etc. HPLC enables identification, qualification and purification of the individual components of the mixture based on their molecular structure. Main components in an HPLC system include the solvent reservoirs, a high-pressure pump, injector system, a column, and a detector (Figure 2-1).
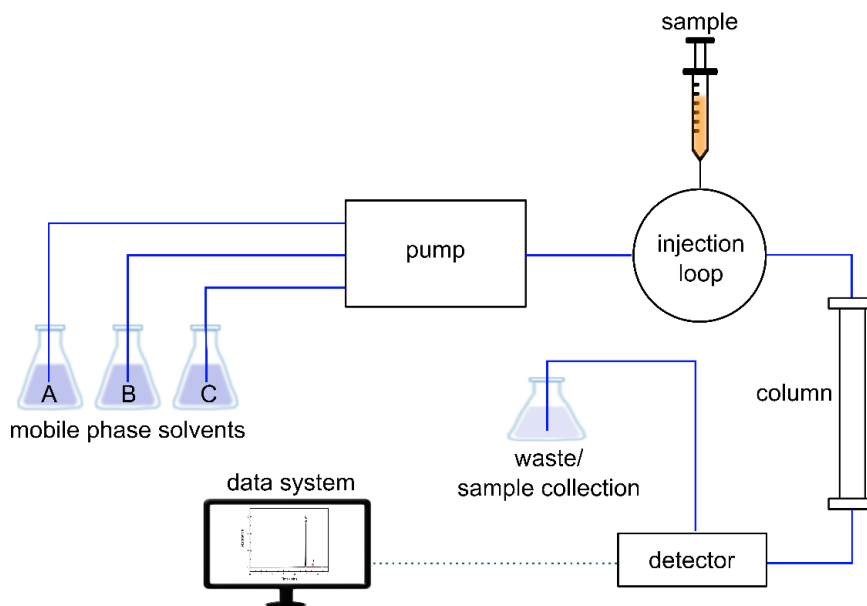

Figure 2-1. High-Performance Liquid Chromatography system.

The reservoirs hold the mobile phase solvents that are used for transporting the sample through the HPLC system. A mobile phase solvent is pumped through the sample injection loop, where the sample is injected into the phase stream that carries the sample into the high pressure column. The reverse phase column

contains the nonpolar stationary phase, while the mobile phase solvent is polar, such as mixtures of water and methanol or acetonitrile. Sample retention time varies depending on the interaction between the stationary phase, the molecules being analyzed, and the solvent. The more nonpolar the compound is, the longer it will be retained; thus the elution order of components is in decreasing order of polarity. The detector is located at the end of the column. The signal from the detector is sent to a computer which generates the chromatogram. As the mobile phase exits the detector, the purified compound may be collected for further study.

The final separation of carotenoid stereoisomers (**Chapter 3**) was carried on HPLC system consisting of Pump Controller Delta 600 and a PDA 2996 detector (Waters, USA), and a reverse phase Eclipse XDB-C18 column (9.4 mm x 250 mm, 5 µm; Agilent, USA). The separation of carotenoids from the pigments mixture (**Chapter 4**) has differed only in the using SunfireTM C8 column (4.6 mm x 250 mm, 5 µm, silica-based, end-capped, Waters, USA). A ternary solvent system was used for the separation on reverse phase. The mobile phase solvent A consisted of methanol/acetonitrile/water (50/25/25, v/v/v), while solvent B was methanol, and solvent C consisted of methanol/n-hexane (4/1, v/v). The flow rate was 1 or 2 mL/min (**Chapter 4**), and 4 mL/min (**Chapter 3**). The injection volume was 100 µl. All pigment samples were dried in the dark in glass desiccator under vacuum made by a membrane vacuum pump and stored at -20 °C for later use.

2.2. Steady-State Absorption Spectroscopy

The absorption spectroscopy is an analytical technique based on the measuring the amount of the light absorbed (determined by the light transmitted) by the molecules as a function of wavelength. A single beam spectrophotometer utilizes one beam of light, which passes through the sample, and the reference signal is measured without the sample or with the cuvette containing the solvent used for the test sample. The intensity of the light at specific wavelength transmitted through the sample ($I(\lambda)$) and intensity of the incident light ($I_0(\lambda)$) are measured. The ratio of the aforementioned light intensities describes transmittance (T):

$$T = \frac{I(\lambda)}{I_0(\lambda)} \qquad (1)$$

The absorbance of a homogenous sample is then calculated from the Eq.1 and is defined by the Beer-Lambert law:[1]

$$A = -logT = log\frac{I_0(\lambda)}{I(\lambda)} = c\epsilon(\lambda)d \qquad (2)$$

It depends on the length of the sample d and the molar concentration c of the absorbing species. The extinction coefficient or molar absorptivity $\epsilon(\lambda)$ is a measure of the probability of absorption of photon with wavelength λ. The absorbance is plotted versus certain wavelength, and the obtained absorption spectra gives the direct information about the energy of the absorbing state. The other important information obtained from the shape of the absorption spectra, is the degree of isomerization, aggregation, or photodamage.
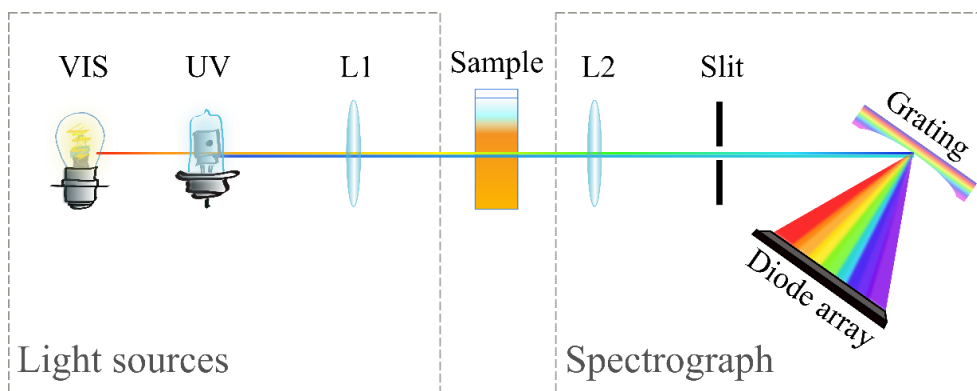

Figure 2-2. Spectrophotometer.

The schematic representation of the UV-VIS spectrophotometer Agilent 8453 used in our laboratory is shown in the Figure 2-2. It consists of three parts, the light source, sample compartment and a spectrograph. The Tungsten lamp provides a visible and near-infrared light, and it is optically combined with the Deuterium lamp, an ultraviolet light sources. The combined emitting light is in the wavelength range from 190 to 1100 nm. The beam is collimated by the lens L1 and goes through the sample. The spectrograph lens L2 focuses the beam on the plane of the slit, and then the beam passes the slit aperture. The holographic

grating disperses the light on the photodiode array, the series of the 1024 individual photodiodes.

2.3. Femtosecond Transient Absorption Spectroscopy

The transient absorption spectroscopy is a powerful tool for studying the excited state dynamics of different molecules. The ultrashort laser pulses ~100 fs allow investigating dynamics of the electronic states in real time. One of the pulses, the *pump*, excites the molecules to the higher states, the other one, the *probe*, is sent to the sample with a delay *t* with respect to the pump pulse. The absorption difference spectra are calculated by subtracting the spectra of the sample in the ground state from the spectra of the sample in the excited state. The difference absorption spectra measured at different delay times after excitation provide the dynamics of various processes.

The simplified scheme of the femtosecond laser system is shown in the Figure 2-3. The ultrafast laser system consists of three parts: the seed laser Mai Tai SP (Spectra-Physics), Empower 30 pump laser (Spectra-Physics), and the Spitfire Ace-100F ultrafast Ti: Sapphire regenerative amplifier (Spectra-Physics). The Mai Tai generates the pulses 100 fs, and the central wavelength is 800 nm with the 400mW output power at the repetition rate 84 MHz. The low-energy pulses from the Mai Tai enter the Spitfire Ace, where they are stretched in duration to achieve lower peak power before amplification. The stretched pulses are further amplified by a two stage (regenerative and multipass) Ti: Sapphire amplifiers. The Ti: Sapphire crystal is additionally pumped by the Empower 30 an intracavity-doubled, Q-switched, diode-pumped Nd-YLF pulsed green laser (527 nm) at1 kHz. The green laser causes the stimulated emission, which amplifies the pulses at the same wavelength and duration as the stretched pulses. Pulses are then directed through the dispersive optics, where they are compressed to their initial duration. The output then consists of pulses with ~100 fs duration, and 4.25 mJ energy per pulse at 1 kHz with the central wavelength at 800 nm.

The output beam is split into the two separate beams (Figure 2-4). The pump beam is tuned by a computer controlled optical parametric amplifier OPA (TOPAS, Light Conversion) in the 240-2500 nm wavelength range, the excitation

wavelength is then chosen based on the experiment requirements. The excitation power of pump pulses usually is set about $\sim 10^{14}$ photons per pulse per cm^2 to avoid sample degradation and non-linear effects. The pump pulse is sent through the chopper whose frequency is synchronized to block every second pulse to record the signal with and without the pump, this helps to decrease the signal-to-noise ratio of the measurements. The mutual polarization between pump and probe pulses was set to the magic angle (54,7°) to eliminate polarization and photoselection effects (see below).
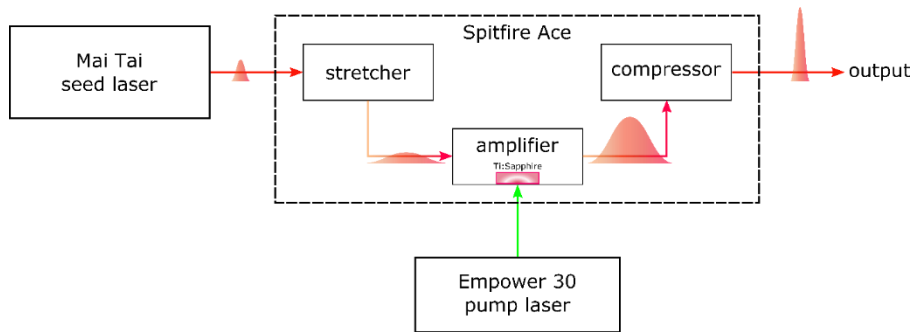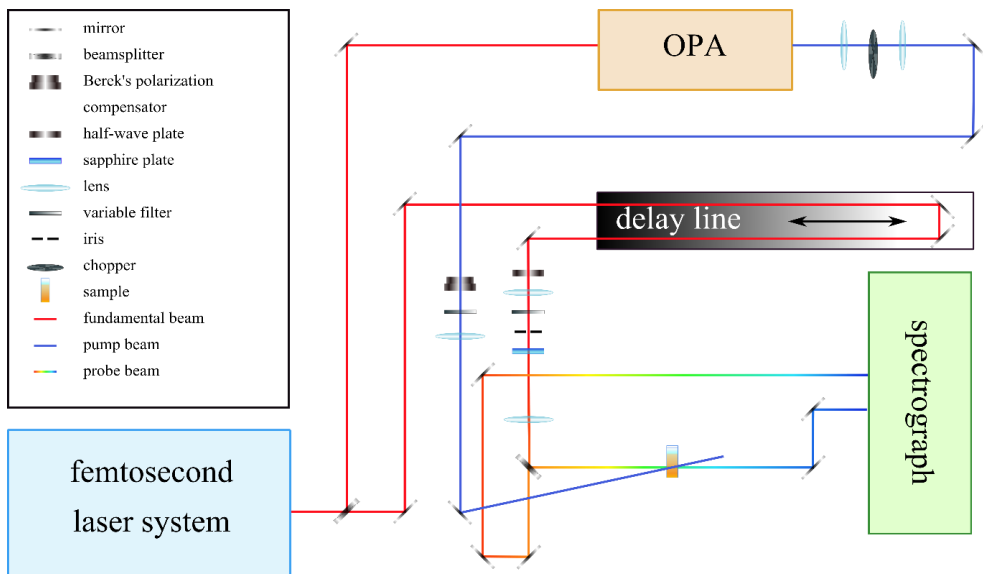

Figure 2-3. Femtosecond laser system

Figure 2-4. A simplified scheme of the pump-probe experiment in our laboratory

Upon excitation of the sample with the linear polarized light, the maximum of the absorption occurs when the polarization of the incident beam is parallel to the transition moment of the chromophore, and the minimum (zero) is reached when they are oriented perpendicular to each other. Then the total transient absorption intensity will be obtained as a sum of three mutually orthogonal (*x, y, z*-axes) intensities measured after excitation with the parallel (*ΔA*$_{//}$ for *z*-axis) and perpendicular (*2×ΔA*$_\perp$ for *x*- and y-axes) polarized light with respect to the pump beam. However, the total transient absorption intensity can be obtained when the measurements performed with the polarization orientation of the probe beam for which *ΔA*$_\perp$ would contribute with a double weight compared to the *ΔA*$_{//}$. Thus the setting of the magic angle between pump and probe beams will be equivalent to the isotropically averaged total intensity. Although, in some experiments the measurement of the anisotropy can be useful, the changes in orientation of the dipole moments of various transition can be calculated. In terms, to define the time-dependent anisotropy, the polarized excitation and probe beams should be applied. The time-dependent anisotropy is defined as:

$$r(t) = \frac{\Delta A_{\parallel}(t) - \Delta A_{\perp}(t)}{\Delta A_{\parallel}(t) + 2\Delta A_{\perp}(t)}. \qquad (3)$$

In its turn, the observed anisotropy is a product of the loss of anisotropy due to photoselection (0.4, the value of anisotropy for a randomly oriented sample), and that due to the angular displacement (θ) of the dipole moments of two transitions

$$r = 0.4 \left(\frac{3 \cos^2 \theta - 1}{2} \right). \quad (4)$$

The probe path includes a computer controlled delay line, which allows monitoring of the dynamic processes by varying the mutual delay between pump and probe pulses. The probe pulse is a white-light continuum generated by 2 mm sapphire plate. Part of the probe beam is split and serves as a reference. The probe and pump beams are focused and overlapped in the sample volume. The changes in the absorption are then recorded by focusing the probe and the reference beams into spectrograph slit, where they are dispersed onto a pair of photodiode array, each with 512 elements.

The change in the absorption $\Delta A(\Delta t, \lambda)$ induced by the pump pulse is calculated using the following expression:

$$\Delta A(\lambda) = A_{pumpON} - A_{pumpOFF} = log \left[\frac{I_{ref}(\lambda)}{I_{probe}(\lambda)}\right]_{pumpON} -$$

$$log \left[\frac{I_{ref}(\lambda)}{I_{probe}(\lambda)}\right]_{pumpOFF} \qquad (5)$$

where the absorbance A_{pumpON} is measured with the pump pulse, $A_{pumpOFF}$ is the absorbance with the blocked pump pulse, I_{ref} is the intensity of the reference beam, and I_{probe} the intensity of the probe. The intensity of the reference beam is measured to eliminate errors which may be introduced by the probe pulse fluctuations. The data is then averaged for more than 20 scans for each time delay to test reproducibility, sample stability, and to average out the laser fluctuations. In addition for each delay setting 250 from 300 shots are averaged in order to achieve satisfactory signal-to-noise ratio.

Three main signal contributions can be seen in the transient absorption spectra: ground state bleaching (GSB), stimulated emission (SE), and excited state absorption (ESA) (Figure 2-5). Those contributions can overlap causing band shifts, resulting in difficulties in separating the dynamics from different processes (see next Section).

The *ground state bleaching* signal has a negative contribution to the signal in the ground state absorption region. Upon excitation some molecules are already in the excited state, which means that the population of the ground state is reduced; thus, fewer photons are absorbed in the probe than in the reference when the pump pulse is unblocked ($A_{pumpON} < A_{pumpOFF}$). The spectral shape of GSB signal is identical to the steady-state absorption spectra, the signal remains until all excited molecules have relaxed to the ground state.

S*timulated emission* occurs when photons from the probe pulse interact with molecules in the excited state causing emission of photons with the same energy. The photons will be emitted in the same direction as the probe photons, consequently resulting in the enhancement of the I_{pumpON} at the detector and

negative difference signal $\Delta A(\Delta t, \lambda)$. For example, in carbonyl carotenoids the SE from the ICT state appears in the NIR spectra region.[2,3]

The *excited state absorption* occurs when new transition from the excited state occurs, and molecules absorb photons from the probe pulse of a certain wavelength. Thus, the positive signal ($A_{pumpON} > A_{pumpOFF}$) will appear on the transient absorption spectra. With the help of ESA we can track the evolution of excited states and their relaxation dynamics. In the case of carotenoids the most pronounced ESA occurs from the first excited state and corresponds to the S_1-S_N transition to a higher state.[4,5]
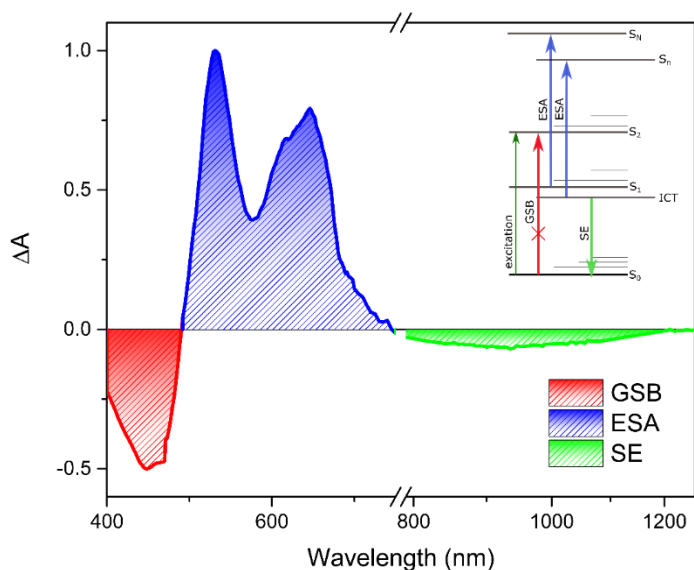
Figure 2-5. Signal contributions in typical transient absorption spectra of carbonyl carotenoid in polar solvent: ground state bleaching (GSB), stimulated emission (SE), and excited state absorption (ESA).

Another contribution to the transient absorption spectra is given by *product absorption*. After excitation of the molecules different reactions may occur which cause long-lived transient molecular states, such as triplet states, charged-

separated states, and isomerized states. One example of product absorption is an energy transfer from carotenoid to chlorophyll in light-harvesting complexes, where the chlorophyll molecules contribute to the spectra, even though they do not interact with the pump pulse. The absorption of the transient products can appear as a positive (e.g. ESA of triplet species) or negative (e.g. GSB of chlorophyll) signal in the difference absorption spectra.

2.4. Global and Target Analysis of the Time-Resolved Data

The time-resolved transient absorption experiment results in a two-dimensional dataset with two axes: the delay time t and the probe wavelength λ. The dependent variable is the differential absorbance $\Delta A\ (t, \lambda)$, the time-resolved spectrum can be rewritten as a superposition of the contributions of the n different components:

$$\psi(t, \lambda_i) = \sum_{j=1}^{n} c_j(t)\epsilon_j(\lambda_i), \quad (6)$$

According to the Beer-Lambert Law the extinction coefficient $\epsilon_j(\lambda)$ is weighed with the time-dependent $c_j(t)$ concentration of absorbing species of component j. The concentrations are described by a set of linear differential equations, the solution of which is given by a set of n exponential decays:

$$c_j(t) = \exp(-k_j t) = \exp(-\frac{t}{\tau_j}) \qquad (7)$$

which is characterized by the decay rate k_j, or lifetime constant τ_j for each component.

To reproduce physically relevant data, it is important to estimate the minimum satisfactory number of components presented in the data. The kinetic scheme should be based on the real physical model. Three kinetic models are usually used to analyze the time-resolved data set (Figure 2-6).

A *parallel* model is used when we have independent mono-exponential decay of each of the components. This method yields decay associated difference spectra (DADS). The DADS represent a loss or gain of a certain component associated with the decay rate k_j.
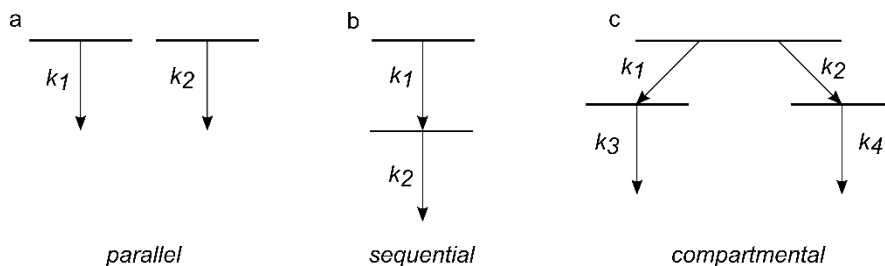
Figure 2-6. Examples of kinetic schemes used for global (a, b) and target (c) analysis.

A *sequential* model refers to the simultaneous fitting of all data sets, where the data are analyzed using a sequential kinetic model, i.e. A→B→C→D…, with an irreversible decay of components into each other. The sequential model enables the extraction of the evolution-associated difference spectra (EADS), which in ideal case represent the true species difference spectra. Although generally EADS estimated by a sequential model represent mixtures of coexisting molecular states, they provide valuable information about the spectral dynamics and time evolution of the whole system.

In order to disentangle the real contributions a more complicated model must be applied such as a *full compartment* model. This model takes into account any possible branching, energy transfer or equilibria between the states. In this case, a target analysis is usually performed, where the target is the proposed de-excitation scheme, including possible spectral assumptions and possibly additional data sets (e.g. from the pump-dump-probe experiments). The resulting spectra are no longer called DADS or EADS but species associated difference spectra (SADS).

Last but not least, the ultrafast spectroscopy data exhibit a wavelength-dependence of time zero (zero delay) due to the group-velocity dispersion of the white light: a phenomenon called "chirp". The data needs to be corrected by a polynomial equation describing the chirp before being global fit. The time resolution of the data is limited by the laser pulse duration, thus a numerical deconvolution of the instrument response function (IRF) is accounted for in the

data analysis as well. The global analysis of the transient absorption data sets presented in the Research Section was implemented using the DAFit software (Pascher Instruments). The target analysis applied in the **Chapter 5** was performed in the Glotaran (Vrije Universiteit Amsterdam).[6]

References

(1)   Lakowicz, J. R. *Principles of Fluorescence Spectroscopy Principles of Fluorescence Spectroscopy*; Springer US, 2006.

(2)   Enriquez, M. M.; Fuciman, M.; Lafountain, A. M.; Wagner, N. L.; Birge, R. R.; Frank, H. A. The Intramolecular Charge Transfer State in Carbonyl-Containing Polyenes and Carotenoids. **2011**, *114* (38), 12416–12426.

(3)   Zigmantas, D.; Polívka, T.; Hiller, R. G.; Yartsev, A.; Sundström, V. Spectroscopic and Dynamic Properties of the Peridinin Lowest Singlet Excited States. *J. Phys. Chem. A* **2001**, *105* (45), 10296–10306.

(4)   Polívka, T.; Sundstrom, V. Ultrafast Dynamics of Carotenoid Excited States-from Solution to Natural and Artificial Systems. *Chem. Rev.* **2004**, *104* (4), 2021–2071.

(5)   Berera, R.; van Grondelle, R.; Kennis, J. T. M. Ultrafast Transient Absorption Spectroscopy: Principles and Application to Photosynthetic Systems. *Photosynth. Res.* **2009**, *101* (2–3), 105–118.

(6)   van Stokkum, I. H. M.; Larsen, D. S.; van Grondelle, R. Global and Target Analysis of Time-Resolved Spectra. *Biochim. Biophys. Acta* **2004**, *1657* (2–3), 82–104.

Research Section

3. Effect of Isomerization on Excited-State Dynamics of Carotenoid Fucoxanthin

This chapter is based on Paper I.:

Abstract

Ultrafast transient absorption spectroscopy and single-wavelength anisotropy measurements were used to study the effect of isomerization on the excited-state properties of fucoxanthin in polar and nonpolar solvents. The excitation wavelengths were 477 nm for all-*trans*-fucoxanthin, and 333 and 477 nm for *cis*-fucoxanthin. All transient absorption spectra of the fucoxanthin isomers in polar solvents show intramolecular charge transfer (ICT) state features, typical for carbonyl carotenoids. Global analysis of the data requires an additional fitting component, originated from the presence of blue and red forms of fucoxanthin in a polar protic solvent. Here we demonstrate that the ICT state decays faster than the S_1 state, due to the significant contribution of the red form to the ICT state dynamics. The isomerization does not affect the S_1 lifetime, but induces a larger difference between the S_1- and ICT-state lifetimes in *cis*-fucoxanthin, which is likely caused by alterations of ICT coupling to either the S_1 or S_0 states; the S^*-state signal is more pronounced for *cis*-isomers in a nonpolar solvent.

3.1. Introduction

Fucoxanthin (Figure 3-1) is an abundant natural pigment belonging to the class of carotenoids, whose chromophore typically consists of a conjugated π-electron chain formed by carbon-carbon double and single bonds that are terminated by various end groups or terminal rings.[1] The characteristic molecular structure of carotenoids results in specific excited-state properties that are characterized by rich relaxation dynamics and the presence of dark states in the carotenoid excited-state manifold.[2–4] The electronic excited states of all carotenoids can be in the first approximation described, in analogy to linear polyenes,[5] by a three-state model consisting of a ground state, S_0, and two excited states denoted by S_1 and S_2.[1,6] On the basis of symmetry consideration originating from linear polyenes, it is expected that the S_0-S_1 transition is forbidden for one-photon processes, whereas the intense absorption that typically occurs in the blue-green spectral region for natural carotenoids is due to the S_0-S_2 transition.[7] Then, upon excitation of the S_2 state, a fast internal conversion (less than a few hundred femtoseconds) occurs to the S_1 state. The S_1-S_0 relaxation then takes place in a picosecond time scale.
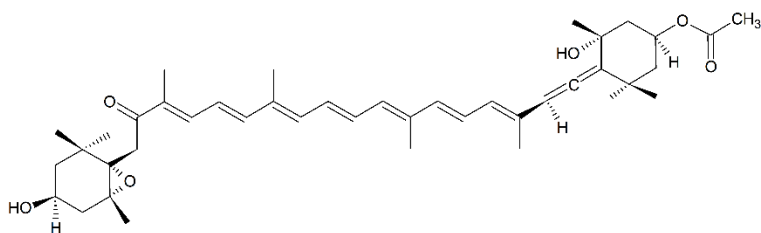

Figure 3-1. Molecular structure of all-*trans*-fucoxanthin.

However, this picture of carotenoid excited states is only a simplified version of the reality because most carotenoids, including fucoxanthin, cannot be

sorted to the C_{2h} symmetry group due to various end groups that break the ideal symmetry of the conjugated backbone.[8] Yet, the S_1 state has not been observed in the absorption spectra of any carotenoid, including those with severely broken symmetry, such as *cis*-isomers. This indicates strongly forbidden S_0-S_1 transitions for all carotenoids regardless of their symmetry; thus, symmetry cannot be the key factor determining the restriction of the S_0-S_1 transition.[8] However, very recently a spectral band associated with the S_1 state was detected in a low-temperature absorption spectrum of a synthetic carotenoid deoxyperidinin, which is a highly substituted molecule containing an allene group and a furanic ring attached to the conjugated backbone.[9] It must also be noted that although the S_0-S_1 transition is, with the exception of deoxyperidinin, dark for all carotenoids, the S_1-S_0 transition, which is detectable through an extremely weak S_1 emission, is somehow correlated to the molecular symmetry of carotenoids.[6,10,11] Further, other dark excited states besides S_1 were identified in the carotenoid excited-state manifold, making it vastly complicated.[12,13] Also, small structural changes that may occur during the relaxation processes following the excitation of the S_2 state were recently proposed to facilitate transitions between the carotenoid excited states,[4,14] underlining the complexity of the excited-state processes in carotenoids and their relation to the carotenoid structure.

Carbonyl carotenoids, such as fucoxanthin, exhibit a typical feature of breaking the ideal symmetry of the chromophore as they always contain a conjugated carbonyl group, which significantly modifies the excited-state properties. Spectroscopic properties of carbonyl carotenoids are dependent on the solvent polarity;[2] when dissolved in a nonpolar solvent, carbonyl carotenoids behave as their noncarbonyl counterparts but increasing the solvent polarity generates significant changes in their excited-state properties.[10,15] These changes are associated with an intramolecular charge transfer (ICT) state that is stabilized in polar solvents.[2,10,16,17] The ICT state is readily identified by its typical excited-state absorption in the 550-700 nm spectral region. It was shown that magnitude of the ICT band in the transient absorption spectrum is correlated with asymmetry of the carbonyl group position. The most intense ICT bands occur when a single

carbonyl group breaks the symmetry of the chromophore, whereas two (or even four[18]) symmetrically positioned carbonyl groups prevent observation of the ICT band.[19,20]

Another process leading to symmetry breaking is isomerization. Many carotenoids readily form various *cis*-isomers, either spontaneously or upon chemical treatment.[21,22] The excited-state properties of *cis*-carotenoids are very similar to those of *trans*-carotenoids; despite the perturbed symmetry, the S_1 state remains dark[8,23,24] and the main absorption band is due to the S_0-S_2 transition. The characteristic spectral feature distinguishing *cis*- and *trans*-carotenoids is the presence of the "*cis*-peak", a pronounced spectral band of *cis*-isomers occurring in the 300-400 nm spectral region. This band results from a transition (usually denoted as S_0-S_3 transition) that is forbidden in all-*trans*-carotenoids, but becomes allowed in *cis*-carotenoids due to the symmetry breaking induced by isomerization.[21,22,24]

Besides this major distinction between *cis*- and all-*trans*-isomers there are a few other differences. First, the S_0-S_2 transition of a *cis*-isomer is shifted to a higher energy,[25,26] and the excited-state absorption bands originating from the S_1 state (the S_1-S_n transition) are broader in *cis*-isomers, indicating larger conformation disorder of *cis*-isomers in the S_1 state. The S_1 lifetime of *cis*-isomers is systematically shorter than that of *trans*-carotenoids, even though the S_1 state energy of the *cis*-carotenoids is 200-500 cm^{-1} higher than that of all-*trans*-isomers,[23,24] breaking the energy gap law that explains the conjugation length dependence of the S_1 lifetime. This clearly points to some changes in coupling between the S_0 and S_1 states induced by isomerization, although the S_0-S_1 transition remains forbidden in both *trans*- and *cis*-isomers.[23,24]

Thus, because isomerization breaks the symmetry of the carotenoid molecule and the ICT state of carbonyl carotenoids is related to the degree of asymmetry induced by the conjugated carbonyl group, we may hypothesize that the spectral markers of the ICT state could be enhanced in *cis*-isomers of carbonyl carotenoids. It is known that a small change in carbonyl carotenoid configuration induced, for example, by specific binding site in a protein can have a significant

effect on the excited-state processes related to the ICT state.[27–29] Yet, effects of isomerization on ICT state have not been studied so far. To test this, fucoxanthin seems to be an ideal candidate. It has a pronounced ICT band in polar solvents, yet the ICT band is clearly separated from the S_1-S_n transition,[16,30] allowing to study the potential effect of isomerization on the ICT state.

Despite the numerous spectroscopic studies on all-*trans*-fucoxanthin,[2,31,32] very little is known about the effect of isomerization on its excited-state properties. Formation of stable fucoxanthin isomers was reported a long time ago by means of iodine-catalyzed isomerization, and these isomers were characterized by steady-state absorption spectroscopy.[33] However, all studies that have been done until now on carotenoid stereoisomers in solution aiming to elucidate details about excited-state dynamics were focused on the noncarbonyl carotenoids;[23,24,34] thus, nothing is known about the effect of isomerization on the ICT state.

Here, we report results of ultrafast transient absorption spectroscopy of *trans-* and *cis-*fucoxanthin in both polar and nonpolar solvents, aiming to reveal isomerization-induced effects on excited-state properties. We show that symmetry breaking induced by isomerization results in clear changes in excited-state properties, yet the magnitude of the ICT band is not markedly affected upon isomerization.

3.2. Materials and Methods

3.2.1. Sample Preparation.

A mixture of fucoxanthin isomers was purchased in solid form from Sigma-Aldrich. High-performance liquid chromatography (HPLC) was applied for separation of carotenoid stereoisomers. (HPLC chromatograms are shown in Figure S3-1, in the Supporting Information.) Fucoxanthin was dissolved in methanol and diluted to the acceptable optical density at the absorption maximum before injection into a Millipore Waters 600 high-performance liquid

chromatograph with Eclipse XDB-C18 column (9.4 mm x 250 mm, 5 µm; Agilent). The mobile phase solvent A consisted of methanol/acetonitrile/water (50/25/25, v/v/v), whereas solvent B was methanol, and solvent C consisted of methanol/n-hexane (4/1, v/v). The flow rate was 4 mL/min. The injection volume was 100 µl. Characteristic elution times were 9.8 min for all-trans-fucoxanthin and 11 min for cis-fucoxanthin. The fractions of both isomers were collected, dried, and stored at -20ºC before use. The cis-fucoxanthin, which constitutes only 3% of the total fucoxanthin in the starting material (Figure S3-1), likely corresponds to a mixture of more than one isomer, and the identification of possible isomeric structures, on the basis of spectroscopic and quantum chemical analysis, is described in Section 3-4.

3.2.2. Steady-State Absorption and Ultrafast Time-Resolved Spectroscopy.

Absorption spectra were recorded at room temperature in methanol and n-hexane using an Agilent 8453 UV-visible spectrophotometer. The optical density was adjusted to ~0.4-0.5 in a 2 mm path length quartz cuvette at the absorption maximum. The absorption spectra were taken before and after each transient absorption experiment to confirm the integrity of the samples. All measurements were carried out at room temperature.

Broadband transient absorption experiments were performed using a Ti:sapphire amplified laser system (Spectra Physics) operating at a 1 kHz repetition rate, producing ~80 fs pulses centered at 800 nm. The pump beam was tuned by an optical parametric amplifier (TOPAS C, Light Conversion) to excite the lowest vibronic band of the S2 state (480 nm) and/or the cis-peak (330 nm). The excitation power of the pump pulses was about 3-15 x·10^{13} photons per pulse per cm2. The probe beam derived from the white-light continuum in the 420-770 nm spectral window was generated by focusing a fraction of the fundamental beam onto a 2 mm sapphire plate. The proper timing between excitation and probe pulses was achieved by a computer-controlled delay line. The pump and the probe

beams were overlapped on the sample, with their relative polarization set to the magic-angle (54.7º) by a Berek polarization compensator placed in the pump-beam path. The sample was placed in a 2-mm path length quartz cuvette with magnetic stirring. The probe and reference beams were focused on the entrance slit of the spectrograph and then dispersed to the linear diode-array detection system. A global fitting of the transient absorption datasets was carried out using a sequential irreversible scheme (DAFit; Pascher Instruments, Lund, Sweden). The evolution-associated difference spectra (EADS) provide information about the time evolution of the studied system, although not necessarily representing the spectra profiles of the individual excited-state species in complex systems.

3.2.3.   Single-Wavelength Anisotropy Measurements.

The output beam from a Ti:sapphire laser was split into two beams, which were used to pump two tunable optical parametric amplifiers (TOPAS C, Light Conversion), which generated excitation and probe beams. The probe beam was further split into two beams whose mutual polarization was set to perpendicular by a periscope. All three beams were overlapped on the sample, with one of the probe beams being set to parallel and the other to perpendicular polarization, with respect to the pump beam. The polarization of the pump beam was set by a Berek polarization compensator. The necessary conditions[35] to avoid significant deviations of the calculated anisotropy have been complied, such as the combination of the low absorbance of the sample with low power of the pump pulse, together with the pump/probe beam ratio being greater than 3.

3.3.   Results

3.3.1.   Steady-State Absorption Spectra.

The steady-state absorption spectra of all-*trans*- and *cis*-fucoxanthin in *n*-hexane and methanol are shown in Figure 3-2. The S_0-S_2 absorption band of *cis*-

fucoxanthin is blue-shifted compared to that of the all-*trans*-fucoxanthin, due to a decrease in the effective conjugation length resulting from isomerization. The absorption spectra of both fucoxanthin isomers in *n*-hexane are narrower than those in methanol and show three resolved vibronic bands at 476, 448, and 426 nm for all-*trans*-isomer and 471, 444, and 422 nm for *cis*-isomer, which correspond to the 0-0, 0-1, and 0-2 vibrational bands of the S_0-S_2 transition. In methanol, the resolution of the vibrational bands is significantly reduced, which is a general feature of carbonyl carotenoids,[2,10,15,16] and the absorption maxima are at 448 and 442 nm for all-*trans*- and *cis*-fucoxanthin, respectively.
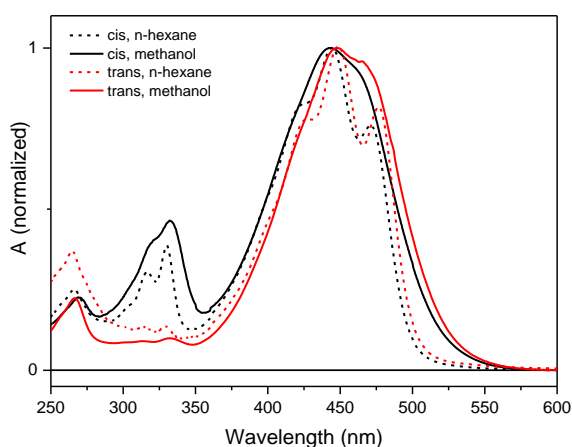

Figure 3-2. Steady-state absorption spectra of *cis*-fucoxanthin (black) and all-*trans*-fucoxanthin (red) in *n*-hexane (dashed lines) and methanol (solid lines) at room temperature. All spectra are normalized to the absorption maximum.

Besides the S_0-S_2 transition that dominates the absorption spectrum of all samples, *cis*-fucoxanthin contains an additional absorption band known as *cis*-peak.[23,24,26,36,37] The *cis*-peak appears in the 300-360 nm spectral region and also exhibits a clear vibronic structure, which is more pronounced in *n*-hexane, mirroring the behavior of the S_0-S_2 transition. The lowest energy band of the *cis*-peak has the largest amplitude and has maximum at 332 nm (methanol) or 330 nm (*n*-hexane). The energy difference between 0-0 and 0-1 vibrational bands of the *cis*-peak is 1300 cm^{-1} in both *n*-hexane and methanol, matching the spacing of the vibrational peaks of the S_2 state. The relative intensity of the *cis*-peak with respect to the maximum of the S_0-S_2 band helps to identify the particular isomer because

it depends on the position of isomerization within the carotenoid molecule.[26,33,38] Here, the *cis*-peak relative intensity yields 30% in *n*-hexane and 34% in methanol.

Table 3-1. Absorption Bands Identified in Various Fucoxanthin Isomers in *n*-Hexane

isomer	S_0-S_2 (λ_{max}, nm)[a]	*cis*-peak[b] (λ_{max}, nm)	D_B/D_{II}[c] (%)	reference
all-*trans*	427,448,476	329	4	this work
	423,448,476	329	8	32
cis	423,444,471	330	30	this work
15-*cis*	418,442,463	327	45	32
13-cis	420,442,467	329	38	32
mixture 13'-cis/9'-cis[d]	422,444,472	329	17	32

[a]The values correspond to the 0-2, 0-1 and 0-0 vibrational bands of the S_0-S_2 transition. [b]*Cis*-peak maximum. [c]Relative intensity of the *cis*-peak calculated as ratio of the cis-peak intensity (D_B) and intensity of the 0-1 band of the S_0-S_2 transition (D_{II}). [d]These two isomers were hardly separable and in *n*-hexane reported only as mixture.

Absorption spectra of both fucoxanthin isomers contain a high-energy band peaking in both solvents at ~266 nm. This band is due to a transition to a higher lying state of B_u^+ symmetry and is typical for all carotenoids.[39] Interestingly, this band in fucoxanthin is essentially "untouched" by polarity. The values of all peaks identified in absorption spectra are listed in the Table 3-1. For comparison, values reported earlier for various fucoxanthin isomers are also shown in the Table 3-1. Molecular structures of fucoxanthin isomers are given in (Figure S3-2).

3.3.2. Transient Absorption.

Transient absorption spectra of both fucoxanthin isomers are shown in Figure 3-3. At 480 nm, all-*trans* fucoxanthin was excited only to the S_2 state, whereas we examined *cis*-fucoxanthin both after excitation to the S_2 state at 480 nm and excitation of the *cis*-peak at 330 nm. The transient absorption spectra depicted in Figure 3-3 are taken at 2 ps after excitation, thus after attaining complete relaxation to the S_1/ICT state.[16,30] Transient absorption spectra at different delay times for all three excitation wavelengths are presented in Figure S3-3.

Transient absorption spectrum of all-*trans*-isomer matches those reported in earlier studies.[16,31] In the nonpolar solvent, *n*-hexane, the narrow peak at 528 nm corresponds to the S_1-S_n excited-state absorption (ESA). Two additional small peaks are visible in the 600-700 nm spectral region, which are characteristic for carbonyl carotenoids. In the polar solvent, methanol, the S_1-S_n peak broadens and shifts to 534 nm, whereas magnitude of the red-shifted peaks grow significantly as compared to that in the data measured in *n*-hexane. These bands, having a maxima at 610 and 650 nm in methanol, are attributed to a transition from the ICT part of the S_1/ICT potential surface and are usually denoted as ICT-S_N transitions.[2,32,40] Note that although the S_1-S_n transition in methanol is red-shifted from that in *n*-hexane, an opposite behavior is observed for the ICT-S_N bands; the reddest and more intense peak is at 654 nm in *n*-hexane, whereas it is at 650 nm in methanol.

The general shape of the transient absorption spectrum of the *cis*-isomer is similar to that of the *trans*-isomer. However, the major difference is in the width of the ESA bands. The S_1-S_n transition of the *cis*-isomer in *n*-hexane is markedly broader, in agreement with earlier studies of isomers of noncarbonyl carotenoids.[23,24] Interestingly, the width of the S_1-S_n transition further increases when *cis*-fucoxanthin is excited at 330 nm into *cis*-peak (Figure 3-3a). There is also a clear difference in the magnitude of a blue shoulder of the S_1-S_n transition (501 nm) that is reminiscent of the S* signal reported for a number of noncarbonyl carotenoids with long conjugations.[12,41] In fucoxanthin, the magnitude of this

shoulder increases bydecreasing the molecular symmetry (it is larger for the *cis*-fucoxanthin), but it increases even more when *cis*-fucoxanthin is excited at 330 nm. The ICT-S_N bands are slightly red-shifted for the *cis*-fucoxanthin. Except for the absence of the blue shoulder of the S_1-S_n transition, differences between *trans*- and *cis*-isomers in methanol mirror those described above for *n*-hexane. The amplitude ratio of the S_1-S_n and ICT-S_N bands in methanol is nearly independent of the fucoxanthin configuration, indicating that isomerization has only a minor effect on the degree of charge transfer character of the S_1/ICT state.

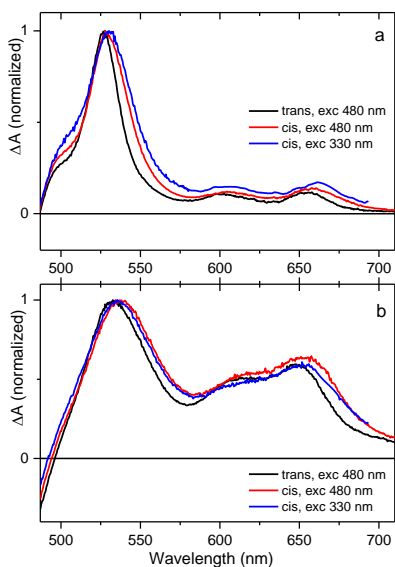Figure 3-3. Transient absorption spectra of fucoxanthin isomers in *n*-hexane (a) and methanol (b). All spectra are measured at 2 ps after excitation at 480 nm *(trans, cis)* or 330 nm *(cis)*. All spectra are normalized to maximum.
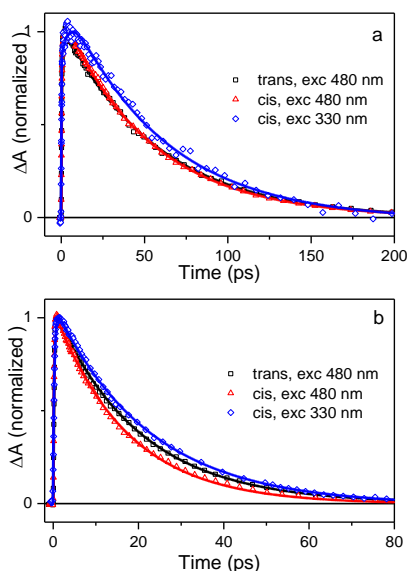
Figure 3-4. Single-kinetic fitting, two panels: (a) normalized S_1-S_n kinetics of all-*trans* and *cis* fucoxanthin in *n*-hexane, (b) normalized S_1-S_n kinetics in methanol.

3.3.3. Excited-State Dynamics.

Basic excited-state dynamics is monitored through kinetics measured at the S_1-S_n maximum shown in Figure 3-4. In *n*-hexane, *trans*- and *cis*-fucoxanthin excited into the lowest vibrational band of the S_2 state at 480 nm exhibit nearly identical dynamics. The kinetic traces obtained after excitation of the *cis*-peak at 330 nm are clearly different, but this difference is caused by a significantly longer vibrational cooling in the S_1 state as evidenced by the global fitting described below. However, in methanol, the S_1 decay is visually different for *cis*- and *trans*-fucoxanthin because the *cis*-isomer excited at 480 nm exhibits a faster S_1 decay than the *trans*-isomer excited at the same wavelengths. Interestingly, the *cis*-isomer excited at 330 nm into the *cis*-peak suggests that the S_1 lifetime is markedly longer than that of *cis*-fucoxanthin excited at 480 nm.

Table 3-2. Summary of time constants obtained from global and single-wavelength fitting.

	Solvent	Fit	τ_1	τ_2	τ_3	τ_x
T480	*n*-hexane	global	100 fs	430 fs	55.2 ps	
	methanol	global	160 fs	270 fs	19.7 ps	12.7 ps
	methanol	probe S_1	50 fs	180 fs	19.9 ps	
	methanol	probe ICT	120 fs	510 fs	18.4 ps	-
C480	*n*-hexane	global	100 fs	560 fs	54.4 ps	
	methanol	global	100 fs	260 fs	19.2 ps	9.5 ps
	methanol	probe S_1	100 fs	140 fs	17 ps	
	methanol	probe ICT	100 fs	220 fs	14.8 ps	-
C330	*n*-hexane	global	280 fs	1.35 ps	57 ps	
	methanol	global	190 fs	1.2 ps	22.2 ps	15.4 ps
	methanol	probe S_1	190 fs	320 fs	22.2 ps	
	methanol	probe ICT	110 fs	300 fs	19.3 ps	

To quantify the differences in the excited-state dynamics shown in Figure 3-4, we have applied a global analysis of the whole spectrotemporal dataset in an attempt to verify the lifetimes extracted from single-kinetic fittings and to obtain a deeper insight into the excited-state dynamics of fucoxanthin isomers. The EADS are shown in Figure S3-4. For fucoxanthin isomers in *n*-hexane we obtained typical spectra of individual excited-state species corresponding to the initially excited S_2 state (~100 fs), to a hot S_1/ICT (0.4-1.4 ps) state and finally the relaxed S_1/ICT state (54-57 ps), with actual lifetimes varying with fucoxanthin configuration and the excitation wavelength (see Table 3-2 for summary of all time constants obtained from global fitting). Although the S_1/ICT lifetimes in the 54-57 ps range are essentially the same, there is a systematical difference in the hot S_1/ICT relaxation time that becomes longer in *cis*-fucoxanthin. Moreover, this relaxation component exhibits a clear excitation-wavelength dependence, as it is about twice as long (1.35 ps) in the *cis*-isomer excited at 330 nm than that in the same molecule excited at 480 nm (560 fs). This difference is also obvious in the rising part of the kinetics shown in Figure 3-4a.

However, in methanol, global fitting analysis of the data recorded for both fucoxanthin isomers failed to generate fits that could be interpreted in the three-state dynamics obtained in *n*-hexane (Figure S3-4). We again obtained EADS corresponding to the three excited-state species described above for fucoxanthin in *n*-hexane, yielding the S_1/ICT state lifetime of fucoxanthin in methanol. These lifetimes are shown in Table 2 and correspond to a depopulation of the initially excited S_2 state (100-150 fs), relaxation of the hot S_1/ICT state that is again significantly longer after 330 nm excitation (0.26-1.2 ps), and decay of the relaxed S_1/ICT state that yields values of 19-22 ps. The significant shortening of the S_1/ICT lifetime in methanol agrees well with previous studies of polarity-dependent excited-state properties of fucoxanthin.[2,10,32] The extracted S_1/ICT lifetime of the *cis*-isomer is longer (22 ps) after a 330 nm excitation compared to that (19 ps) obtained after excitation of the S_2 state, confirming the difference in kinetics shown in Figure 3-4. Also, the much longer relaxation time of the hot S_1/ICT state (1.2 ps) obtained after excitation of the *cis*-peak at 330 nm matches

with the behavior in *n*-hexane, although the amplitude of this component in methanol is much smaller than that in *n*-hexane (Figure S3-4). However, besides these three lifetimes, one extra time component in the 9-15 ps range, having a relaxed S_1/ICT-type spectrum, was needed to obtain satisfactory global fits (Figure S3-4). This component was not reported in any previous studies of fucoxanthin[32,42] and speculation of this discrepancy is discussed in Section 3-4.

3.3.4. Single-Wavelength Anisotropy.

Because isomerization changes the configuration of the fucoxanthin molecule, which may further lead to changes in orientations of the dipole moments of various transitions, we have also applied polarization measurements to measure time-dependent anisotropy which is defined as

$$r(t) = \frac{I_\parallel(t) - I_\perp(t)}{I_\parallel(t) + 2I_\perp(t)}$$

where $I_\parallel(t)$ and $I_\perp(t)$ are the time-dependent signal intensities detected with parallel- and perpendicular-polarized probe beams with respect to the polarization of the excitation beam.[43] To avoid spectral regions with overlapping contributions from various transitions, we have chosen the spectral region of ICT state-stimulated emission in the near-IR region. The ICT state-stimulated emission of fucoxanthin has maximum around 930 nm.[2,30] Such an arrangement can provide information on the mutual orientation of dipole moments of the absorbing (S_0-S_2) and emitting (ICT-S_0) transitions. Kinetic traces measured for parallel and perpendicular polarizations along with calculated time-dependent anisotropy for all-*trans* and *cis*-fucoxanthin, are shown in Figure 3-5. For a randomly oriented sample, the initial anisotropy, probing the same transition that is excited, should be equal to 0.4.[43] The anisotropy decay shown in Fig. 5c indeed has the initial anisotropy close to 0.4, although the precise value is not easy to extract from our data as the kinetic traces cross zero within the first 200 fs (Figure 3-5a,b). The initial anisotropy decreases within ~2 ps to its final values of 0.32 (*cis*) and 0.27 (*trans*) that remain nearly constant within the lifetime of the S_1/ICT state (Figure 3-5c). This final anisotropy (r_{fin}) can be used to calculate angular displacement α

between the dipole moments of the absorbing (S_0-S_2) and emitting (ICT-S_0) transitions:[43]

$$r_{fin} = 0.2(3cos^2\alpha - 1)$$

Using the values for r_{fin} as 0.32 and 0.27 for *cis*- and *trans*-isomer, respectively, gives the angles between the S_0-S_2 and ICT-S_0 transitions of 22 and 28° for *cis*-fucoxanthin and all-*trans*-fucoxanthin, respectively. This shows that isomerization affects the mutual orientation of the transition dipole moments of these two transitions only marginally.
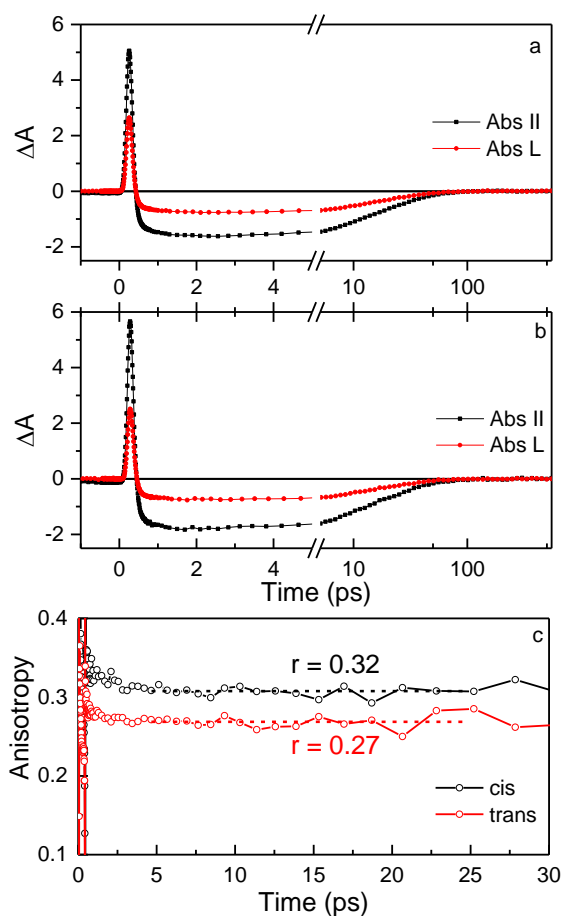

Figure 3-5. Single-wavelength kinetic traces recorded at 925 nm for all-*trans*-fucoxanthin (a) and *cis*-fucoxanthin (b) in methanol. The kinetics were measured for parallel (black) and perpendicular (red) mutual polarization of the excitation and probe beams. (c) Time-dependent anisotropy calculated for all-*trans* (red) and *cis* (black) fucoxanthin.

3.4. Discussion

3.4.1. Identification of the *cis*-Isomer in the Sample.

To identify the type of *cis*-isomer, we use steady-state absorption data measured in *n*-hexane because this solvent preserves the vibrational structure of the S_0-S_2 transition, making determination of the individual peak maxima much easier. If we compare our data with those reported earlier by Haugan et al.[33] (see Table 3-1), it is obvious that our isomer is not the central-*cis*-isomer as both the wavelength of the 0-0 band of the S_2 state and relative intensity of the *cis*-peak do not match the values expected for the central-*cis*-isomer. Spectrally, our *cis*-isomer is closest to the mixture of 13'-*cis*- and 9'-*cis*-isomers, but the relative intensity of the *cis*-peak in our sample (30%) is by far higher than that in Haugan's mixture (17%). All presumed isomers were optimized by ab initio density fumctional theory (DFT) calculations using the B3LYP/def-TZVP level of theory, with the resolution of the identity approximation (RI-J) in Turbomole software. Thus, the optimized minimum energies of isomers increase in the following order all-*trans*<9'-*cis*<13'-*cis*<13-*cis*<9-*cis*<15-*cis*<15'-*cis*. Since the 13'-*cis*- and 9'-*cis*-fucoxanthin-isomers are of higher stability and thermodynamically more favorable due to a relatively small steric hindrance between hydrogen atoms and methyl groups,[21,26,33] we conclude that our sample indeed contains these two isomers. In contrast to Haugan's analysis, our sample is rather dominated by the 13'-*cis*-isomer, resulting in a much larger intensity of the *cis*-peak and slight blueshift of the absorption spectrum in comparison to that in Haugan's mixture (Table 3-1). Comparing the values of the *cis*-peak magnitude in Haugan's and our sample, we can estimate that our sample contains the 13'-*cis*- and 9'-*cis*-isomers in a ~3:2 ratio. Further, even though there are no data for separated 13'-*cis*- and 9'-*cis*-isomers in *n*-hexane, preventing direct comparison with our data, in a solvent mixture used as the eluent in HPLC,[33] the relative intensity of the *cis*-peak is 4.3 times larger for the 13'-*cis*-isomer. This implies that excitation of the *cis*-peak at 330 nm should preferentially excite the 13'-*cis*-isomer, whereas a larger contribution from the 9'-*cis*-isomer is expected after a 480 nm excitation.

We note here that although we cannot precisely determine the structure of the isomers (as could be done, for example, by NMR for which the required quantities are far beyond the amount of material available for this study) our spectroscopic and quantum chemical analyzes presented above provide a reasonable estimation to address the key question of this manuscript – whether the *cis*-configuration and associated symmetry breaking affects the ICT state of fucoxanthin. Even though we can only estimate the structure of *cis*-isomers, it is beyond doubt that we should compare two distinct fucoxanthin configurations: all-*trans*-fucoxanthin that has no *cis*-peak in theabsorption spectra, and *cis*-fucoxanthin whose absorption spectrum contains a distinct *cis*-peak, which is a reliable marker of *cis*-isomers.

3.4.2. Excited-State Dynamics of Fucoxanthin.

Let us first look at the excited-state dynamics of fucoxanthin in methanol in general, without specifying differences between *cis*- and all-*trans*-configuration. Although the excited-state dynamics in *n*-hexane is in agreement with earlier reports[31,32] in methanol, the global fitting reveals an additional 9-15 ps component that was not observed earlier. It must be noted that complete EADS extracted from global fitting of fucoxanthin in methanol have not been reported so far. Yet, indications that three components are not enough to fit the data can be traced in earlier reports from the Hashimoto group, who showed that extra components, albeit with low amplitude, are needed to obtain satisfactory fits.[16]

The reason for this lies in the observation that two forms of fucoxanthin can be found when the molecule is dissolved in methanol: a "blue" form that exhibits weaker coupling between the S_1 and ICT state and a "red" form having a stronger S_1-ICT coupling.[31] The different S_1-ICT coupling, which results in a different degree of the charge transfer character of the S_1/ICT state, leads to slightly different lifetimes of these two forms. In excited-state dynamics, this is manifested as the difference in lifetimes measured in the S_1-S_n band (where the blue form dominates) and that in the ICT-S_N band where the red form has a

significant contribution. This difference was nicely demonstrated in the kinetics recorded at S_1 and ICT bands by Kosumi et al.,[16,42] leading to lifetimes of 18 and 23 ps for the red and blue form, respectively. The same behavior was earlier reported for another carbonyl carotenoid peridinin in methanol, for which the corresponding lifetimes were 4.5 and 10.5 ps.[44] This behavior is exclusive for protic polar solvents such as methanol. In the polar aprotic solvent acetonitrile, which has polarity comparable to that of methanol, no additional lifetimes were required either for peridinin[44] or for fucoxanthin[45].

Thereafter, when global fitting is applied to datasets obtained for both *trans*- and *cis*-fucoxanthin in methanol, the small difference between the blue and red forms cannot be reliably captured, leading to a necessity of the fourth component, marked as τ_x in Table 3-2. To demonstrate this, we compare the kinetics recorded at the S_1-S_n maximum and that at the ICT-S_N peak in Figure 3-6 for both fucoxanthin configurations. Indeed, the kinetics are not identical, which is even better demonstrated by plotting the time-dependence of the magnitude ratios of the S_1-S_n and ICT-S_N bands (Figure 3-6, insets). The ratio increases with time, demonstrating a somewhat faster decay of the ICT band. To quantify this difference, we have fitted individually the kinetics shown in Figure 3-6 and the results are summarized in Table 3-2. For these individual fits, three decay components are enough to obtain a good fit, corroborating our conclusion that the fourth (τ_x) decay component in global fitting is an artifact created by two different lifetimes of the blue and red forms. The single-wavelength fits clearly show that the ICT-state decay is about 3 ps faster than the S_1 decay for the *cis*-isomer. The *trans*-isomer follows this trend, although the difference between S_1 and ICT decays is less than that for the *cis*-isomer.

3.4.3.   Difference in the Excited-State Properties of the Fucoxanthin Isomers.

It was demonstrated for *cis*-isomers of carotenoids that their S_1-state lifetimes are systematically shorter than the S_1-state lifetimes of *trans*-isomers.[23,24,46] However, this trend is not observed here as the S_1/ICT lifetimes of both *trans*- and *cis*-fucoxanthin are very close. When comparing the decay of the S_1-S_n bands, the lifetimes in methanol yield ~20 ps for *trans*-fucoxanthin, 17 ps for *cis*-fucoxanthin excited at 480 nm, and 22 ps for *cis*-fucoxanthin excited at 330 nm. As noted above, at 330 nm we assume preferential excitation of the 13'-*cis*-isomer, which thus has the S_1/ICT lifetime even longer than that of *trans*-fucoxanthin. When comparing the decays of the ICT-like band, the results are the same although the lifetimes are slightly shorter than those extracted from the S_1-S_n decay. The same is observed in *n*-hexane; thus, it is not a polarity-induced effect (Table 3-2).

Because all *cis*-carotenoids studied earlier did not have the conjugated carbonyl group in their structure,[23,24,46] it is tempting to conclude that the conjugated carbonyl of fucoxanthin is the structural feature responsible for the observed absence of shortening of the S_1 lifetime of isomer. However, a closer inspection of earlier reports shows that there is one xanthophyll, neoxanthin, which also exhibits an identical S_1 lifetime for the *trans*- and central-*cis*-isomer.[24] The molecular structure of neoxanthin is actually very similar to that of fucoxanthin, except for the missing conjugated C=O group. The central structural feature shared by neoxanthin and fucoxanthin is the allenic group terminating one side of the conjugated chain, making the conjugated backbone asymmetric. Becasue all other carotenoids that were used to study effects of isomerization on their excited-state properties had fully symmetrical chromophores, we conclude that shortening of the S_1 lifetime in *cis*-isomers occurs only for carotenoids having symmetric conjugated backbones. Deviation from symmetry, caused, for example, by extension of the conjugation to the asymmetric allenic group of neoxanthin or fucoxanthin, will render the S_1 lifetimes of *cis*- and trans-isomers nearly identical. Whether this occurs only for the allenic group or it has general validity, needs to be tested in future studies.

In terms of excited-state dynamics, the major difference between *cis*- and *trans*-fucoxanthin is the mismatch between the decays of the S_1-like and ICT-like bands, which is obvious also from the time-dependent magnitude ratios of these two transitions (Figure 3-6). Although for *trans*-fucoxanthin, the difference obtained by single-wavelength fitting is only about 1.5 ps (20 vs 18.5 ps, Table 3-2), it becomes more than 2 ps for *cis*-fucoxanthin excited at 480 nm (17 vs 14.8 ps) and it further grows even to 3 ps for *cis*-fucoxanthin excited at 330 nm. Because at 330 nm we preferentially excite the 13'-*cis*-fucoxanthin, this shows that isomerization closer to the center of the molecule enhances this effect. The difference in lifetimes measured in the S_1 and ICT bands was first reported by Kosumi et al.[32] and taken as evidence to support that the S_1-like and ICT-like transitions must be due to two separate, although coupled, S_1 and ICT states. This hypothesis was recently proven by pump-dump-probe spectroscopy data reported by Redeckas et al.[30] who unequivocally showed that the populations of the S_1 and ICT states are differently affected by a dump pulse. In a model proposed by Redeckas et al., the difference between the S_1 and ICT lifetimes is determined by the S_1-ICT coupling and by coupling of the S_1 and ICT states to the ground state.[30] The S_1 lifetime obviously remains unaffected by isomerization because it does not change upon isomerization even in *n*-hexane, the large difference between S_1 and ICT lifetimes in *cis*-fucoxanthin must be caused by alterations of ICT coupling to either the S_1 or S_0 states. It is possible that change of orientation of the ICT-S_0 transition dipole moment revealed here by anisotropy measurements may lead to a change in the ICT-S_1 coupling, resulting in the observed larger difference between S_1 and ICT lifetimes of *cis*-fucoxanthin in methanol.

The most intriguing result is the absence of any pronounced isomerization-induced spectral changes in transient absorption spectra taken for both isomers in the polar solvent methanol. Because the magnitude of the ICT band in transient absorption spectra of carbonyl carotenoids in polar solvent was associated with the asymmetry of the molecule,[3,15] we expected an increase of the ICT band magnitude for *cis*-fucoxanthin. Yet, as evidenced by the transient spectra shown in Fig. 3, no such increase was observed. Instead, the only isomerization-induced

effect is the slight increase of width of both the S_1-like and ICT-like bands indicating larger conformation disorders in both S_1 and ICT states for the *cis*-isomer. However, this effect is known for all carotenoid isomers[23,24,46] and has therefore nothing to do with the polarity-induced changes in the excited-state properties of fucoxanthin.

The nearly identical magnitude of the ICT band in transient absorption spectra of *cis*- and all-*trans*-fucoxanthin is especially surprising for 330 nm excitation, which should preferentially excite the 13'-*cis*-isomer (see Figure S3-2 for molecular structure). In contrast to 9'-*cis*-isomer, the 13'-*cis*-isomer introduces significant asymmetry, which should be reflected in magnitude of the ICT band. Becasue this was not observed, it is likely that not asymmetry of the whole molecule, but solely asymmetry of the carbonyl group position is the key factor determining the magnitude of the ICT-band. Thus, in fucoxanthin, the fact that it contains a single conjugated carbonyl group positioned at the end of the conjugated chain determines the magnitude of the ICT-band. Increasing asymmetry of the whole conjugated chain by isomerization has no further effect on the ICT-band magnitude. It should be mentioned here that in a recent study on synthetic β-carotene derivatives containing a lactone ring,[47] the ICT band was not observed at all even though the molecules had the asymmetric single conjugated carbonyl group and the polarity-induced change of the S_1 lifetime was observed.[47] This clearly shows that the relation between the asymmetry of the chromophore and magnitude of the ICT band for carbonyl carotenoids in polar solvents is more complicated than thought previously.

Another important difference between the all-*trans*- and *cis*-fucoxanthin is the amplitude of signal in the 500-520 nm region. This part of the transient absorption spectrum is typically associated with the so-called S* signal whose origin still remains a subject of ongoing discussions.[12,13,48–52] Although it is often observed in carotenoids with long ($N>10$) conjugation length, it has never been reported for fucoxanthin. Yet, comparison of transient absorption spectra in *n*-hexane (Figure 3-3a) reveals a clear increase of the signal amplitude in the characteristic S* region for *cis*-isomer. Moreover, the signal further increases

when *cis*-isomer is excited at 330 nm. Especially, the increase of the signal after high-energy excitation indicates that the signal is indeed due to the S* feature which was shown to gain amplitude after excess energy excitation.[39]

The observation of the increased S* signal in *cis*-isomer of fucoxanthin supports the hypothesis that S* signal is associated with specific carotenoid conformations.[49,53] These conformations are more easily generated for the *cis*-fucoxanthin, and excess energy excitation at 330 nm further increases probability of the formation of these conformers. The transient absorption spectra in Fig. 3a also show a correlation between broadening of the S_1-S_n band toward red and amplitude of the S* signal; the larger the broadening, signaling wider distribution of conformers in the S_1 state, the larger the S* signal. This further supports the "conformation hypothesis" associating the S* signal with specific conformations.
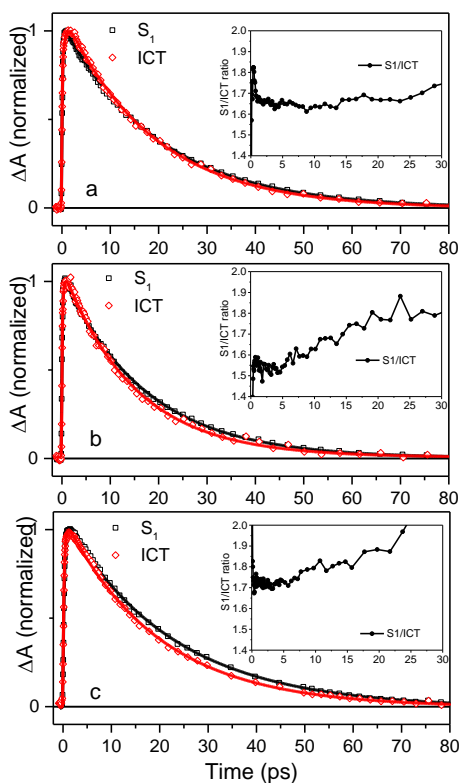

Figure 3-6. Single-kinetic fitting, three panels: normalized S_1-S_n (maximum of S_1-S_n transition), ICT-S_N (650 nm peaks) kinetics in methanol of all-*trans*-fucoxanthin excited at 480 nm (a), *cis*-fucoxanthin excited at 480 nm (b) and 330 nm (c). Inset: S_1/ICT ratio

So far, the S* signal was associated either with a hot ground state[13,52] or with the S_1 state of these conformers. The distinction between these two cases seems to be determined by the conjugation length of the carotenoid. Although for very long conjugated systems ($N>11$) the S* signal likely comes from the hot ground state, for shorter carotenoids ,S_1 state conformations are responsible for the S* signal.[49,54,55] Thus, for fucoxanthin, which has an effective conjugation length of 8.1,[45] the S* signal observed in transient absorption spectra in *n*-hexane is attributed to the S_1 state. This conclusion also matches the correlation between the distribution of the S_1 conformers, manifested as spectral broadening of the S_1-S_n band, and amplitude of the S* signal.

References

(1)   Polívka, T.; Sundstrom, V. Ultrafast Dynamics of Carotenoid Excited States-from Solution to Natural and Artificial Systems. *Chem. Rev.* **2004**, *104* (4), 2021–2071.

(2)   Zigmantas, D.; Hiller, R. G.; Sharples, F. P.; Frank, H. A. ; Sundstrom, V.; Polívka, T. Effect of a Conjugated Carbonyl Group on the Photophysical Properties of Carotenoids. *Phys. Chem. Chem. Phys.* **2004**, *6*, 3009–3016.

(3)   Chábera, P.; Fuciman, M.; Hríbek, P.; Polívka, T. Effect of Carotenoid Structure on Excited-State Dynamics of Carbonyl Carotenoids. *Phys. Chem. Chem. Phys.* **2009**, *11* (39), 8795–8803.

(4)   Beck, W. F.; Bishop, M. M.; Roscioli, J. D.; Ghosh, S.; Frank, H. A. Excited State Conformational Dynamics in Carotenoids: Dark Intermediates and Excitation Energy Transfer. *Arch. Biochem. Biophys.* **2015**, *572*, 175–183.

(5)   Tavan, P.; Schulten, K. Electronic Excitations in Finite and Infinite Polyenes. *Phys. Rev. B: Condens.Matter*, **1987**, *36*, 4337–4358.

(6)   Christensen, R. L. The Electronic States of Carotenoids. In *The Photochemistry of Carotenoids*; Frank, H. A., Young, A. J., Britton, G., Cogdell, R. J., Eds.; Kluwer Academic Publishers: Dordrecht, The Netherlands, **1999**; pp 137–159.

(7)   Britton, G. UV/Visible Spectroscopy. In *Carotenoids: Spectroscopy;* Britton, G., Liaaen, S., Pfander, H., Eds.; Birkhäuser Verlag: Basel, Switzerland, **1995**; Vol. 1B, pp 13–63.

(8)   Fiedor, L.; Heriyanto; Fiedor, J.; Pilch, M. Effects of Molecular Symmetry on the Electronic Transitions in Carotenoids. *J. Phys. Chem. Lett.* **2016**, *7* (10), 1821–1829.

(9)   Greco, J. A.; LaFountain, A. M.; Kinashi, N.; Shinada, T.; Sakaguchi, K.; Katsumura, S.; Magdaong, N. C. M.; Niedzwiedzki, D. M.; Birge, R. R.; Frank, H. A. Spectroscopic Investigation of the Carotenoid Deoxyperidinin: Direct Observation of the Forbidden S_0-S_1 Transition. *J. Phys. Chem. B* **2016**, *120* (10), 2731–2744.

(10)   Frank, H. A.; Bautista, J. A.; Josue, J.; Pendon, Z.; Hiller, R. G.; Sharples, F. P.; Gosztola, D.; Wasielewski, M. R. Effect of the Solvent Environment on the Spectroscopic Properties and Dynamics of the Lowest Excited States of Carotenoids. *J. Phys. Chem. B* **2000**, *104* (18), 4569–4577.

(11)   Mimuro, M.; Nishimura, Y.; Takaichi, S.; Yamano, Y.; Ito, M.; Nagaoka, S.; Yamazaki, I.; Katoh, T.; Nagashima, U. The Effect of Molecular Structure on the Relaxation Processes of Carotenoids Containing a Carbonyl Group. *Chem. Phys. Lett.* **1993**, *213* (5), 576–580.

(12)   Polívka, T.; Sundström, V. Dark Excited States of Carotenoids: Consensus and Controversy. *Chem. Phys. Lett.* **2009**, *477* (1–3), 1–11.

(13)   Balevičius, V. Jr.; Abramavicius, D.; Polívka, T.; Galestian Pour, A.; Hauer, J. A Unified Picture of S* in Carotenoids. *J. Phys. Chem. Lett.* **2016**, *7* (17) , 3347–3352.

(14)   Ghosh, S.; Bishop, M. M.; Roscioli, J. D.; Mueller, J. J.; Shepherd, N. C.; LaFountain, A. M.; Frank, H. A.; Beck, W. F. Femtosecond Heterodyne Transient-Grating Studies of Nonradiative Decay of the S_2 (1 1Bu+) State of β-Carotene: Contributions from Dark Intermediates and Double-Quantum Coherences. *J. Phys. Chem. B* **2015**, *119* (47), 14905–14924.

(15)   Enriquez, M. M.; Fuciman, M.; LaFountain, A. M.; Wagner, N. L.; Birge, R. R.; Frank, H. A. The Intramolecular Charge Transfer State in Carbonyl-Containing Polyenes and Carotenoids. *J. Phys. Chem. B* **2010**, *114* (38), 12416–12426.

(16)   Kosumi, D.; Fujii, R.; Sugisaki, M.; Oka, N.; Iha, M.; Hashimoto, H. Characterization of the Intramolecular Transfer State of Marine Carotenoid Fucoxanthin by Femtosecond Pump-Probe Spectroscopy. *Photosynth. Res.* **2014**, *121* (1), 61–68.

(17)   Ragnoni, E.; Di Donato, M.; Iagatti, A.; Lapini, A.; Righini, R. Mechanism of the Intramolecular Charge Transfer State Formation in All-trans-β-Apo-8′-Carotenal: Influence of Solvent Polarity and Polarizability. *J. Phys. Chem. B* **2015**, *119* (2), 420–432.

(18)   Polívka, T.; Frank, H. A.; Enriquez, M. M.; Niedzwiedzki, D. M.; Liaaen-Jensen, S.; Hemming, J.; Helliwell, J. R.; Helliwell, M. X-Ray Crystal

Structure and Time-Resolved Spectroscopy of the Blue Carotenoid Violerythrin. *J. Phys. Chem. B* **2010**, *114* (26), 8760–8769.

(19)   Enriquez, M. M.; Fuciman, M.; Lafountain, A. M.; Wagner, N. L.; Birge, R. R.; Frank, H. A. The Intramolecular Charge Transfer State in Carbonyl-Containing Polyenes and Carotenoids. *J. Phys. Chem. B* **2010**, *114* (38), 12416–12426.

(20)   Chábera, P.; Fuciman, M.; Razi Naqvi, K.; Polívka, T. Ultrafast Dynamics of Hydrophilic Carbonyl Carotenoids – Relation between Structure and Excited-State Properties in Polar Solvents. *Chem. Phys.* **2010**, *373* (1–2), 56–64.

(21)   Zechmeister, L. *Cis-Trans Isomeric Carotenoids, Vitamins A and Arylpolyenes*; Springer-Verlag: Vienna, 1962.

(22)   Andersson, P. O.; Takaichi, S.; Cogdell, R. J.; Gillbro, T. Photophysical Characterization of Natural Cis-Carotenoids. *Photochem. Photobiol.* **2001**, *74* (4), 549–557.

(23)   Niedzwiedzki, D. M.; Sandberg, D. J.; Cong, H.; Sandberg, M. N.; Gibson, G. N.; Birge, R. R.; Frank, H. A. Ultrafast Time-Resolved Absorption Spectroscopy of Geometric Isomers of Carotenoids. *Chem. Phys.* **2009**, *357* (1–3), 4–16.

(24)   Niedzwiedzki, D. M.; Enriquez, M. M.; Lafountain, A. M.; Frank, H. A. Ultrafast Time-Resolved Absorption Spectroscopy of Geometric Isomers of Xanthophylls. *Chem. Phys.* **2010**, *373* (1–2), 80–89.

(25)   Hashimoto, H.; Miki, Y.; Kuki, M.; Shimamura, T.; Utsumi, H.; Koyama, Y. Isolation by High-Pressure Liquid Chromatography of the Cis-Trans Isomers of .beta.-Apo-8'-carotenal. Determination of Their S_0-State Configurations by NMR Spectroscopy and Prediction of Their S_1- and T_1-State Configurations by Transient Raman Spectroscopy. *J. Am. Chem. Soc.* **1993**, *115* (20), 9216–9225.

(26)   Crupi, P.; Toci, A. T.; Mangini, S.; Wrubl, F.; Rodolfi, L.; Tredici, M. R.; Coletta, A.; Antonacci, D. Determination of Fucoxanthin Isomers in Microalgae (Isochrysis Sp.) by High-Performance Liquid Chromatography Coupled with Diode-Array Detector Multistage Mass Spectrometry Coupled with Positive Electrospray Ionization. *Rapid Commun. Mass Spectrom.* **2013**, *27* (9),

1027–1035.

(27)   Enriquez, M. M.; Hananoki, S.; Hasegawa, S.; Kajikawa, T.; Katsumura, S.; Wagner, N. L.; Birge, R. R.; Frank, H. A. Effect of Molecular Symmetry on the Spectra and Dynamics of the Intramolecular Charge Transfer (ICT) State of Peridinin. *J. Phys. Chem. B* **2012**, *116* (35), 10748–10756.

(28)   Šlouf, V.; Chábera, P.; Olsen, J. D.; Martin, E. C.; Qian, P.; Hunter, C. N.; Polívka, T. Photoprotection in a Purple Phototrophic Bacterium Mediated by Oxygen-Dependent Alteration of Carotenoid Excited-State Properties. *Proc. Natl. Acad. Sci. U.S.A.* **2012**, *109* (22), 8570–8575.

(29)   Šlouf, V.; Kuznetsova, V.; Fuciman, M.; de Carbon, C. B.; Wilson, A.; Kirilovsky, D.; Polívka, T. Ultrafast Spectroscopy Tracks Carotenoid Configurations in the Orange and Red Carotenoid Proteins from Cyanobacteria. *Photosynth. Res.* **2017**, *131* (1), 105–117.

(30)   Redeckas, K.; Voiciuk, V.; Vengris, M. Investigation of the S1/ICT Equilibrium in Fucoxanthin by Ultrafast Pump–dump–probe and Femtosecond Stimulated Raman Scattering Spectroscopy. *Photosynth. Res.* **2016**, *128* (2), 169–181.

(31)   Kosumi, D.; Kusumoto, T.; Fujii, R.; Sugisaki, M.; Iinuma, Y.; Oka, N.; Takaesu, Y.; Taira, T.; Iha, M.; Frank, H. A; et al. Ultrafast Excited State Dynamics of Fucoxanthin: Excitation Energy Dependent Intramolecular Charge Transfer Dynamics. *Phys. Chem. Chem. Phys.* **2011**, *13* (22), 10762–10770.

(32)   Kosumi, D.; Kusumoto, T.; Fujii, R.; Sugisaki, M.; Iinuma, Y.; Oka, N.; Takaesu, Y.; Taira, T.; Iha, M.; Frank, H. A.; et al. Ultrafast S_1 and ICT State Dynamics of a Marine Carotenoid Probed by Femtosecond One- and Two-Photon Pump-Probe Spectroscopy. *J. Lumin.* **2011**, *131* (3), 515–518.

(33)   Haugan, J. A.; Englert, G.; Glinz, E.; Liaaen-Jensen, S. Structural Assignments of Geometrical Isomers of Fucoxanthin. *Acta Chem. Scand.* **1992**, *46*, 389–395.

(34)   Wirtz, A. C.; van Hemert, M. C.; Lugtenburg, J.; Frank, H. A.; Groenen, E. J. J. Two Stereoisomers of Spheroidene in the Rhodobacter sphaeroides R26 Reaction Center: A DFT Analysis of Resonance Raman Spectra. *Biophys. J.* **2007**, *93* (3), 981–991.

(35)   van Wilderen, L. J. G. W.; Lincoln, C. N.; van Thor, J. J. Modelling Multi-Pulse Population Dynamics from Ultrafast Spectroscopy. *PLoS One* **2011**, *6* (3).

(36)   Koyama, Y.; Takatsuka, I.; Kanaji, M.; Tomimoto, K.; Kito, M.; Shimamura, T.; Yamashita, J.; Saiki, K.; Tsukida, K. Configurations Of Carotenoids in the Reaction Center and the Light-Harvesting Complex of Rhodospirillum rubrum. Natural Selection of Carotenoid Configurations by Pigment Protein Complexes. *Photochem. Photobiol.* **1990**, *51* (1), 119–128.

(37)   Koyama, Y.; Kanaji, M.; Shimamura, T. Configurations of Neurosporene Isomers Isolated from the Reaction Center and the Light-Harvesting Complex of Rhodobacter Spheroides G1C. a Resonance Raman, Electronic Absorption, and 1H-NMR Study. *Photochem. Photobiol.* **1988**, *48* (1), 107–114.

(38)   Koyama, Y.; Fujii, R. Cis-Trans Carotenoids in Photosynthesis: Configurations, Excited-State Properties and Physiological Functions. In *The Photochemistry of Carotenoids*; Frank, H. A., Young, A. J., Britton, G., Gogdell, R. J., Eds.; Kluwer Academic Publishers: Dordrecht, The Netherlands, **1999**; pp 161–188.

(39)   Billsten, H. H.; Pan, J.; Sinha, S.; Pascher, T.; Sundstrom, V.; Polívka, T. Excited-State Processes in the Carotenoid Zeaxanthin after Excess Energy Excitation. *J. Phys. Chem. A* **2005**, *109* (31), 6852–6859.

(40)   Wagner, N. L.; Greco, J. A.; Enriquez, M. M.; Frank, H. A.; Birge, R. R. The Nature of the Intramolecular Charge Transfer State in Peridinin. *Biophys. J.* **2013**, *104* (6), 1314–1325.

(41)   Niedzwiedzki, D.; Koscielecki, J. F.; Cong, H.; Sullivan, J. O.; Gibson, G. N.; Birge, R. R.; Frank, H. A. Ultrafast Dynamics and Excited State Spectra of Open-Chain Carotenoids at Room and Low Temperatures. *J. Phys. Chem. B* **2007**, *111* (21), 5984–5998.

(42)   Kosumi, D.; Kusumoto, T.; Fujii, R.; Sugisaki, M.; Iinuma, Y.; Oka, N.; Takaesu, Y.; Taira, T.; Iha, M.; Frank, H. A.; et al. One- and Two-Photon Pump-Probe Optical Spectroscopic Measurements Reveal the S_1 and Intramolecular Charge Transfer States Are Distinct in Fucoxanthin. *Chem. Phys.*

Lett. **2009**, *483* (1–3), 95–100.

(43)   Lakowicz, J. R. *Principles of Fluorescence Spectroscopy Principles of Fluorescence Spectroscopy*; Springer: New York, 2006.

(44)   Zigmantas, D.; Hiller, R. G.; Yartsev, A.; Sundstrom, V.; Polívka, T. Dynamics of Excited States of the Carotenoid Peridinin in Polar Solvents: Dependence on Excitation Wavelength, Viscosity, and Temperature. *J. Phys. Chem. B* **2003**, *107*, 5339–5348.

(45)   Keşan, G.; Durchan, M.; Tichý, J.; Minofar, B.; Kuznetsova, V.; Fuciman, M.; Šlouf, V.; Parlak, C.; Polívka, T. Different Response of Carbonyl Carotenoids to Solvent Proticity Helps to Estimate Structure of the Unknown Carotenoid from Chromera velia. *J. Phys. Chem. B* **2015**, *119* (39), 12653–12663.

(46)   Bautista, J. A.; Chynwat, V.; Cua, A.; Jansen, F. J.; Lugtenburg, J.; Gosztola, D.; Wasielewski, M. R.; Frank, H. A. The Spectroscopic and Photochemical Properties of Locked-15,15'-cis-Spheroidene in Solution and Incorporated into the Reaction Center of Rhodobacter Sphaeroides R-26.1. *Photosynth. Res.* **1998**, *55* (1), 49–65.

(47)   Kosumi, D.; Kajikawa, T.; Sakaguchi, K.; Katsumura, S.; Hashimoto, H. Excited State Properties of β-Carotene Analogs Incorporating a Lactone Ring. *Phys. Chem. Chem. Phys.* **2017**, *19* (4), 3000–3009.

(48)   Gradinaru, C. C.; Kennis, J. T.; Papagiannakis, E.; van Stokkum, I. H.; Cogdell, R. J.; Fleming, G. R.; Niederman, R. A; van Grondelle, R. An Unusual Pathway of Excitation Energy Deactivation in Carotenoids: Singlet-to-Triplet Conversion on an Ultrafast Timescale in a Photosynthetic Antenna. *Proc. Natl. Acad. Sci. U.S.A.* **2001**, *98* (5), 2364–2369.

(49)   Niedzwiedzki, D. M.; Sullivan, J. O.; Polívka, T.; Birge, R. R.; Frank, H. A. Femtosecond Time-Resolved Transient Absorption Spectroscopy of Xanthophylls. *J. Phys. Chem. B* **2006**, *110* (45), 22872–22885.

(50)   Christensson, N.; Milota, F.; Nemeth, A.; Sperling, J.; Kauffmann, H. F.; Pullerits, T.; Hauer, J. Two-Dimensional Electronic Spectroscopy of β-Carotene. *J. Phys. Chem. B* **2009**, *113* (51), 16409–16419.

(51)   Kloz, M.; Weissenborn, J.; Polívka, T.; Frank, H. A.; Kennis, J. T. M. Spectral Watermarking in Femtosecond Stimulated Raman Spectroscopy:

Resolving the Nature of the Carotenoid S* State. *Phys. Chem. Chem. Phys.* **2016**, *18* (21), 14619–14628.

(52)   Lenzer, T.; Ehlers, F.; Scholz, M.; Oswald, R.; Oum, K. Assignment of Carotene S* State Features to the Vibrationally Hot Ground Electronic State. *Phys. Chem. Chem. Phys.* **2010**, *12* (31), 8832–8839.

(53)   Lukeš, V.; Christensson, N.; Milota, F.; Kauffmann, H. F.; Hauer, J. Electronic Ground State Conformers of β-Carotene and Their Role in Ultrafast Spectroscopy. *Chem. Phys. Lett.* **2011**, *506* (1–3), 122–127.

(54)   Ostroumov, E. E.; Reus, M. G. M. M.; Holzwarth, A. R.; Holzwarth, A. R. On the Nature of the "Dark S*" Excited State of β-Carotene. *J. Phys. Chem. A* **2011**, *115* (16), 3698–3712.

(55)   Balevičius, V.; Pour, A. G.; Savolainen, J.; Lincoln, C. N.; Lukes, V.; Riedle, E.; Valkunas, L.; Abramavicius, D.; Hauer, J. J. Vibronic Energy Relaxation Approach Highlighting Deactivation Pathways in Carotenoids. *Phys. Chem. Chem. Phys.* **2015**, *17*, 1166–1169.
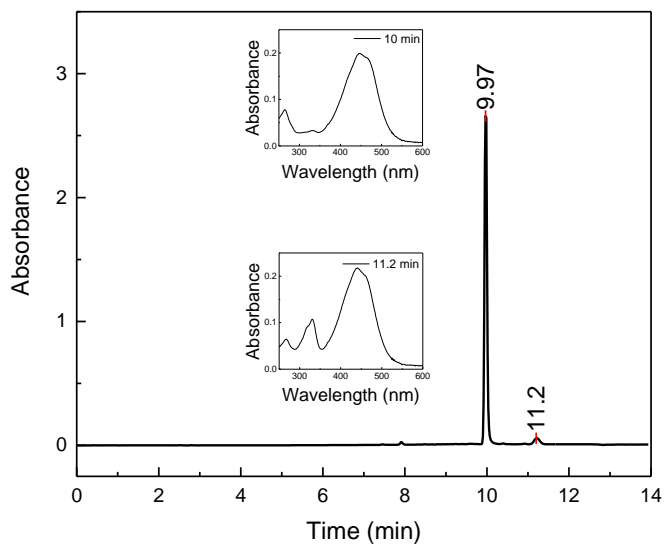
Supporting Information

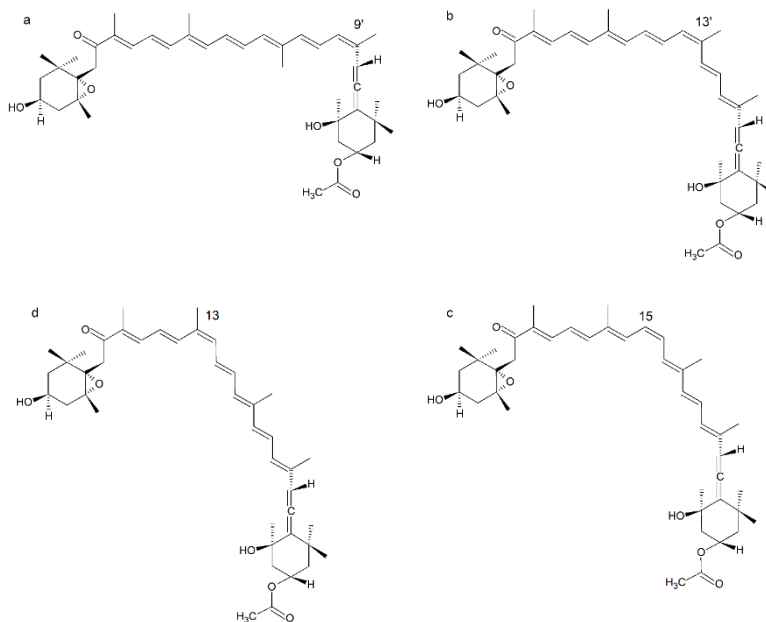Figure S3-1. HPLC profile of fucoxanthin isomers extracted from the sample detected at 440 nm.

Figure S3-2. Molecular structures of fucoxanthin isomers: 9'-*cis* (a), 13'-*cis* (b), 15-*cis* (c), 13-*cis* (d).
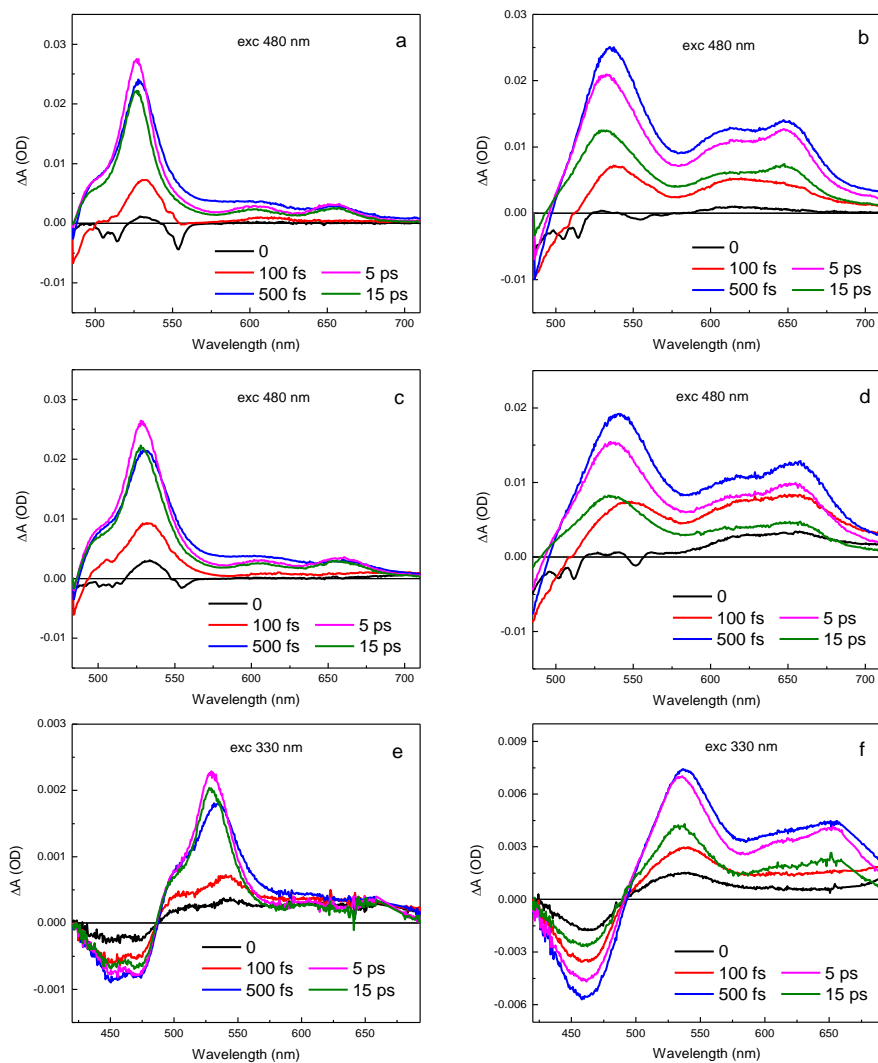
Figure S3-3. Transient absorption spectra of all-*trans* fucoxanthin (a, b) and *cis*-fucoxanthin (c-f) in *n*-hexane (left column) and methanol (right column) at different time delays after excitation. Excitation wavelengths are indicated in each panel.
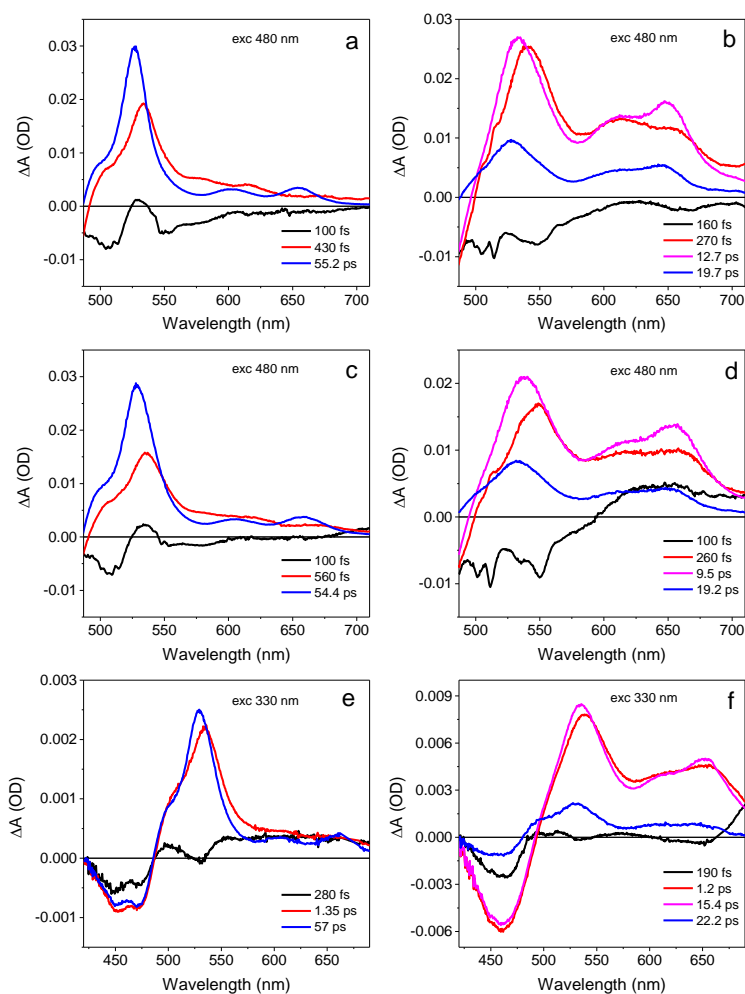
Figure S3-4. EADS obtained from global fitting of all-*trans* fucoxanthin (a,b) and *cis*-fucoxanthin (c-f) in *n*-hexane (left column) and methanol (right column). Excitation wavelengths are indicated in each panel. The first, (black) EADS component is ascribed to a spectrum of the initially-excited S_2 state. The second, (red) EADS represents the non-relaxed, hot S_1/ICT generated by relaxation from the S_2 state, while the blue EADS is due to the relaxed S_1/ICT state. These components are found in both *cis-* and all-*trans*-conformation, though they are generally longer in non-polar solvent. This is especially pronounced for the S_1/ICT state whose lifetime is ~20 ps in methanol and nearly 60 ps in *n*-hexane. The EADS shown in magenta corresponds to the additional 9-12 ps component observed exclusively in methanol.

4. Different Response of Carbonyl Carotenoids to Solvent Proticity Helps to Estimate Structure of the Unknown Carotenoid from *Chromera velia*

Abstract

In order to estimate the possible structure of the unknown carbonyl carotenoid related to isofucoxanthin from Chromera velia denoted as isofucoxanthin-like carotenoid (Ifx-l), we employed steady-state and ultrafast time-resolved spectroscopic techniques to investigate spectroscopic properties of Ifx-l in various solvents. The results were compared with those measured for related carotenoids with known structure, fucoxanthin (Fx) and isofucoxanthin (Ifx). The experimental data were complemented by quantum chemistry calculations and molecular modeling. The data show that Ifx-l must have longer effective conjugation length than Ifx. Yet, the magnitude of polarity-dependent changes in Ifx-l is larger than for Ifx, suggesting significant differences in structure of these two carotenoids. The most interesting spectroscopic feature of Ifx-l is its response to solvent proticity. The transient absorption data show that (1) the magnitude of the ICT-like band of Ifx-l in acetonitrile is larger than in methanol, and (2) the S_1/ICT lifetime of Ifx-l in acetonitrile, 4 ps, is markedly shorter than in methanol (10 ps). This is opposite behavior than for Fx and Ifx whose S_1/ICT lifetimes are always shorter in protic solvent methanol (20 and 13 ps) than in aprotic acetonitrile

(30 and 17 ps). Comparison with other carbonyl carotenoids reported earlier showed that proticity response of Ifx-l is consistent with presence of a conjugated lactone ring. Combining the experimental data and quantum chemistry calculations, we estimated a possible structure of Ifx-l.

4.1. Introduction

Photophysics of carotenoids received much attention during the past few decades. These molecules are essential constituents of many biological systems where they play a number of significant roles ranging from light-harvesting and photoprotection in photosynthetic organisms[1-4] to radical and singlet oxygen scavenging[5,6] in nearly all living organisms. Most of the carotenoid actions in living systems are triggered by light; thus, knowledge of excited-state processes is a key prerequisite to describe their actions on molecular level. Numerous studies of carotenoid photophysics revealed a complex network of excited state pathways involving also dark excited states.[7,8] Basic photophysical properties of carotenoids may be described in a simplified three-level scheme consisting of the ground state (S_0), the lowest excited state S_1 which is a dark state since the S_0-S_1 transition is forbidden by symmetry rules, and the strongly absorbing S_2 state through which the carotenoids acquire their typical color.[7] Energies and lifetimes of the S_1 and S_2 excited states depend on number of conjugated C=C bonds (N).[7,9,10] Both S_1 and S_2 states are involved in photophysical processes such as light-harvesting,[1,7] photoprotection,[11,12] or radical formation[13] in photosynthetic systems.

Though this simple three-level scheme is useful for basic description of excited-state dynamics of carotenoids, it is known that it cannot provide a full description of the light-triggered processes as other dark excited states exist within the S_2-S_1 energy gap.[8,14,15] Whether these additional dark states affect the excited-state dynamics depends on carotenoid structure. There is now solid experimental evidence that for carotenoids with N>10 additional states, usually denoted as B_u^- state and the S* state, are involved in relaxation pathways following the excitation of the S_2 state.[14-16]

Another dark excited state with a charge transfer character, an intramolecular charge transfer (ICT) state exists in an excited-state manifold of a specific family of carotenoids, the carbonyl carotenoids. These carotenoids have in their structure one or more keto (C=O) groups that are in conjugation with the

main C=C conjugated chain. Since the seminal paper describing excited-state dynamics of a member of this carotenoid family, the carotenoid peridinin,[17] it is known that carbonyl carotenoids exhibit polarity-dependent spectroscopic properties. New band(s) induced by the ICT state appear in their transient absorption spectra and their S_1 lifetime, most likely due to a coupling to the ICT state, has a polarity-dependent lifetime. During the past decade, a number of carbonyl carotenoids were studied by time-resolved spectroscopy. Studies of carbonyl carotenoids with one,[17-23] two[24-26] and even four[27] conjugated C=O groups showed that magnitude of the polarity-dependent behavior depends on carotenoid structure. First, the asymmetrically positioned conjugated C=O group greatly enhances the polarity dependence.[25] Second, the shorter the carbonyl carotenoid, the larger the polarity-dependent effect.[20,28-30] Thus, for short carotenoids with asymmetrical conjugated C=O group such as peridinin, the S_1 lifetime changes over nearly two orders of magnitude when switching from nonpolar to polar solvent, while for long carotenoids with symmetrically positioned C=O groups such as astaxanthin essentially no polarity effect is observed.

Recently, a lot of attention was devoted to studies of excited-state dynamics of the carbonyl carotenoid fucoxanthin (Figure 4-1). It is the most abundant carotenoid on earth and is commonly found in photosynthetic marine algae where it serves as efficient light-harvesting pigment.[31] Fucoxanthin (Fx) has seven conjugated C=C bonds terminated by one conjugated C=O group at one side and an allene group at other side. This configuration results in a rather short conjugation length with asymmetrically positioned C=O group, making it a good candidate to study polarity-dependent effects. Indeed, the Fx S_1 lifetime decreases from 60 ps in nonpolar solvent *n*-hexane to about 20 ps in polar solvent methanol. In addition, the spectral band attributable to the ICT state appears in transient absorption spectra in methanol.[18,21,28,32] A series of studies from Hashimoto's group characterized this carotenoid in great detail, showing that 1) the excited-state dynamics is also excitation-wavelength dependent due to large conformational disorder in the ground state in polar solvents;[21,32,33] 2) shortening

of the conjugated chain of Fx enhances the polarity-dependent behavior;[28] 3) an allene group mildly enhances the ICT character of the lowest excited state;[34] 4) the ICT state is possible to excite directly via two-photon excitation.[32]
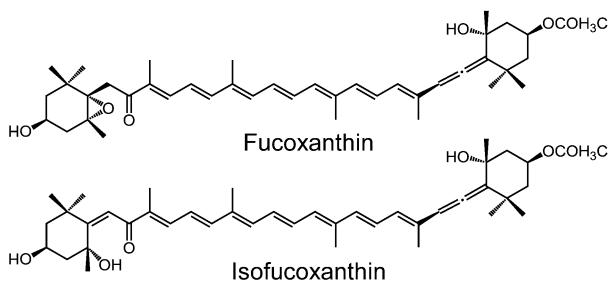

Figure 4-1. Molecular structures of fucoxanthin and isofucoxanthin.

While Fx and even its analogues with varying conjugation lengths[28] were studied in great detail by time-resolved spectroscopy, there are close relatives of this highly-abundant carotenoid that were not studied at all. One such relative is isofucoxanthin (Figure 4-1) which has one extra conjugated C=C bond in the conjugated system. In contrast to Fx, isofucoxanthin (Ifx) has never been identified as a photosynthetic pigment, but it is known as a metabolite of Fx.[35] Ifx was isolated from seaweeds[36] or from egg yolk,[37] though the presence of Ifx was hypothesized to be an isolation artifact formed from Fx during the isolation.[38] Recently, however, pigment analysis of a newly discovered photosynthetic organism, *Chromera velia*, showed that major carotenoid in this organism is a so-far unidentified pigment related to Ifx.[39] Electrospray mass spectrometry in combination with chemical analysis demonstrated that composition ($C_{42}H_{58}O_6$) and chemical properties of the unknown carotenoid resembled those of Ifx. Yet the absorption spectrum in methanol is red-shifted from that of Ifx, indicating longer conjugation length.[39]

This unknown carotenoid was denoted as isofucoxanthin-like (Ifx-l) carotenoid and its basic spectroscopic characterization showed the typical polarity-dependent behavior of carbonyl carotenoids.[40] It is the major carotenoid in the Chromera light harvesting (CLH) protein.[41] The unknown carotenoid transfers energy to Chl-a with nearly 100% efficiency but, in contrast to other light-harvesting complexes with carbonyl carotenoids, optimization of carotenoid-to-chlorophyll energy transfer is achieved in CLH by decreasing the charge transfer character of the S_1/ICT state of Ifx-l upon binding to protein.[40] Here, to explore the spectroscopic properties of Ifx-l in detail, we measured transient absorption spectroscopy data on Ifx-l in a number of solvents with different polarity and compared the data with Fx and Ifx. Combination of spectroscopic data with quantum chemical calculations and classical molecular dynamics (MD) simulations allowed to discern specific spectroscopic properties of Ifx-1 and to estimate possible structure of this unknown carotenoid.

4.2.　　Materials and Methods

4.2.1. Sample Preparation.

Ifx was prepared by treatment of Fx by KOH in methanol according to ref. 35. Fx (0.2 mg, 0.3 μmol, Sigma-Aldrich) was dissolved in 0.05% KOH in methanol (250 μL), molar ratio KOH: Fx = 11. After 40 min in dark at room temperature, ether (ca. 700 μL) and water (ca. 1000 μL) were added. The ether phase was washed with saturated aqueous NaCl solution (ca. 1000 μL) and water (3 x 1000 μL) and dried. The dried sample was resolved in 100% methanol and the mixture of products was separated by high-performance liquid chromatography (HPLC) on a reverse phase. Ifx-l was isolated from *Chromera velia*. Frozen cells of *Chromera velia* were used as a source of Ifx-l. The cells were resuspended with methanol, homogenized in glass homogenizer and broken by 10 cycle circulation in an EmulsiFlex-C5 high pressure cell disrupter (Avestin Inc., Canada) at a pressure of 100-150 MPa, while keeping the apparatus refrigerated

on ice in the dark. Insoluble material was removed by centrifugation for 6 min at 6000g. The methanol extract was then dried. Prepared cell extracts were dissolved in 100% methanol, and the mixture was separated by HPLC on a reverse phase column as described in ref. 41.

The final separation of carotenoids from mixtures was carried on a HPLC system consisting of Pump Controller Delta 600, a PDA 2996 detector (Waters, USA), and a reverse phase Sunfire C8 column (4.6 x 250 mm, 5 µm, silica-based, end-capped, Waters, USA). For the separation on reverse phase a ternary solvent system was used (0-1 min 40% A, 60% B, 11-13 min 100% B, 14 min 100% C; where the solvent A was 50% methanol, 25% acetonitrile and 25% water, B was 100% methanol, and C was 80% methanol and 20% n-hexane). Flow rate was 1 or 2 mLmin^{-1}. All pigment samples were dried in the dark in glass desiccator under vacuum made by a membrane vacuum pump and stored at -20 °C for later use.

4.2.2. Spectroscopy.

Steady-state absorption spectra of the samples were measured by Jasco V-530 spectrophotometer. A femtosecond spectrometer employing an amplified Ti:sapphire laser system as the source of femtosecond pulses (1 kHz, 110 fs, 800 nm) was used for transient absorption measurements. The 800 nm femtosecond pulses were divided into two beams by a beam splitter. Most of the output intensity was used to generate pump pulse to excite sample. Excitation pulses were further modified by an optical parametric amplifier (TOPAS, Light Conversion) to excite the lowest vibrational band of the S_0-S_2 transition. The rest of the split beam was focused to a 2 mm sapphire plate to generate broadband (450-750 nm) white-light probe pulses. Time-resolved absorption changes were measured in a broad spectral range by detecting the dispersed white light by a double-diode array, the time delay between excitation and probe pulses was introduced by a computer-controlled delay line. For each time delay, about 300 spectra were collected and averaged. The full spectrotemporal data set consisted typically of

150-200 time points. Mutual polarization of the excitation and probe beams was set to the magic angle (54.7°). For all measurements, a 2 mm path length quartz cuvette was used. The sample was mixed by a microstirrer to prevent degradation of the sample during the measurements. To keep the excitation intensity at $\sim 10^{14}$ photons pulse^{-1} cm^{-2}, a neutral-density filter was used. All measurements were carried out at room temperature.

The collected data were fitted globally using the software DAFit (Pascher Instruments, Lund, Sweden). To visualize the excited-state dynamics, we assume that the excited states evolves according to a sequential, irreversible scheme, in which the extracted time constants correspond to lifetimes of the individual excited-state species in the sequential scheme. The spectral profile of each species is called the evolution-associated difference spectrum (EADS).

4.2.3. Computational details.

The geometries of the ground states of carotenoids were optimized with standard ground-state density functional theory (DFT)[42] using the Becke3−Lee−Yang−Parr (B3LYP)[42] with the 6-31G(d,p) basis set. Vertical transition energies were calculated by means of time-dependent density functional theory within the Tamm−Dancoff approximation (TD-DFT/TDA)[44] using the hybrid exchange−correlation functional (Cam-B3LYP)[45] with the TZVP[46] basis set which is larger than the commonly used 6-31G(d,p) basis set. Calculations were carried out in the gas phase. All quantum chemical computations were performed by Gaussian09 software package,[47] while Gauss View 5.0.8 was used for visualization of the structures. Classical molecular dynamics (MD) simulations were performed with general AMBER force field (GAFF)[48] with Gromacs package.[49]

4.3.   Results

Absorption spectra of Fx, Ifx and Ifx-l are compared in nonpolar and polar solvent in Figures 4-2a and 4-2b. Diethyl ether was used as a nonpolar solvent due to very low solubility of Ifx in nonpolar solvents. Diethyl ether was the least polar solvent in which we could reach concentrations required for experiments. The vibronic structure of the S_0-S_2 transition is visible in both solvents, though in polar acetonitrile the resolution of vibrational bands is diminished. The preserved vibronic structure even in the polar solvent allows to readily read the energy of the S_2 state, which is given by the 0-0 band of the S_0-S_2 transition. In diethyl ether, the S_2 energies of Fx and Ifx are essentially identical, with the 0-0 band peaking at 470 nm. The 0-0 band of Ifx-l is shifted to ~495 nm, indicating longer conjugation length in comparison with Fx and Ifx. In the polar solvent acetonitrile there is slight difference between absorption maxima of Fx and Ifx. While the 0-0 band of Fx remains unchanged (470 nm) when switching from diethyl ether to acetonitrile, for Ifx the 0-0 band in polar acetonitrile is redshifted to 473 nm. Structure of vibrational bands of Ifx-l is nearly gone in acetonitrile, but it is still possible to determine the position of the 0-0 band at ~495 nm. Thus, no significant shift of the S_2 energy is observed for Ifx-l upon change of solvent polarity.

To study the influence of solvent polarity on spectroscopic properties of Ifx-l in more detail, the carotenoid was dissolved in various other solvents and absorption spectra of these samples are shown Figure 4-2c. Ifx-l exhibits typical polarity-dependent behavior known for a number of other carbonyl carotenoids. Vibrational structure diminishes with increasing polarity and characteristic asymmetric broadening toward longer wavelengths is observed. The S_2 energy remains essentially untouched by solvent polarity, though the vibrational bands broaden with increasing polarity, resulting in the characteristic decrease of resolution of vibrational bands in polar solvents. In tetrahydrofuran (THF), we observe an ~7 nm red-shift of the whole absorption spectrum due to high polarizability of THF. In contrast to other carbonyl carotenoids such as peridinin

or astaxanthin whose absorption spectra in polar solvents are completely featureless,[18,19,26] Ifx-l retains certain resolution of vibrational bands even in the most polar solvents. The observed polarity-dependent behavior is a clear indicator that Ifx-l must contain a conjugated carbonyl group.

Transient absorption spectra of all samples are shown in Figure 4-3. The differences among the three carotenoids and their response to solvent polarity observed in steady-state absorption (Figure 4-2) are further enhanced in transient absorption. The transient absorption spectra were recorded in the visible spectral region, 480-700 nm, where the characteristic features of the S_1/ICT state of carbonyl carotenoids can be monitored. The most prominent feature in all transient spectra is the excited-state absorption band peaking in the 520-560 nm region. This band is attributed to an S_1-S_n transition[7] and is most pronounced in nonpolar solvents. The bands in the 600-700 nm region are much more sensitive to polarity, and they are usually attributed to an ICT-S_n transition.[7,18,19] Since the precise nature of the lowest excited state of carbonyl carotenoids remains unknown and a few hypotheses were proposed,[32,50,51] these two bands are often denoted as S_1-like and ICT-like due to the similarity of the former to the standard S_1-S_n transition of non-carbonyl carotenoids and polarity-dependent behavior of the latter.

While the absorption spectra of Fx and Ifx are nearly identical in diethyl ether (Figure 4-2a), their transient absorption spectra depicted in Figure 4-3a are distinct. The S_1-S_n transition of Fx peaks at 520 nm while it is red-shifted to 525 nm for Ifx. Moreover, the S_1-S_n band of Ifx is slightly broader indicating larger conformation disorder in the S_1/ICT state for Ifx. The small red-shift and broadening is also manifested in the two clearly-pronounced ICT bands which peak at 594 and 643 nm (Fx) and at 600 and 650 nm (Ifx). As for absorption spectra, Ifx-l exhibits significant red shift compared to Fx and Ifx; its S_1-S_n band has maximum at 555 nm, and the ICT bands have their maxima at 630 and 686 nm.
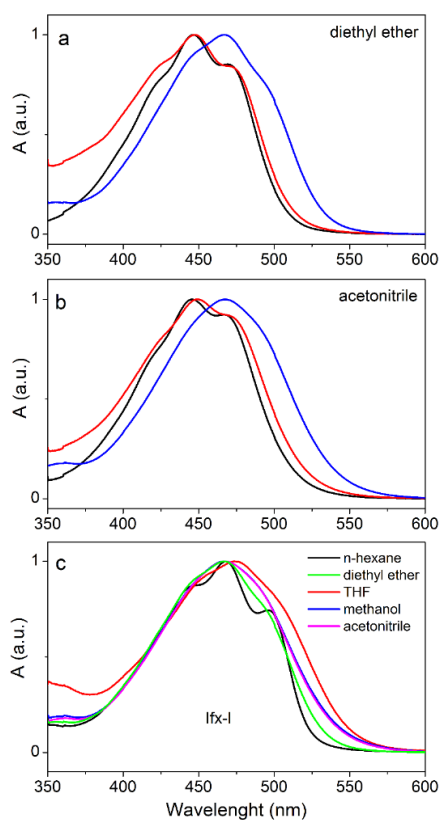
Figure 4-2. Normalized absorption spectra of Fx, Ifx and Ifx-l. (a) Comparison of absorption spectra of Fx (black), Ifx (red) and Ifx-l (blue) in the non-polar solvent diethyl ether. (b) Comparison of absorption spectra of Fx (black), Ifx (red) and Ifx-l (blue) in the polar solvent acetonitrile. (c) Absorption spectra of Ifx-l in various solvents.

In the polar acetonitrile (Figure 4-3b), the S_1-S_n bands of all three carotenoids are broadened and slightly shifted to longer wavelengths with maxima located at 523 nm (Fx), 531 nm (Ifx), and 564 nm (Ifx-l). Increasing polarity led to an increase of the ratio of amplitudes of the S_1-like and ICT-like bands. While in diethyl ether the S_1-like bands dominated the transient spectrum, switching to acetonitrile made the intensities of the ICT-like bands comparable to the S_1-S_n bands. It is known that the ICT-to-S_1 intensity ratio monitors the degree of the

charge transfer character of the S_1/ICT state. For the carbonyl carotenoids with the most pronounced polarity dependence this ratio can be even larger than one.[18-20,29] Thus, transient absorption spectra shown in Figure 4-3b would indicate that the S_1/ICT state exhibits increased charge transfer character according to Fx < Ifx < Ifx-l. For Ifx-l in acetonitrile, the ICT-like band has the same intensity as the S_1-like band, suggesting strong polarity-dependent behavior. This is a rather surprising observation, because it is known that for carbonyl carotenoids with similar structure the degree of charge transfer character of the S_1/ICT state increases with shortening the conjugation length.[28-30] Here, Ifx-l, which must have a longer conjugation length than Fx and Ifx as evidenced by both absorption and transient absorption spectra, exhibits stronger charge transfer character of the S_1/ICT state.

Figure 4-3c compares transient absorption spectra of Ifx-l in a few solvents with different polarity. It is obvious that three polarity-dependent effects can be traced in the figure. First, the S_1-S_n band broadens with increasing polarity, mirroring the polarity effects on the S_0-S_2 transition (Figure 4-2c). Second, the maximum of the S_1-S_n band shifts to longer wavelengths. This results from comparison of S_1-S_n peaks in *n*-hexane and methanol (or acetonitrile) which have comparable polarizability. The peak is shifted from 555 nm (*n*-hexane and diethyl ether) to 565 nm (methanol and acetonitrile). In THF, which has moderate polarity, the S_1-S_n band is shifted even further to 575 nm, but this shift is induced by large polarizability of THF. Third, the magnitude of the ICT bands increases with polarity. While in *n*-hexane no ICT bands are observed, in acetonitrile they have intensity compared to the S_1-like transition. Interestingly, there is a significant increase of ICT band intensity when going from methanol to acetonitrile. Although acetonitrile has slightly larger polarity than methanol (Table 4-1), only mild differences in transient absorption spectra measured in these two solvents were observed for other carbonyl carotenoids such as peridinin or apo-carotenals.[17,18,20]
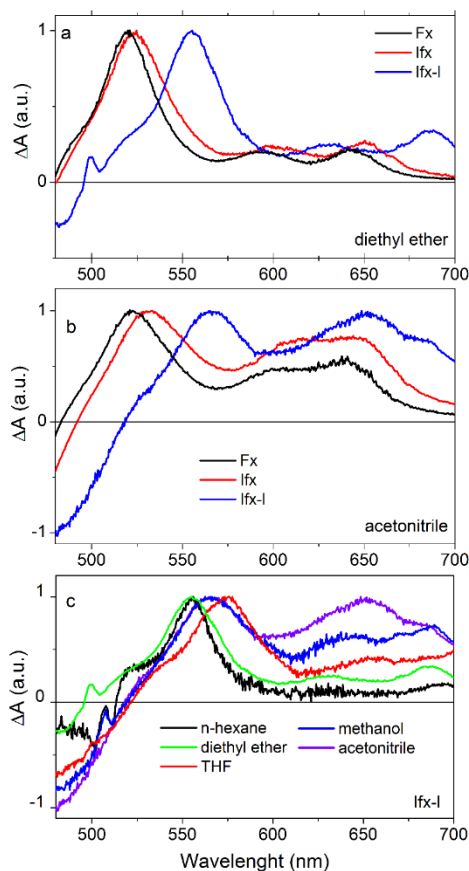
Figure 4-3. Transient absorption spectra of Fx, Ifx and Ifx-l measured 1 ps after excitation at 480 nm (Fx and Ifx) or 510 nm (Ifx-l). Transient absorption spectra of Fx, Ifx, and Ifx-l in diethyl ether (a), and in acetonitrile (b), and transient absorption spectra of Ifx-l in various solvents (c).
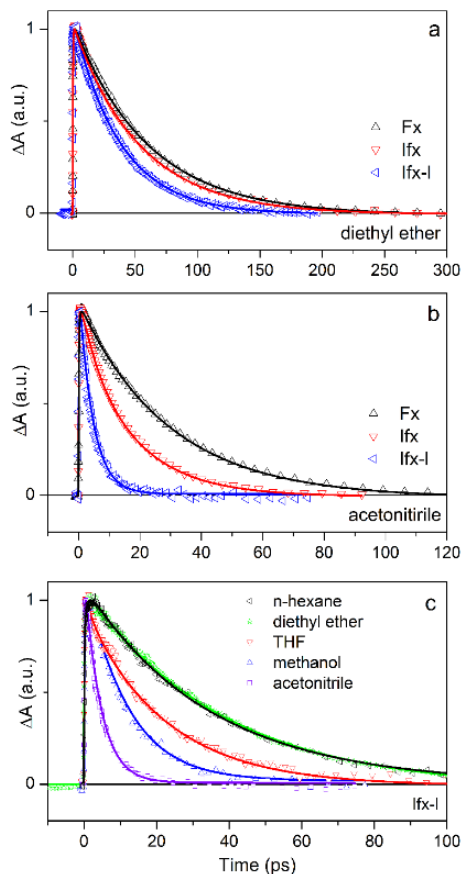
Figure 4-4. Kinetics recorded at the S_1-like maxima of the transient absorption spectra of Fx, Ifx, and Ifx-l. Comparison of kinetics for different carotenoids in diethyl ether (a), acetonitrile (b) and comparison of Ifx-l kinetics in various solvents (c). All kinetics are normalized to maximum, excitation wavelengths were 480 nm (Fx and Ifx) or 510 nm (Ifx-l). Solid lines are fits.

The increased degree of charge transfer character of the S_1/ICT state is usually accompanied by changes in the S_1/ICT lifetime. Figure 4-4 shows kinetics measured at the S_1-S_n maxima of all three carotenoids in various solvents. Since the S_1-like and ICT bands in most cases decay with the same time constant,[18,19,21,29] the kinetics measured at the maximum of the S_1-like band monitors dynamics of the S_1/ICT state, as further evidenced by global fitting (see below). In the nonpolar diethyl ether, the lifetimes of Fx, Ifx and Ifx-l are 60, 53 and 37 ps, respectively. The shortening of the S_1 lifetime in the nonpolar solvent reflects the change of effective conjugation length of the carotenoids, further confirming that while one additional C=C bond of Ifx compared to Fx does not affect much the effective conjugation, Ifx-l must have markedly longer effective conjugation length. As for the magnitude of the ICT bands in transient absorption spectra, the polarity effect on the S_1/ICT lifetime increases in a series Fx < Ifx < Ifx-l. In acetonitrile, the S_1/ICT lifetime is shortened to 29 ps (Fx), 17 ps (Ifx), and even to 4 ps for Ifx-l. Thus, for Ifx-l the S_1/ICT lifetime is shortened by 1 order of magnitude when going from diethyl ether to acetonitrile, further underscoring the large polarity effect on excited-state properties of this carotenoid. Global analysis shown in Figure 4-5 demonstrates that the S_1/ICT lifetimes are the same in the spectral regions associated with S_1-like and ICT-bands. Also, a subpicosecond time component of 0.3-0.5 ps is detected in all data sets. In diethyl ether the spectral shape of this component corresponds to a hot S_1 state and, therefore, reflects vibrational cooling in the S_1 state.[52,53] In polar solvent it rather reflects stabilization of the ICT state as it is pronounced only in the ICT-like band. Figure 4-4c demonstrates the dependence of the S_1/ICT lifetime of Ifx-l on polarity. There is almost no change in the S_1/ICT lifetime between *n*-hexane and diethyl ether, which may justify using the diethyl ether as a nonpolar solvent. With further increase of solvent polarity the S_1/ICT lifetime of Ifx-l decreases to 22 ps in THF, to 11 ps in methanol, and further to 4 ps in acetonitrile. The S_1/ICT lifetimes in various solvents are summarized in Table 4-1.

Table 4-1. S_1/ICT Lifetimes of Ifx-l in Various Solvents.

Solvent	Polarity $P(\varepsilon)^{a}$	S_1/ICT lifetime (ps)
n-hexane	0.229	42
diethyl ether	0.526	37
tetrahydrofuran	0.687	22
2-propanol	0.852	19
acetone	0.868	9
methanol	0.913	11
acetonitrile	0.921	4

a) polarity factor calculated from dielectric constant as $P(\varepsilon) = (\varepsilon-1)/(\varepsilon+2)$

The most surprising observation is the large difference between the S_1/ICT lifetimes of Ifx-l in methanol and acetonitrile. Since earlier studies reported also different S_1/ICT lifetimes of Fx, yielding 18-23 ps in methanol[18,21,28,32,33] and 30-35 ps in acetonitrile,[18,19] we have compared dynamics of all three carotenoids in these two polar solvents. The results are shown in Figure 4-6. Indeed, data confirm the different S_1/ICT lifetimes of Fx in polar, but aprotic, acetonitrile and in both polar and protic methanol. The decay of the S_1/ICT state is markedly slower in acetonitrile, at 29 ps as compared to 19 ps in methanol. Interestingly, this change in the S_1/ICT lifetime is not mirrored in transient absorption spectra measured in methanol and acetonitrile; they are nearly identical. For Ifx, a carotenoid which has not been studied by time-resolved spectroscopy so far, the trend is the same though the difference is smaller than for Fx; the S_1/ICT lifetime is 13 ps in methanol and 17 ps in acetonitrile. Transient absorption spectra have a comparable shape in both solvents, but the spectrum of Ifx in methanol is slightly red-shifted. Finally, for Ifx-l the S_1/ICT lifetime exhibits opposite dependence on solvent proticity, as it is markedly shorter in aprotic acetonitrile (4 ps) than in protic methanol (11 ps). The different response of Ifx-l in these two solvents is underscored by changes in transient absorption spectra. These results show that a solvent's ability to form hydrogen bonds is crucial for determining the excited state properties of Ifx-l in polar solvents. This is further demonstrated by measurements of the S_1/ICT lifetime of Ifx-l in 2-propanol and acetone (Table 4-

1) resulting in lifetimes of 19 and 9 ps, respectively. Thus, even though polarity of methanol is larger than that of acetone, the S_1/ICT lifetime of Ifx-l in acetone (9 ps) is shorter than in methanol (11 ps). Clearly, protic alcohols make the S_1/ICT lifetime longer than aprotic solvents with comparable polarity.
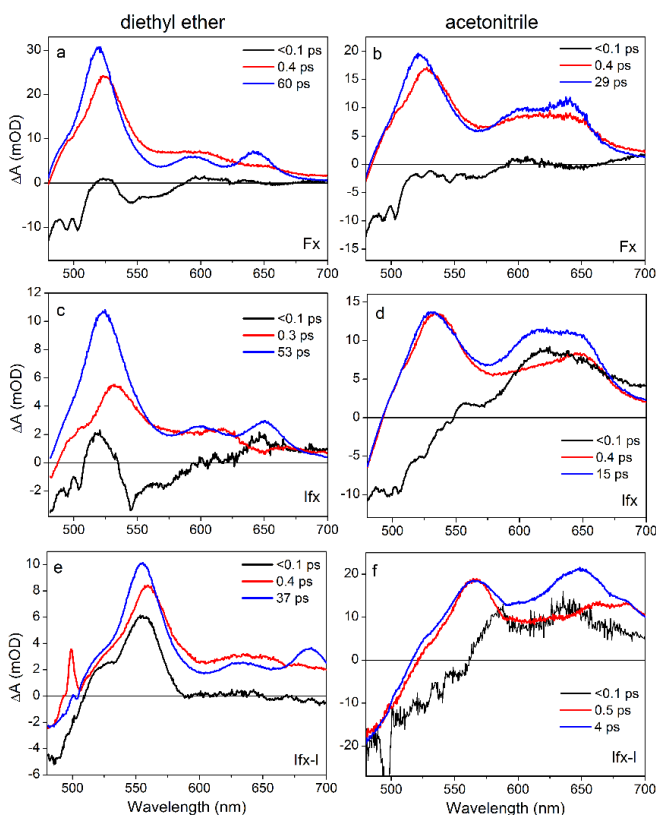

Figure 4-5. . EADS obtained from global fitting the transient absorption data measured for Fx, Ifx, and Ifx-l in diethyl ether (a, c and e) and in acetonitrile (b, d and f).

4.4.   Discussion

Transient absorption data confirm the prediction reported by Moore et al.[39] that Ifx-l must have longer conjugation length than Ifx. Both position of the S_1-S_n band and lifetime of the S_1/ICT state indicate a conjugation length longer than that of Ifx. On the basis of comparison with other carotenoids we may estimate the

effective conjugation length, N_{eff}.[54,55] For carotenoids containing conjugated carbonyl group, the S_2 energy extracted from absorption spectrum is not suitable for determining N_{eff}, because carbonyl carotenoids have usually lower S_2 energy than their non-carbonyl counterparts, and this effect is independent of solvent polarity.[19] Instead, the S_1/ICT lifetime in nonpolar solvent is better parameter to estimate N_{eff} as the behavior of the S_1/ICT state of carbonyl carotenoids in nonpolar solvents is comparable to that of the S_1 state of non-carbonyl carotenoids.[18,19]
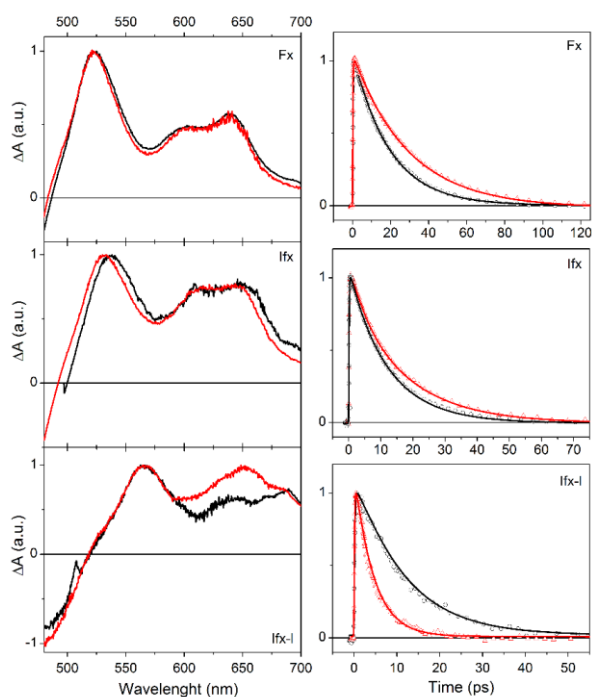

Figure 4-6. Comparison of transient absorption spectra at 1 ps (left column) and kinetics measured at the maximum of the S_1-like transition (right column) for Fx, Ifx and Ifx-l in methanol (black) and acetonitrile (red). All data are normalized to maximum. Solid lines are fits. Excitation wavelength were 480 nm (Fx and Ifx) or 510 nm (Ifx-l).

A comparison of the S_1/ICT lifetimes of Fx, Ifx, and Ifx-l in diethyl ether with known S_1 lifetimes of linear carotenoids is shown in Figure 4-7. It is clear that when the S_1 lifetimes of linear carotenoids are plotted on a logarithmic scale vs. $1/N$, they can be fitted by a linear function. Placing the S_1/ICT lifetimes in nopolar solvents of the carotenoids studied here on this graph results in N_{eff} values of 8.5 for Ifx-l, 8.2 for Ifx, and 8.1 for Fx. N_{eff} values suggest that extension of the

conjugated system of Fx by one extra C=C bond located beyond the conjugated C=O group (Ifx, see Figure 4-1) leaves N_{eff} almost unaffected. This is in line with observation of the essentially identical S_2 energies of Fx and Ifx (Figure 4-2) as well as with the mild difference in energy of the S_1-S_n transition in diethyl ether for these two carotenoids shown in Figure 4-3a. In contrast, there must be structural feature in Ifx-l that extends N_{eff}. Even though our estimation gives the prolongation of N_{eff} by about ~0.5 when going from Fx to Ifx-l, for carotenoids with $N_{eff} < 10$ such seemingly small changes in effective conjugation markedly affect the spectroscopic properties.

All three carotenoids exhibit typical polarity-dependent behavior characteristic of carbonyl carotenoids. Their S_1/ICT lifetimes become shorter in polar solvents and ICT-bands in the 600-700 nm spectral region gain intensity with increasing polarity. The magnitude of the polarity-induced effect is, however, different. The S_1/ICT lifetime of Ifx-l in polar acetonitrile is 4 ps, being the shortest S_1/ICT lifetime in solution reported so far. For most carbonyl carotenoids studied so far, the S_1/ICT lifetime in the most polar solvents converges to values of 8-10 ps,[20,29] independent of their S_1/ICT lifetimes in nonpolar solvent. Moreover, the polarity-induced effects usually diminishes with increase of conjugation length. This is especially obvious when comparing a set of carbonyl carotenoids with identical structure but different conjugation lengths, such as β-apo-carotenals,[20] peridinin[29,30] or Fx[28] analogues. The magnitude of the ICT-like band, which reflects the degree of a charge transfer character of the S_1/ICT state,[18,19,28-30] always increases with decrease of conjugation length for carbonyl carotenoids in solution.

Here, although Ifx-l has the longest conjugation of the carotenoids reported here, it exhibits largest magnitude of the polarity-induced effects. The S_1/ICT lifetime shortens from 40 ps in *n*-hexane to 4 ps in acetonitrile (Figure 4-4c), and the magnitude of the ICT-like band is also the largest (Figure 4-3b). Even in absorption spectra, the loss of vibrational structure of the S_0-S_2 transition in polar solvents, which is another characteristic polarity-induced effect, is most pronounced for Ifx-l (Figure 4-2). This implies that Ifx-l cannot be a longer version

of Ifx. To achieve enhanced response to polarity, Ifx-l must have different structure of the conjugated chain than Fx and Ifx. Since the polarity-dependent behavior is driven by the conjugated carbonyl group, the expected differences in structure most likely involve the conjugated carbonyl group.
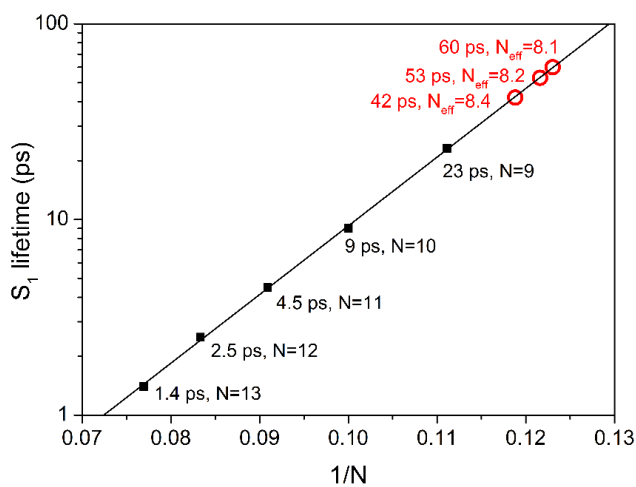

Figure 4-7. Dependence of the S_1 lifetimes on conjugation length. Black symbols denote the S_1 lifetimes of linear carotenoids in *n*-hexane plotted against $1/N$. The solid line is a linear fit to the S_1 lifetimes of linear carotenoids. Red circles show the S_1/ICT lifetimes of fucoxanthin, and isofucoxanthin-like carotenoid in a non-polar solvent. Placing these lifetimes on the black line allows to determine the effective conjugation length, N_{eff}, of these carotenoids. Each point is labeled by a corresponding S_1 (or S_1/ICT) lifetime and N (or N_{eff}).

The qualitative difference between Ifx-l and Ifx (Fx) is further underscored by different response of Ifx-l to solvent proticity. For Fx and Ifx the hydrogen-bonding solvent methanol produces the S_1/ICT lifetime that is shorter than in aprotic solvent acetonitrile, but Ifx-l exhibits opposite response to proticity (Figure 4-6). The S_1/ICT lifetimes in protic methanol and aprotic acetonitrile reported in the literature for various carbonyl carotenoids are summarized in Table 4-2. According to data in Table 4-2, we can divide carbonyl carotenoids into three

groups. The first group contains apo-carotenals, for which the conjugated carbonyl group terminates the conjugated system, which do not exhibit any effect of solvent proticity; the S_1/ICT lifetimes are the same in methanol and acetonitrile regardless the conjugation length. In the second group are Fx, Ifx and uriolide acetate. These carotenoids have their S_1/ICT lifetimes shorter in methanol than in acetonitrile. Moreover, the difference between the S_1/ICT lifetime in protic and aprotic solvent increases with decrease of conjugation length. The carbonyl group of the carotenoids from the second group is also at the end of the conjugated system, but it is positioned in s-cis configuration with respect to the main conjugation (see Figure S4-1, Supporting Information for the structure of uriolide acetate). For Ifx, the conjugated C=O group is not truly at the end of the conjugated system (see Figure 4-1), but the extra C=C bond beyond the carbonyl group has a minimal effect on spectroscopic properties. The third group involves peridinins and Ifx-l. Only these carotenoids have the S_1/ICT lifetime shorter in aprotic acetonitrile. In this group, the difference between the S_1/ICT lifetime in protic and aprotic solvent increases with increasing effective conjugation. The characteristic structural feature in peridinins is the presence of a lactone ring through which the carbonyl group is attached asymmetrically to the main conjugated backbone (Figure S4-1). It must be noted that uriolide acetate, which exhibits opposite response to solvent proticity, has also a lactone ring, but attached in a way that places the carbonyl group at the end of the conjugated system (Figure S4-1). Thus, only if the conjugated carbonyl group at the lactone ring does not terminate the conjugated system, do we observe behavior typical for the third group.

Thus, it is tempting to conclude that Ifx-l contains a lactone ring positioned in a way comparable to that of peridinin. In fact, C39-peridinin (C39P), explored in detail by Niedzwiedzki et al.,[29,30,56] exhibits spectroscopic properties closest to those reported here for Ifx-l. The S_1/ICT lifetimes of C39P are 40, 10 and 6 ps in *n*-hexane, methanol and acetonitrile, respectively, while for Ifx-l these values yield 40, 11 and 4 ps. Moreover, the S_2 energies in *n*-hexane, ~20,000 cm^{-1} (C39P) and 20,200 cm^{-1} (Ifx-l), underscore the spectroscopic similarity of C39P and Ifx-

l. Then, naturally, a question arises: could the unknown carotenoid in *Chromera velia* actually be the C39P? The answer is no for the reasons given below.

Table 4-2. Lifetimes of S_1/ICT States (in picoseconds) for Various Carbonyl Carotenoids in *n*-Hexane, Methanol and Acetonitrile.[a]

carotenoid	*n*-hexane	methanol	acetonitrile	Reference
12'-apo-β-carotenoic acid	200	58	56	23
12'-apo-β-carotenal	200	7	8	**Error! Bookmark not defined.**
8'-apo-β-carotenal	25	8	8	20,51
uriolide acetate	70	26	46	18
fucoxanthin	60	20	30	18,19,21
isofucoxanthin	53	13	17	This work
C35-peridinin	> 1000	12	11	29,30
peridinin	160	10	8	17-19,29,30
C39-peridinin	40	10	6	29,30
isofucoxanthin-like	37	11	4	This work

a) The S_1/ICT lifetimes of peridinin, fucoxanthin, 12'-apo-β-carotenal and 8'-apo-β-carotenal represent mean values obtained from various experiments.

First, there is a difference in maxima of the S_1-S_n bands in *n*-hexane that peak at 540 nm (C39P) and 555 nm (Ifx-l). Second, the detailed mass spectroscopy studies carried out by Moore et al.[39] rule out C39P as a candidate for Ifx-l. The major differences between C39P and Ifx-l are the following. (1) The molecular mass of Ifx-l is 658.42167, corresponding to a composition of $C_{42}H_{58}O_6$ while composition of C39P is $C_{41}H_{52}O_7$; (2) Ifx-l does not contain an epoxy group. On the other hand, it is known that the part of the molecule containing the allene group and the terminal ring attached to the allene is the same for Fx, Ifx, Ifx-l, and C39P.[39]

It is, however, obvious that Ifx-l should share certain structural features with C39P due to their common specific response to solvent proticity. To evaluate

the effect of solvent on local structure of Fx, Ifx, and C39P, molecular dynamics (MD) simulations have been performed. MD simulations of all three carotenoids in methanol and acetonitrile showed that in all cases the carbonyl group is solvated though in the case of methanol long-lived hydrogen bonds appear between the carotenoid C=O group and OH groups of methanol. In order to understand this effect further, we performed *ab initio* DFT calculations with B3LYP/CC-PVDZ level of theory to calculate the interaction energies of C39P-acetonitrile and Fx-acetonitrile complexes (Figure S4-2). Calculated interaction energies are -2.75 kcal/mol for Fx complex and -3.02 kcal/mol for C39P complex. The stability of complexes is achieved through dispersion interaction and nonstandard hydrogen bonding.[57] Such hydrogen bonds were also reported in solutions of acetonitrile with benzene, acetone and dimethyl sulphoxide.[58] Thus, even though the aprotic acetonitrile cannot make standard hydrogen bonds with C=O group, DFT calculations proved the existence of nonstandard hydrogen bonds in acetonitrile. The lifetime and strength of hydrogen bonding between solvent and C=O group can be further influenced by intramolecular interactions. MD simulations showed that in the structure of Ifx there is a potential for intramolecular hydrogen bond between the OH group attached to carbon C1 and the C=O group, which may make the hydrogen bonding between the C=O group and solvent molecules less frequent.

Thus, both experimental data and calculations indicate that the different response of carbonyl carotenoids to solvent proticity is related to presence of a lactone ring. Only carbonyl carotenoids with a lactone ring whose C=O group does not terminate the conjugated system have the S_1/ICT lifetime shorter in acetonitrile than in methanol. DFT calculations indicate that this could be related to stronger nonstandard hydrogen bonds formed between acetonitrile and C=O group located at the lactone ring. Moreover, intramolecular hydrogen bonding may play its role by diminishing formation of hydrogen bonds with methanol as it is in the case of Ifx.

We have used this knowledge to construct a series of hypothetical structures denoted as models 1-5 (Table 4-3). For these molecules, quantum
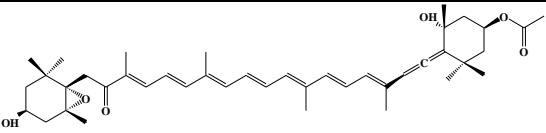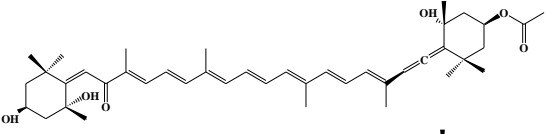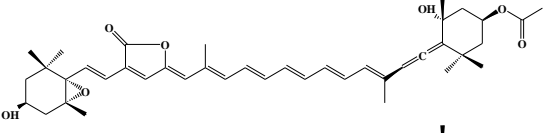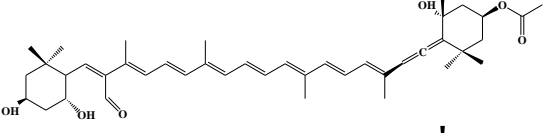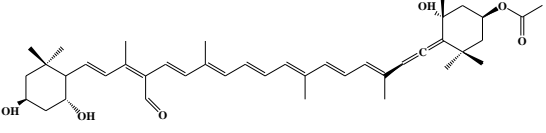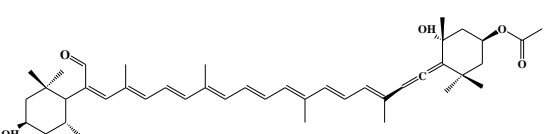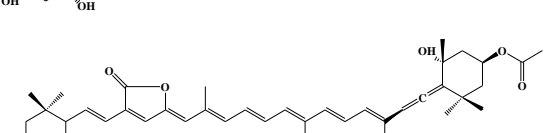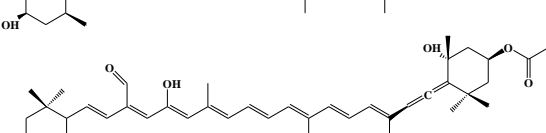
chemical calculations were used to compute the S_2 energy to find out whether it matches the S_2 energy of C39P and Ifx-l. The calculations provide energies of vertical S_0-S_2 transition in a vacuum so they do not reproduce the experimental values, but they can monitor shifts of the S_2 energy induced by changes in structure. To test this, we have calculated the S_2 energies of Fx, Ifx and C39P. The calculations fairly reproduce the nearly identical S_2 energies of Fx and Ifx, confirming that position of the one extra C=C group of Ifx does not significantly prolong the effective conjugation length. The calculated S_2 energy of C39P is downshifted by 1180 cm^{-1} from that of Ifx, which reasonably matches the measured ~900 cm^{-1}.

Models 1 and 2 are just slight modifications of Ifx structure, which is taken as the basis for the structure of Ifx-l.[39] Model 1 retains the possibility of intramolecular hydrogen bond identified in Ifx, but the calculations show that neither model 1 nor model 2 downshifts the S_2 energy and thus cannot be taken as a possible structure of Ifx-l. Model 3, which puts the conjugated carbonyl group at the end of the conjugated system induces the desirable shift of the S_2 energy. Yet, placing the carbonyl group at the end of the conjugation should produce different response to proticity than observed for Ifx-l as evidenced by the data in Table 4-2. Model 4 introduces the lactone ring into the structure and this feature induces the correct shift of the S_2 energy. However, the structure with the lactone ring has an incorrect composition of $C_{42}H_{56}O_6$, so further modifications are needed. Opening the lactone ring (model 5) then gives the correct S_2 energy and correct chemical formula. Attaching the conjugated carbonyl group via one of the methyls is known to generate large polarity-induced effects as evidenced by report on bacteriorubixanthinal;[59] thus, even the structure with opened lactone ring is expected to likely lead to spectroscopic behavior observed here for Ifx-l.

The different response to solvent proticity of Fx, Ifx, and Ifx-l is another interesting feature of carbonyl carotenoids which has not been addressed earlier although the different S_1/ICT lifetimes in methanol and acetonitrile were reported earlier for Fx.[18,19,28] The experimental and theoretical results presented here helped to estimate structure of the unknown carotenoid from CLH complexes of

Chromera velia. The specific response of Ifx-l to solvent proticity, the S_1/ICT lifetime being markedly shorter in polar aprotic solvent than in a protic one, and comparison of data with spectroscopic properties of known carotenoid structures reported earlier showed that a 'hybrid' structure somewhere between Ifx and C39P should be expected for Ifx-l. Final structure elucidation will require detailed NMR or X-ray diffraction studies. So far, the amount of purified Ifx-l was not enough to obtain reliable NMR data, preventing us from determining final structure of Ifx-l.

Table 4-3. Molecular Structures of Fucoxanthin, Isofucoxanthin and C39P together with Five Modelled Structures and their Calculated S_0-S_2 Energies.

molecular structure	name chemical formula	S_0-S_2	
		nm	cm^{-1}
	Fucoxanthin $C_{42}H_{58}O_6$	399	25 062
	Isofucoxanthin $C_{42}H_{58}O_6$	402	24 875
	C_{39} Peridinin $C_{41}H_{52}O_7$	422	23 696
	Model 1 $C_{42}H_{58}O_6$	397	25 188
	Model 2 $C_{42}H_{58}O_6$	396	25 252
	Model 3 $C_{42}H_{58}O_6$	416[a] 413[b]	24 038 24 213
	Model 4 $C_{42}H_{56}O_6$	424	23 585
	Model 5 $C_{42}H_{58}O_6$	423	23 641

[a] cis conformation. [b] trans conformation.

References

(1) Polívka, T.; Frank, H. A. Molecular Factors Controlling Photosynthetic Light-Harvesting by Carotenoids. *Acc. Chem. Res*. **2010**, *43*, 1125–1134.

(2) Croce, R.; van Amerongen, H. Natural Strategies for Photosynthetic Light Harvesting. *Nat. Chem. Biol*. **2014**, *10*, 492-501.

(3) Ruban, A.V.; Johnson, M. P.; Duffy, C. D. P. The Photoprotective Molecular Switch in the Photosystem II Antenna, *Biochim. Biophys. Acta* **2012**, *1817,* 167-181.

(4) Jahns, P.; Holzwarth, A. R. The Role of the Xanthophyll Cycle and of Lutein in Photoprotection of Photosystem II. *Biochim. Biophys. Acta* **2012**, *1817*, 182-193.

(5) Stahl, W.; Sies, H. Antioxidant Activity of Carotenoids. *Molecular Aspects of Medicine,* **2003**, *24*, 345-351.

(6) Edge, R.; Truscott, T. G. Carotenoid Radicals and the Interaction of Carotenoids with Active Oxygen Species. In *The Photochemisry of Carotenoids*; Frank, H. A; Young, A. J; Britton, G.; Cogdell, R. J.; Eds. Kluwer Academic Publishers, Dordrecht 1999, p. 223-234.

(7) Polívka, T.; Sundström, V. Ultrafast Dynamics of Carotenoid Excited States. From Solution to Natural and Artificial Systems. *Chem. Rev*. **2004**, *104*, 2021–2071.

(8) Polívka T.; Sundström, V. Dark Excited States of Carotenoids: Consensus and Controversy. *Chem. Phys. Lett*. **2009**, *477*, 1–11.

(9) Christensen, R. L.; Enriquez, M. M.; Wagner, N. L.; Peacock-Villada, A. Y.; Scriban, C.; Schrock, R. R.; Polívka, T.; Frank, H. A.; Birge, R. R. Energetics and Dynamics of the Low-Lying Electronic States of Constrained Polyenes: Implications for Infinite Polyenes. *J. Phys. Chem. A*. **2013**, *117*, 1449-1465

(10) Christensen, R. L. The Electronic States of Carotenoids. In *The Photochemistry of Carotenoids*; Frank, H. A., Young, A. J., Britton, G., Cogdell, R. J., Eds.; Kluwer Academic Publishers: Dordrecht, The Netherlands, 1999; Vol. 8, pp 137−159.

(11) Ruban, A. V.; Berera, R.; Ilioaia, C.; van Stokkum, I. H. M.; Kennis, J. T. M.; Pascal, A. A.; van Amerongen, H.; Robert, B.; Horton, P.; van Grondelle, R. Identification of a Mechanism of Photoprotective Energy Dissipation in Higher Plants. *Nature,* **2007**, *450*, 575-578.

(12) Staleva, H.; Komenda, J.; Shukla, M. K.; Šlouf, V.; Kaňa, R.; Polívka, T.; Sobotka, R. Mechanism of Photoprotection in the Cyanobacterial Ancestor of Plant Antenna Proteins. *Nat. Chem. Biol*. **2015**, *11*, 287-291.

(13) Polívka,T.; Pullerits,T.; Frank,H.A.; Cogdell,R.J.; Sundström,V. Ultrafast Formation of a Carotenoid Radical in LH2 Antenna Complexes of Purple Bacteria. *J. Phys. Chem. B* **2004**, *108*, 15398- 15407.

(14) Maiuri, M.; Polli, D.; Brida, D.; Luer, L.; LaFountain, A.M.; Fuciman, M.; Cogdell, R.J.; Frank, H.A.; Cerullo, G. Solvent-Dependent Activation of Intermediate Excited States in the Energy Relaxation Pathways of Spheroidene. *Phys. Chem. Chem. Phys*. **2012**, *14*, 6312–6319.

(15) Buckup, T.; Motzkus, M. Multidimensional Time-Resolved Spectroscopy of Vibrational Coherence in Biopolyenes. *Annu. Rev. Phys. Chem*. **2014**, *65*, 39-57.

(16) Balevičius, V.; Pour, A. G.; Savolainen, J.; Lincoln, C. N.; Lukeš, V.; Riedle, E.; Valkunas, L.; Abramavicius, D.; Hauer, J. Vibronic Energy Relaxation Approach Highlighting Deactivation Pathways in Carotenoids. *Phys. Chem. Chem. Phys*. **2015**, *17*, 19491-19499.

(17) Bautista, J. A.; Connors, R. E.; Raju, B. B.; Hiller, R. G.; Sharples, F. P.; Gosztola, D.; Wasielewski, M. R.; Frank, H. A. Excited State Properties of Peridinin: Observation of a Solvent Dependence of the Lowest Excited Singlet State Lifetime and Spectral Behavior Unique Among Carotenoids. *J. Phys. Chem. B* **1999**, *103*, 8751-8758.

(18) Frank, H.A.; Bautista, J.A.; Josue, J.; Pendon, Z.; Hiller, R.G.; Sharples, F.P.; Gosztola, D.; Wasielewski, M.R. Effect of the Solvent Environment on the Spectroscopic Properties and Dynamics of the Lowest Excited States of Carotenoids. *J. Phys. Chem. B* **2000**, *104*, 4569–4577.

(19) Zigmantas, D.; Hiller, R.G.; Sharples, F.P.; Frank, H.A.; Sundström, V.; Polívka, T. Effect of a Conjugated Carbonyl Group on the Photophysical Properties of Carotenoids. *Phys. Chem. Chem. Phys*. **2004**, *6*, 3009–3016.

(20) Kopczynski, M.; Ehlers, F.; Lenzer, T.; Oum, K. Evidence for an Intramolecular Charge Transfer State in 12'-apo-β-caroten-12'-al and 8'-apo-β-caroten-8'-al: Influence of Solvent Polarity and Temperature. *J. Phys. Chem. A* **2007**, *111*, 5370–5381.

(21) Kosumi, D.; Kusumoto, T.; Fujii, R.; Sugisaki, M.; Iinuma, Y.; Oka, N.; Takaesu, Y.; Taira, T.; Iha, M.; Frank, H. A; et al. Ultrafast Excited State Dynamics of Fucoxanthin: Excitation Energy Dependent Intramolecular Charge Transfer Dynamics. *Phys. Chem. Chem. Phys.* **2011**, *13*, 10762–10770.

(22) Di Donato, M.; Ragnoni, E.; Lapini, A. Foggi, P.; Hiller, R. G.; Righini, R. Femtosecond Transient Infrared and Stimulated Raman Spectroscopy Shed Light on the Relaxation Mechanism of Photoexcited Peridinin. *J. Chem. Phys*. **2015**, *142*, 212409.

(23) Stalke, S.; Wild, D. A.; Lenzer, T.; Kopczynski, M.; Lohse, P. W.; Oum, K. Solvent-Dependent Ultrafast Internal Conversion Dynamics of n'-apo-β-carotenoic-n'-acids (n=8, 10, 12). *Phys. Chem. Chem. Phys*. **2008**, *10*, 2180-2188.

(24) Chábera, P.; Fuciman, M.; Hříbek, P.; Polívka, T. Effect of Carotenoid Structure on Excited State Dynamics of Carbonyl Carotenoids. *Phys. Chem. Chem. Phys.* **2009**, *11*, 8795-8803.

(25) Enriquez, M. M.; Fuciman, M.; LaFountain, A. M.; Wagner, N. L.; Birge, R. R.; Frank, H. A. The Intramolecular Charge Transfer State in Carbonyl-Containing Polyenes and Carotenoids. *J. Phys. Chem. B* **2010**, *114*, 12416-12426.

(26) Ilagan, R. P.; Christensen, R. L.; Chapp, T. W.; Gibson, G. N.; Pascher, T.; Polívka, T.; Frank, H. A. Femtosecond Time-Resolved Absorption Spectroscopy of Astaxanthin in Solution and in α-crustacyanin. *J. Phys. Chem. A* **2004**, *109,* 3120-3127.

(27) Polívka, T.; Frank, H. A.; Enriquez, M. M.; Niedzwiedzki, D. M.; Liaaen-Jensen, S.; Hemming, J.; Helliwell, J. R.; Helliwell, M. X-ray Crystal Structure and Time-Resolved Spectroscopy of the Blue Carotenoid Violerythrin. *J. Phys. Chem. B* **2010**, *114*, 8760-8769.

(28) Kosumi, D.; Kajikawa, T.; Okumura, S.; Sugisaki, M.; Sakaguchi, K.; Katsumura, S.; Hashimoto, H. Elucidation and Control of an Intramolecular Charge Transfer Property of Fucoxanthin by a Modification of Its Polyene Chain Length. *J. Phys. Chem. Lett.* **2014**, *5*, 792-797.

(29) Niedzwiedzki, D. M.; Chatterjee, N.; Enriquez, M. M.; Kajikawa, T.; Hasegawa, S.; Katsumura, S.; Frank, H. A. Spectroscopic Investigation of Peridinin Analogues Having Different π-Electron Conjugated Chain Lengths: Exploring the Nature of the Intramolecular Charge Transfer State. *J. Phys. Chem. B* **2009**, *113*, 13604-13612.

(30) Niedzwiedzki, D. M.; Kajikawa, T.; Aoki, K.; Katsumura, S.; Frank, H. A. Excited States Energies and Dynamics of Peridinin Analogues and the Nature of the Intramolecular Charge Transfer State in Carbonyl-Containing Carotenoids. *J. Phys. Chem. B* **2013**, *117,* 6874-6887.

(31) Macpherson, A. N.; Hiller, R. G. Light-Harvesting Systems in Chlorophyll-c Containing Algae. In *Light-Harvesting Antennas in Photosynthesis*; Green, B. R; Parson, W. W; Eds. Kluwer Academic Publishers, Dordrecht 2004, p. 323-352.

(32) Kosumi, D.; Kusumoto, T.; Fujii, R.; Sugisaki, M.; Iinuma, Y.; Oka, N.; Takaesu, Y.; Taira, T.; Iha, M.; Frank, H. A.; Hashimoto, H. One- and Two-Photon Pump-Probe Optical Spectroscopic Measurements Reveal the S1 and Intramolecular Charge Transfer States are Distinct in Fucoxanthin. *Chem. Phys. Lett*. **2009**, *483*, 95-100.

(33) Kosumi, D.; Fujii, R.; Sugisaki, M.; Oka, N.; Iha, M.; Hashimoto, H. Characterization of the Intramolecular Transfer State of Marine Carotenoid Fucoxanthin by Femtosecond Pump-Probe Spectroscopy. *Photosynth. Res*. **2014**, *121*, 61-68.

(34) Kosumi, D.; Kajikawa, T.; Yano, K.; Okumura, S.; Sugisaki, M.; Sakaguchi, K.; Katsumura, S.; Hashimoto, H. Roles of Allene Group in an Intramolecular Charge Transfer Character of a Short Fucoxanthin Homolog as Revealed by Femtosecond Pump-Probe Spectroscopy. *Chem. Phys. Lett*. **2014**, *602*, 75–79.

(35) Haugan, J. A.; Englert, G.; Liaaen-Jensen, S. Alkali Lability of Fucoxanthin − Reactions and Products. *Acta Chem. Scand*. **1992**, *46*, 614-624.

(36) Bonnett, R.; Mallams, A. K.; Spark, A. A.; Tee, J. L.; Weedon, B. C. L., McCormick, A. Carotenoids and Related Compounds. 20. Structure and Reactions of Fucoxanthin. *J. Chem. Soc. C* **1969,** *3*, 429-454.

(37) Jensen, A. Effect of Seaweed Carotenoids on Egg Yolk Coloration. *Poultry Sci*. **1963**, *42*, 912.

(38) Strand, A.; Herstad, O.; Liaaen-Jensen, S. Fucoxanthin Metabolites in Egg Yolks of Laying Hens. *Comp. Biochem. Physiol. A* **1998**, *119*, 963-974.

(39) Moore, R. B.; Oborník, M.; Janouškovec, J.; Chrudimský, T.; Vancová, M.; Green, D. H.; Wright, S. W.; Davies, N. W.; Bolch, C. J. S.; Heimann, K.; et al. A Photosynthetic Alveolate Closely Related to Apicomplexan Parasites. *Nature* **2008**, *451*, 959–963.

(40) Durchan, M.; Keşan, G.; Šlouf, V.; Fuciman, M.; Staleva, H.; Tichý, J.; Litvín, R.; Bína, D.; Vácha, F.; Polívka, T. Highly Efficient Energy Transfer from a Carbonyl Carotenoid to Chlorophyll a in the Main Light Harvesting Complex of Chromera Velia. *Biochim. Biophys. Acta* **2014**, *1837,* 1748–1755.

(41) Tichý, J.; Gardian, Z.; Bína, D.v Koník, P.; Litvín, R.; Herbstová, M.; Pain, A.; Vácha, F. Light Harvesting Complexes of Chromera velia, Photosynthetic Relative of Apicomplexan Parasites. *Biochim. Biophys. Acta* **2013**, *1827*, 723–729.

(42) Kohn, W.; Sham, L. J. Self-Consistent Equations Including Exchange and Correlation Effects. *Phys. Rev.* **1965**, *140*, A1133-A1138.

(43) Becke, A. D. Density-Functional Thermochemistry. III. The Role of Exact Exchange. *J. Chem. Phys*. **1993**, *98*, 5648−5652.

(44) Hirata, S.; Head-Gordon, M. Time-Dependent Density Functional Theory within the Tamm-Dancoff Approximation. *Chem. Phys. Lett*. **1999**, *314*, 291−299.

(45) Yanai, T.; Tew, D. P.; Handy, N. C. A New Hybrid Exchange-Correlation Functional Using the Coulomb-Attenuating Method (CAM-B3LYP). *Chem. Phys. Lett*. **2004**, *393*,51−57.

(46) Schaefer, A.; Huber, C.; Ahlrichs, R. Fully Optimized Contracted Gaussian Basis Sets of Triple Zeta Valence Quality for Atoms Li to Kr. *J. Chem. Phys.* **1994**, *100*, 5829−5853.

(47) Frisch, M. J.; Trucks, G. W.; Schlegel, H. B.; Scuseria, G. E.; Robb, M. A.; Cheeseman, J. R.; Scalmani, G.; Barone, V.; Mennucci, B.; Petersson, G. A.; et al. *Gaussian, 09W*; Gaussian Inc.: Wallingford,CT, 2009.

(48) Wang, J.; Wolf, R. M.; Caldwell, J. W.; Kollman, P. A.; Case, D. A. Development and Testing of a General AMBER Force Field. *J. Comput. Chem.* **2004**, *25*, 1157-1174.

(49) Hess, B.; Kutzner, C.; van der Spoel, D.; Lindahl, E. GROMACS 4: Algorithms for Highly Efficient, Load-Balanced, and Scalable Molecular Simulation. *J. Chem. Theory Comput.* **2008**, *4*, 435-447.

(50) Wagner, N. L.; Greco, J. A.; Enriquez, M. M.; Frank, H. A.; Birge, R. R. The Nature of the Intramolecular Charge Transfer State in Peridinin. *Biophys. J*. **2013**, *104*, 1314-1325.

(51) Durchan, M.; Fuciman, M., Šlouf, V.; Keşan, G.; Polívka, T. Effect of Polarity and Aggregation on Excited-State Dynamics of 8'-apo-β-carotenal. *J. Phys. Chem. A*. **2012**, *116*, 12330−12338.

(52) Billsten, H. H.; Zigmantas, D.; Sundström, V.; Polívka, T. Dynamics of Vibrational Relaxation in the S1 State of Carotenoids Having 11 Conjugated C=C bonds. *Chem. Phys. Lett.* **2002**, *355*, 465-470.

(53) Niedzwiedzki, D.; Koscielecki, J. F.; Cong, H.; Sullivan, J. O.; Gibson, G. N.; Birge, R. R.; Frank, H. A. Ultrafast Dynamics and Excited State Spectra of Open-Chain Carotenoids at Room and Low Temperatures. *J. Phys. Chem. B* **2007**, *111*, 5984- 5998.

(54) Fuciman, M.; Keşan, G.; LaFountain, A.; Frank, H. A., Polívka, T. Tuning the Spectroscopic Properties of Aryl Carotenoids by Slight Changes in Structure. *J. Phys. Chem. B.* **2015**, *119*, 1457–1467.

(55) Mendes-Pinto, M. M.; Sansiaume, E.; Hashimoto, H.; Pascal, A. A.; Gall, A.; Robert, B. Electronic Absorption and Ground State Structure of Carotenoid Molecules. *J. Phys. Chem. B* **2013**, *117*, 11015–11021.

(56) Kajikawa, T.; Hasegawa, S.; Iwashita, T.; Kusumoto, T.; Hashimoto, H.; Niedzwiedzki, D. M.; Frank, H. A.; Katsumura, S. Syntheses of C33-, C35-, and C39-Peridinin and their Spectral Characteristics. *Org. Lett.* **2009**, *11*, 5006-5009.

(57) Zierkiewicz, W.; Michalska, D.; Havlas, Z.; Hobza, P. Study of the Nature of Improper Blue-Shifting Hydrogen Bonding and Standard Hydrogen Bonding in the X3CH-OH2 and XH-OH2 Complexes (X = F, Cl, Br, I): A Correlated ab initio Study. *Chem. Phys. Chem.* **2002**, *3*, 511–518.

(58) Stolov, A. A.; Kamalova, D. I.; Borisover, M. D.; Solomonov, B. N. Hydrogen Bonds Formed by Methyl Groups of Acetonitrile – Infrared and Calorimetric Study. *Spectrochim. Acta A* **1994**, *50*, 145-150.

(59) Šlouf, V.; Fuciman, M.; Dulebo, A.; Kaftan, D.; Koblížek, M.; Frank, H.;A.; Polívka, T. Carotenoid Charge Transfer States and Their Role in Energy Transfer Processes in LH1-RC Complexes from Aerobic Anoxygenic Phototrophs. *J. Phys. Chem. B*. **2013**, *117*, 10987−10999.
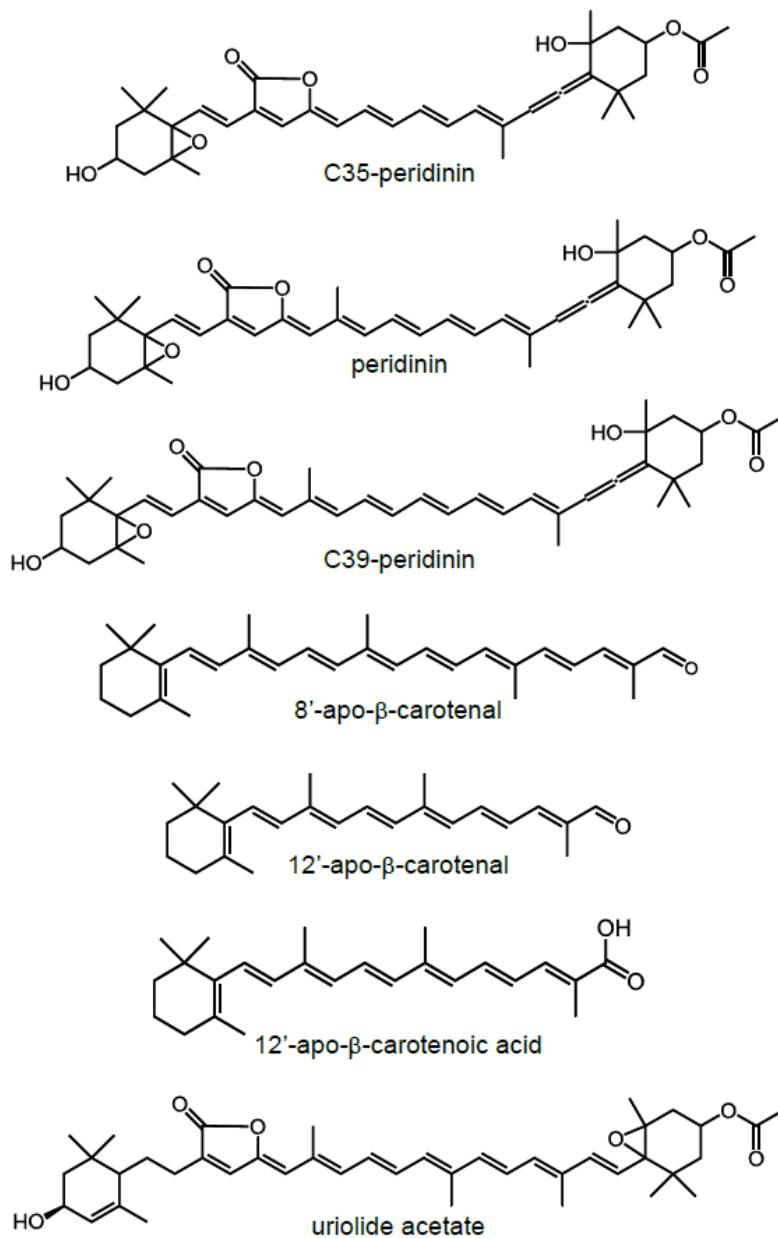
Supporting Information

Figure S4-1. Molecular structures of carbonyl carotenoids discussed in the main text.
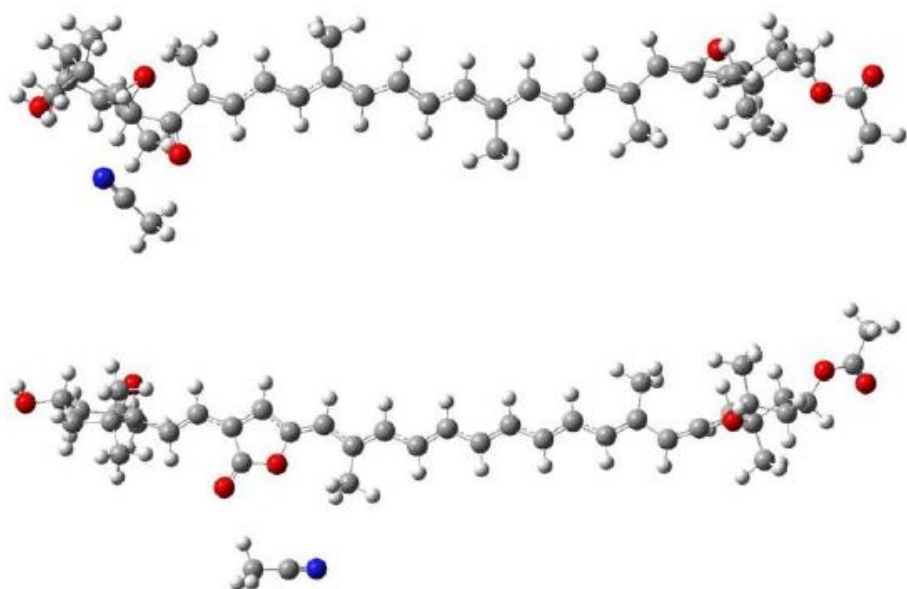
Figure S4-2. Molecular structures of Fx-acetonitrile (top) and C39P-acetonitrile (bottom) complexes. Only the acetonitrile molecule closest to the keto group forming the complex is shown.

5. Spectroscopic properties of the S_1 state of linear carotenoids after excess energy excitation

This chapter is based on Paper III.:

Abstract

Properties of the S_1 state of neurosporene, spheroidene and lycopene were studied after excess energy excitation in the S_2 state. Excitation of carotenoids into higher vibronic levels of the S_2 state generates excess vibrational energy in the S_1 state. The vibrationally hot S_1 state relaxes faster when carotenoid is excited into the S_2 state with excess energy, but the S_1 lifetime remains constant regardless of which vibronic level of the S_2 state is excited. The S* signal depends on excitation energy only for spheroidene, which is likely due to asymmetry of the molecule, facilitating conformations responsible for the S* signal.

5.1. Introduction

Excited states of carotenoids, linear, methyl-substituted polyenes, have been a subject of numerous theoretical and experimental studies,[1-5] mainly because of their rich photophysics that stems from the presence of forbidden, dark excited states that participate in relaxation processes. Understanding the excited-state dynamics of carotenoids is crucial for disentangling their multiple roles in photosynthetic light-harvesting proteins where they serve as both light-harvesting and photoprotective pigments.[6,7] When carotenoids are excited into the strongly absorbing state, S_2, they relax within a few hundred femtoseconds to the S_1 state, which is forbidden for one-photon transitions from the ground state (S_0). The S_1 state undergoes non-radiative internal conversion on the time scale of a few picoseconds to the ground state. The S_1 state lifetime correlates with the conjugation length (N, number of conjugated C=C bonds of the chromophore) of a carotenoid; the S_1 lifetime varies from ~60 ps for N=8 to ~1.5 ps to N=13.[2]

This basic representation of relaxation dynamics is, however, only a very simplified model. First, the S_2-S_1 internal conversion, which likely occurs via a conical intersection,[8-10] reaches the S_1 potential surface far from the S_1 energy minimum, thereby creating a vibrationally hot S_1 state. Vibrational relaxation in the S_1 state occurs on the sub-picosecond time scale,[11,12] but dependence on the conjugation length remain unclear though some experiments suggest it becomes faster with increase of N.[13] Second, other dark states except the S_1 state may be involved in relaxation dynamics: 1) the elusive B_u^- state proposed on the basis of quantum chemical calculations[14,15] to be located below the S_2 state for carotenoids with N>10,[16] and 2) the S* state, which is readily identified by a distinct band in the transient absorption spectra,[17-19] and is often explained as a signal originating from specific carotenoid conformations either in the ground or S_1 states,[20-22] though alternative explanations have also been proposed.[23]

To account for various transient signals in ultrafast time-resolved experiments a few studies proposed a model involving small structural changes

during relaxation of a carotenoid molecule after excitation into the S_2 state.[10,11,24] In these models, potential surfaces of carotenoid excited states have multiple minima along the torsional coordinate, suggesting that some experimentally observed transition features earlier assigned to a separate electronic states may actually be transition structures on a complicated potential surface. [10,11,24] However, if the models with complicated potential surfaces are correct, they imply that the relaxation channels may take different paths depending on which part of the S_2 potential surface the excitation is prepared. Similarly, it was suggested that excitation of the S_1 state directly from the ground state, either by sensitization through energy transfer from another molecule or via two-photon excitation, may populate different minimum of the S_1 state than that reached via internal conversion from the S_2 state.[25]

Excitation of a carotenoid molecule with excess energy into higher vibrational levels of the S_2 state could provide a way to activate alternative relaxation pathways. There are only a few studies comparing the excited-state dynamics of carotenoids after excitation into the lowest vibrational band and after excess energy excitation. Nakamura et al.[26] explored stimulated emission from the S_2 state of a short spheroidene derivative (N=8) after excitation of higher vibrational levels, and Zuo et al.[27] studied relaxation in the S_2 state after exciting either 0-1 or 0-2 vibrational band of neurosporene (N=9). Both these studies focused on redistribution of energy within the S_2 state and addressed possible mixing with the B_u^- state. Billsten et al.[28] studied zeaxanthin (N=11) after excess energy excitation showing that the signal associated with the S* state is enhanced when the excess energy is provided.

Here we apply transient absorption spectroscopy to study properties of the S_1 state of three linear carotenoids with different conjugation lengths after excitation into higher vibrational levels of the S_2 state. We show that excess of vibrational energy in the S_2 state affects the vibrational cooling in the S_1 state in all studied carotenoids, but the S* signal is enhanced by excess energy excitation only for the carotenoid spheroidene.

5.2.   Material and Methods

Neurosporene and spheroidene were isolated and purified from cells of *Rhodobacter sphearoides* strains G1C and 2.4.1 respectively, as previously described.[29] Lycopene was purchased from CaroteNature (Switzerland). Prior to transient absorption measurements, all carotenoids were dissolved in n-hexane to obtain the absorbance OD ~0.4-0.5 at the absorption maximum in a 2 mm quartz cuvette. The absorption spectra were measured before and after each transient absorption experiment to confirm integrity of the samples. All measurements were carried out at room temperature.

Femtosecond pump-probe measurements were carried out on the femtosecond laser system (Spectra-Physics) producing pulses of ~100 fs duration at 1 kHz repetition rate with 800 nm central wavelength. The output is split into the two separate beams. The pump beam is tuned by an optical parametric amplifier (TOPAS, Light Conversion). The excitation intensity of pump pulses was ~2.10^{14} photons.pulse^{-1}.cm^{-2}. For probing, a white-light continuum covering the 440-700 nm spectral window generated by focusing a fraction of the primary 800 nm beam to a 2 mm sapphire plate was used. The probe beam was further split into the probe (overlapping at the sample with pump) a reference (passing outside the sample) beams which were focused to the entrance slit of a spectrograph where the beams were dispersed onto a double CCD array. The time delay between the excitation and probe pulses was introduced by a computer-controlled delay line. The mutual polarization between pump and probe beams was set to the magic angle (54.7°).

5.3. Results and Discussion

5.3.1. Steady-State Absorption Spectroscopy

Absorption spectra of all three linear carotenoids dissolved in *n*-hexane are shown in Figure 5-1. The lowest energy bands (0-0) of the S_0-S_2 transition peak at 469 nm (neurosporene), 482 nm (spheroidene) and 503 nm (lycopene) (Table 5-1). The red shift of the S_2 energy is due to extension of the conjugation length that varies from $N=9$ (neurosporene), to $N=10$ (spheroidene) and $N=11$ (lycopene). Energy separation between the 0-0 and 0-1 vibrational peaks, representing the combination of the C=C and C-C stretching modes, is 1460 cm^{-1} (neurosporene), 1420 cm^{-1} (spheroidene) and 1350 cm^{-1} (lycopene). The 0-1 and 0-2 vibrational bands, which were used to excite the carotenoids into higher vibronic levels, have maxima at 439 nm and 415 nm (neurosporene), 451 nm and 426 nm (spheroidene), and 471 nm and 444 nm (lycopene).

5.3.2. Transient Absorption Spectroscopy

The S_1 state. To provide basic characterization of the S_1 state after excitation into different vibrational levels of the S_2 state we show in Figure 5-2 normalized transient absorption spectra measured at delays that ensure that all relaxation processes (S_2-S_1 internal conversion and S_1 vibrational relaxation) are completed. We note here that our limited time resolution (~100 fs) is insufficient to reveal any relaxation processes within the S_2 state. However, the global analysis (Supporting Information, Figures S5-1, S5-2, S5-3) implies that the time needed to form the hot S_1 spectrum slightly prolongs if the higher vibronic bands of the S_2 state are excited.

The dominating feature in Figure 5-2 is the narrow excited state absorption band corresponding to the S_1-S_n transition. The full width half maximum (FWHM) yields values of 545 cm^{-1} (neurosporene), 570 cm^{-1} (spheroidene) and 610 cm^{-1} (lycopene) when obtained from the S_1-S_n bands measured after excitation into the

lowest, 0-0 band of the S_2 state, demonstrating increase of FWHM with conjugation length. Such increase of the S_1-S_n bandwidth was typically observed for carotenoids with conjugation extended to terminal rings or for carotenoid isomers and was assigned to and increased conformational disorder in the S_1 state.[30,31] Thus, correlation between the FWHM of the S_1-S_n band and conjugation length suggests that longer conjugation length facilitates increase of conformational disorder in the S_1 state. The FWHM of the S_1-S_n band also increases when carotenoids are excited into the higher vibrational levels (Table 5-1), indicating that excess vibrational energy in the S_2 state further increases the conformational disorder in the S_1 state.
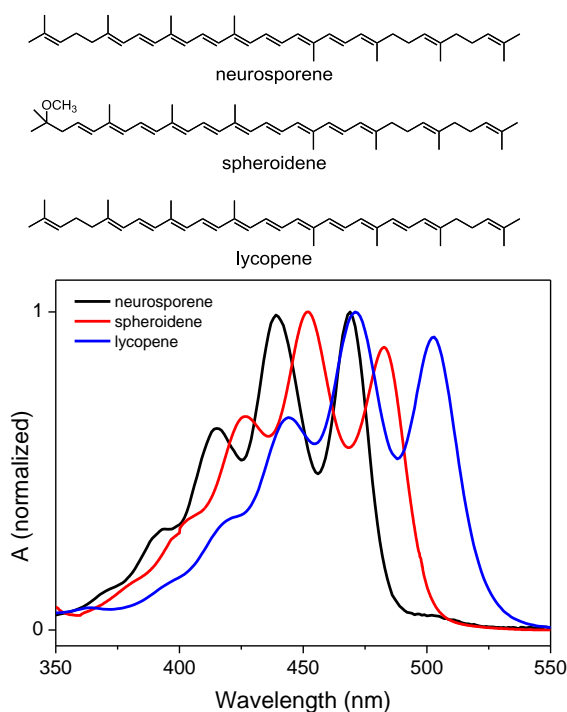

Figure 5-1. Molecular structures (top) and absorption spectra in n-hexane (bottom) of the studied carotenoids.

The maximum of the S_1-S_n band mirrors the shift of the S_2 energy with conjugation length and peaks at 510 nm (neurosporene), 525 nm (spheroidene)

and 554 nm (lycopene) after excitation into the 0-0 band of the S_2 state. For neurosporene and lycopene, the peak position does not change with increasing excitation energy, but for spheroidene the S_1-S_n peak red shifts to 528 nm when either 0-1 or 0-2 vibrational bands of the S_2 state are excited (Table 5-1). This shows that spheroidene exhibits slightly different behavior than the other two carotenoids, which is also underlined by the blue shoulder of the S_1-S_n band, which is typically denoted as the S^* signal.[17,19,32] Although this shoulder is observed in all data in Figure 5-2, only for spheroidene its magnitude depends on excitation wavelength. Origin and dynamics of this band will be discussed later.

Table 1. Spectroscopic parameters of the studied carotenoids.

	S_2 0-0 band (nm)[a]	λ_{exc} (nm)	S_1 lifetime (ps)[a]	S_1-S_n max (nm)	S_1-S_n FWHM (cm^{-1})	S_1 vibr. relaxation[b] (ps)[a]	ΔV^c (a.u.)
neurosporene	469	475	20.7	510	545	0.66	26
		436	20.4	509	582	0.54	30
		410	21.4	510	555	0.48	41
spheroidene	482	488	8.2	525	569	0.6	18
		450	8.1	527	611	0.61	20
		420	8.1	528	627	0.42	32
lycopene	503	510	4	554	612	0.5	15
		473	4.2	554	639	0.45	17
		443	4.2	553	697	0.47	21

a) the error margins for the time constants do not exceed 10%
b) values obtained from fitting the decay of band integral (Fig. 4)
c) difference between the value of the band integral at early (0.2-0.3 ps) and later (3-4 ps) delay times. See Fig. 4a for definition.

Finally, insets in Figure 5-2 show kinetics monitoring the decay of the S_1 state after excitation into different vibrational levels of the S_2 state, demonstrating that the S_1 lifetime is not affected by the excess energy provided by excitation into higher vibrational levels. The S_1 lifetimes extracted from global fitting (Supporting Information, Figures S5-1, S5-2, S5-3) are 21 ps (neurosporene), 8 ps (spheroidene) and 4.2 ps (lycopene), matching the values reported in a number of previous reports.[12,13,33,34] The independence of the S_1 lifetime on excitation wavelength implies that the population always reaches the same part of the S_1 potential surface, regardless of where the S_2 state is excited.
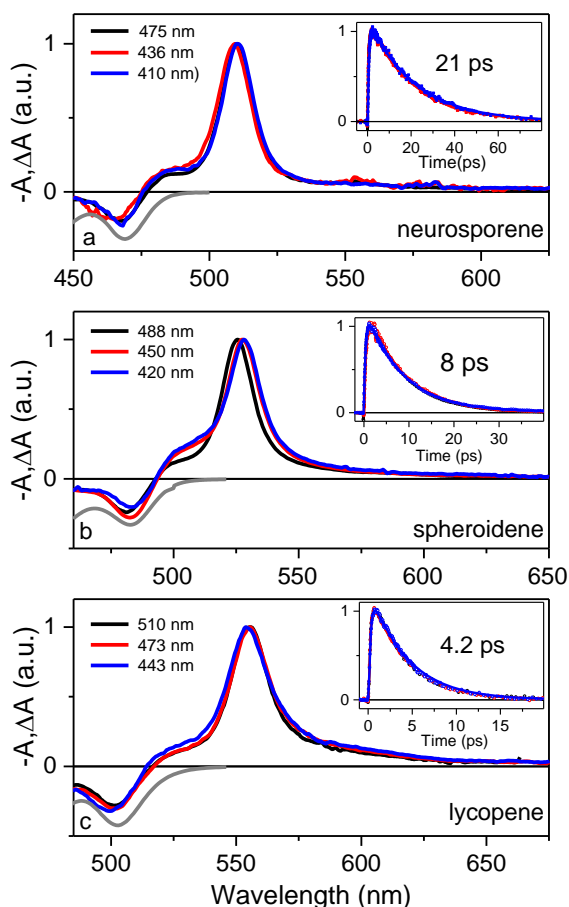
Figure 5-2. Transient absorption spectra taken at the maximum of the S_1-S_n transition after excitation into different vibrational levels of the S_2 state (excitation wavelengths are indicated in each graph). Inverted absorption spectrum in the spectral region of the 0-0 band of the S_0-S_2 transition is shown in grey for each carotenoid. Kinetic traces taken at the maximum of the S_1-S_n band for different excitations are shown in insets.

Vibrational relaxation in the S_1 state. The vibrational relaxation in the S_1 state of carotenoids takes place on a sub-picosecond time scale.[12,13] It is well-established fact that the internal conversion from the S_2 state generates hot S_1 state that is characterized by a broad and red-shifted spectrum, compared to the spectrum of the relaxed S_1 state. The vibrational relaxation times are usually extracted from global fitting, but since for some carotenoids the S_2 lifetime and S_1 vibrational relaxation time do not differ much,[13] the precise values may suffer from error. Thus, to evaluate vibrational relaxation in the S_1 state of linear carotenoids after excitation of different vibrational levels of the S_2 state, we have applied a different approach. The vibrational relaxation is readily visualized in transient absorption spectra measured at delays in the 0.2-4 ps range after excitation, which are normalized to the S_1-S_n maximum. We show such normalized spectra of spheroidene excited at 488 nm as an example in Figure 5-3a. The excess vibrational energy in the hot S_1 state is manifested as the extra signal in the red part of the normalized transient absorption spectra.

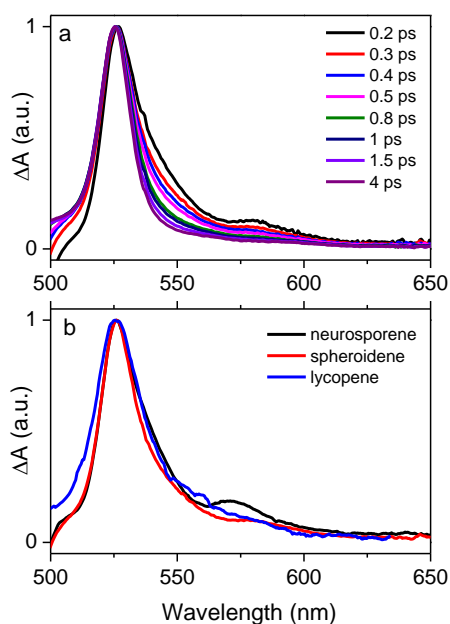Figure 5-3. (a) Normalized transient absorption spectra of spheroidene measured at different time delays after excitation to the 0-2 vibrational level of the S_2 state. (b) Normalized transient absorption spectra of neurosporene, spheroidene and lycopene taken at 0.3 ps after excitaiton to the 0-0 vibrational level of the S_2 state. The spectra are shifted to align the maxima of the S_1-S_n transition.

Note that at early times (0.2 – 0.3 ps), a weak band at ~577 nm is clearly visible. This band is shifted by ~1760 cm^{-1} from the main S_1-S_n peak, matching the frequency of the C=C stretching mode in the S_1 state of carotenoids.[35-37] Thus, the weak band at 577 nm represents a transition from the first vibrational level of the S_1 state to the S_n state of spheroidene. Figure 5-3b compares the 0.3 ps spectra of different carotenoids, demonstrating that the resolution of this band decreases with increasing conjugation length. This observation corroborates the assumption of the increase of conformational disorder in the S_1 state with increasing conjugation.

We use the normalized transient absorption spectra shown in Figure 5-3a to characterize the vibrational relaxation. If we calculate the area under each normalized spectrum, we obtain dynamics of vibrational relaxation, because decrease of area reflects the narrowing of the S_1-S_n band due to decay of excited vibrational modes. Similar fitting approach employing dynamics of a band integral was recently used to study properties of the S_1 state of β-carotene.[38] The dynamics of the band integral of the normalized spectra are shown in Figure 5-4. These dynamics should reflect pure S_1 vibrational relaxation without interference from other processes. The decays shown in Figure 5-4 can be fitted by a single exponential decay yielding values summarized in Table 5-1. We note two trends concerning the vibrational relaxation dynamics.

First, the vibrational relaxation after excitation of the lowest energy band of the S_2 state becomes faster with increase of conjugation length, but the differences are much smaller than obtained earlier from global fitting analyses. For example, Niedzwiedzki et al.[13] reported shortening of the S_1 vibrational relaxation time from 640 fs (neurosporene) to 370 fs (rhodopin glucoside, N=11). Here our analysis confirms the value for neurosporene (660 fs, Table 5-1), but for lycopene, which has the same conjugation length as rhodopin glucoside, our approach gives the value of 500 fs thus longer than was reported for rhodopin glucoside.

Second, the vibrational relaxation is faster if the carotenoid is excited into higher vibrational levels of the S_2 state. The population of the vibrational hot S_1

state is also larger after excess energy excitation as evidenced by larger value ΔV (see Figure 5-4), which characterizes the difference between the area under the normalized spectrum at early times (0.2-0.3 ps) and at times when vibrational relaxation is finished (4 ps, the plateau in kinetics shown in Figure 5-4). The ΔV values are summarized in Table 5-1. Thus, excess vibrational energy in the S_2 state generates excess vibrational energy in the S_1 state.

The S* signal. The transient absorption spectra of all three carotenoids contain a blue shoulder of the S_1-S_n band, which is in the literature referred to as the S* signal.[10,17,19,32] Its origin remains a matter of a debate,[21,22,39-41] but there is accumulating evidence that for carotenoids with N<12 the shoulder has its origin in the S_1 excited state[5,42] while for very long conjugated systems the S* signal corresponds to a hot ground state.[32,40] In the first approximation, whether the S* signal is due to an excited or a ground state can be decided on the basis of decay properties of the S* signal; if it decays with the same lifetime as the S_1 state, it likely comes from the S_1 state, but if it has a lifetime markedly longer than the S_1 state, it may have its origin in the hot ground state.

Since all carotenoids studied here belong to the group having N<12, we may expect the identical lifetimes of the S_1 state and the S* signal, which is indeed the case if the carotenoids are excited into the 0-0 band of the S_2 state. Global analysis of the spectro-temporal datasets, shown in Figures S5-1, S5-2, S5-3 (Supporting Information) shows that data measured after excitation into the 0-0 band can be successfully fitted with three components, corresponding to the S_2, hot S_1 and S_1 lifetimes. It is, however, known that excitation into higher vibrational levels of the S_2 state increases the amplitude of the S* signal.[28] The same effect can be also traced in transient absorption spectra depicted in Figure 5-2. While for neurosporene and lycopene the increase of the S* signal amplitude after excess energy excitation is negligible (yet visible in data), for spheroidene this effect is significant.
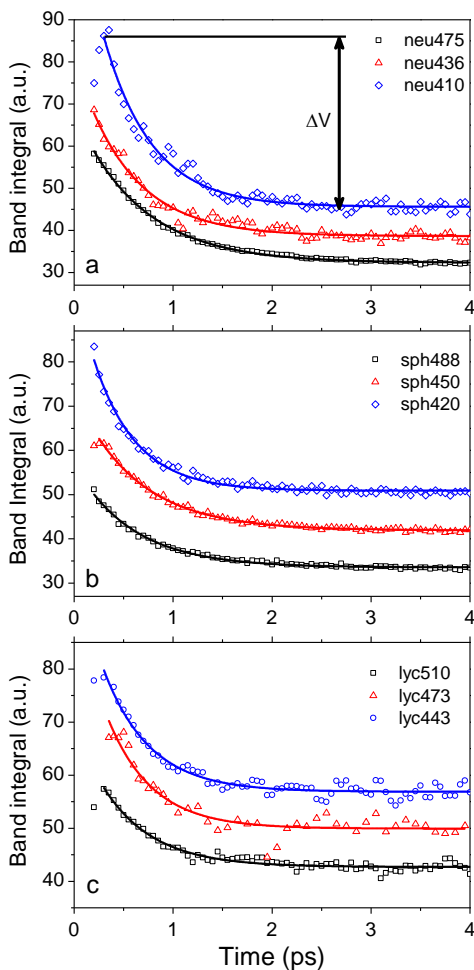
Figure 5-4. Dynamics of the vibrational relaxation of the S_1 state of neurosporene (a), spheroidene (b), lycopene (c) after excitation into the 0-2 (blue), 0-1 (red), and 0-0 (black) vibrational levels of the S_2 state. The band integrals are calculated for the wavelength range 490-620 nm (neurosporene), 510-640 nm (spheroidene), and 530-660 nm (lycopene). For the blue and red curves, an arbitrary vertical offset was introduced to prevent overlap of the curves. In the top panel, the quantity ΔV, which is introduced to quantify the vibrational relaxation, is depicted.

The difference in response to excess energy excitation between spheroidene and the other two linear carotenoids is further underscored by dynamics of the S* signal. For neurosporene and lycopene the slight increase of the S* signal after excitation into higher vibrational levels of the S_2 state does not affect the dynamics. The data can be still fitted with three components and no additional decay is required to account for the S* signal (Figures S5-1, S5-2, S5-3). For spheroidene, however, one extra component, significantly longer than the S_1 lifetime, must be included in fitting (Figure S5-2). This is demonstrated in Figure 5-5 that compares transient absorption spectra at 25 ps (Figure 5-5a) and

kinetics measured at the maximum of the S* signal at 506 nm (Figure 5-5b). The S* signal of spheroidene clearly decays longer than the S_1 state and global fitting extracts the S* lifetimes of 19 ps (excitation into the 0-1 band) and even 54 ps (0-2 band).

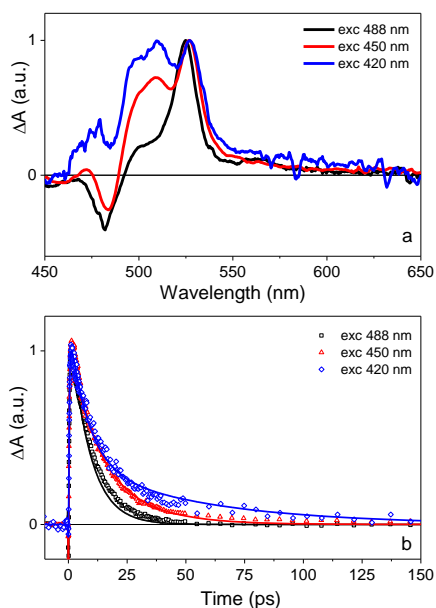
Figure 5-5. Transient absorption spectra taken at 25 ps (a) and kinetic traces measured at the maximum of the S* signal at 506 nm (b), after excitation into the 0-0 (black), 0-1 (red), and 0-2 (blue) vibrational levels of the S_2 state of spheroidene.

Such long lifetimes can hardly be assigned to an S_1 state thus other explanation is needed. First, there is an issue of possible contamination of the sample by shorter fragments that would absorb at shorter wavelengths thus might be preferentially excited when excitation is shifted to the blue part of the absorption spectrum. This question was in detail addressed for β-carotene.[42] Indeed, shorter fragments would have a longer S_1 lifetime and S_1-S_n band blue-shifted from that of "real" spheroidene, thus mimicking the spectra and dynamics of spheroidene data shown in Figure 5-5. However, if this were the case, the bleaching band would have to be also blue-shifted as these hypothetical shorter fragments would absorb only at shorter wavelengths. A closer inspection of data in Figure 5-5 and also EADS (see Figure S5-2) clearly shows that this is not the case. The bleaching band in the EADS of the longest decay component of

spheroidene has a maximum nearly identical with that seen in the spectrum associated with the "normal" S_1 state. This confirms that the long S^* decay is associated with spheroidene ruling out possible involvement of any shorter fragments.

It is also important to note that the 19 ps decay component was identified earlier for spheroidene excited into the lowest 0-0 band of the S_2 state, but dissolved in CS_2 [13]. Using CS_2 as a solvent does not change the S_1 lifetime, but it significantly increases the conformational disorder in the S_1 state (even though the conformational disorder in the ground state remains unaffected).[13] This observation supports the hypothesis of the S^* signal (regardless its origin) being associated with a specific conformations that may exist either in the ground or in excited state.[3,20,30,40] The final question that remains to answer is why we see this effect only for spheroidene and not for the shorter neurosporene and longer lycopene. Examination of structures of the three carotenoids shown in Figure 5-1 reveals that while neurosporene and lycopene are nearly ideally symmetric molecules, certain asymmetry is introduced by the methoxy group of spheroidene. Although the methoxy group is not part of the conjugation and consequently cannot affect spectroscopic properties, it can influence formation of the specific conformations needed to observe the S^* signal. However, an alternative hypothesis could be that other dark states may be involved in the population of the S^*. For example, recent study[37] on the vibrational dynamics of a similar group of carotenoids showed that for carotenoids with N~10 there exists diabatic mixing between the B_u^+ and B_u^- states. It is thus possible that such mixing in spheroidene opens new relaxation channel preferring the S^* signal.

5.4. Conclusions

Ultrafast transient absorption spectroscopy of three linear carotenoids with different conjugation length, neurosporene, spheroidene and lycopene has been employed to study effect of excess vibrational energy in the S_2 state on dynamics

of the S_1 state. We show that the S_1 lifetimes of all three carotenoids remain unaffected by excitation into higher vibronic levels of the S_2 state, demonstrating that relaxation pathways from the S_2 potential surface always reach the same minimum at the S_1 potential surface. The excess excitation energy in the S_2 state however affect the vibrational relaxation in the S_1 state. The hot S_1 state, generated by internal conversion from the S_2 state, relaxes faster when the S_2 state is excited if higher vibrational states of the S_2 state are excited. Finally, the excess excitation energy in the S_2 state enhances the S^* signal, but exclusively for spheroidene. This effect likely stems from the asymmetry of the spheroidene molecule which facilitates generation of specific conformations in the S_1 state that are responsible for the S^* signal. These conformations are preferentially generated if the S_2 state is excited with excess vibrational energy.

References

(1)   Christensen, R. L. The Electronic States of Carotenoids. In *The Photochemistry of Carotenoids*; Frank, H. A., Young, A. J., Britton, G., Gogdell, R. J., Eds.; Kluwer Academic Publishers: Dordrecht, The Netherlands, 1999; pp 137–159.

(2)   Polívka, T.; Sundstrom, V. Ultrafast Dynamics of Carotenoid Excited States-from Solution to Natural and Artificial Systems. *Chem. Rev.* **2004**, *104* (4), 2021–2071.

(3)   Hashimoto, H.; Sugisaki, M.; Yoshizawa, M. Ultrafast Time-Resolved Vibrational Spectroscopies of Carotenoids in Photosynthesis. *Biochim. Biophys. Acta* **2014**, *1847* (1), 1–10.

(4)   Bautista, J. A.; Connors, R. E.; Raju, B. B.; Hiller, R. G.; Sharples, F. P.; Gosztola, D.; Wasielewski, M. R.; Frank, H. A. Excited State Properties of Peridinin: Observation of a Solvent Dependence of the Lowest Excited Singlet State Lifetime and Spectral Behavior Unique among Carotenoids. *J. Phys. Chem. B* **1999**, *103* (41), 8751–8758.

(5)   Balevičius, V.; Pour, A. G.; Savolainen, J.; Lincoln, C. N.; Lukes, V.; Riedle, E.; Valkunas, L.; Abramavicius, D.; Hauer, J. J. Vibronic Energy Relaxation Approach Highlighting Deactivation Pathways in Carotenoids. *Phys. Chem. Chem. Phys.* **2015**, *4* (8), 1166–1169.

(6)   Polívka, T.; Frank, H. A. Molecular Factors Controlling Photosynthetic Light Harvesting by Carotenoids. *Acc. Chem. Res.* **2010**, *43* (8), 1125–1134.

(7)   Duffy, C. D. P.; Ruban, A. V. Dissipative Pathways in the Photosystem-II Antenna in Plants. *J. Photochem. Photobiol. B* **2015,** *152*, 215-226.

(8)   Fuss, W.; Haas, Y.; Zilberg, S. Twin States and Conical Intersections in Linear Polyenes. *Chem. Phys.* **2000**, *259*, 273–295.

(9)   Hauer, H.; Buckup, T.; Motzkus, M. Pump-Degenerate Four Wave Mixing as a Technique for Analyzing Structural and Electronic Evolution: Multidimensional Time-Resolved Dynamics near a Conical Intersection. *J. Phys.*

Chem. A **2007**, *111* (2007) 10517–10529.

(10)   Beck, W. F.; Bishop, M. M.; Roscioli, J. D.; Ghosh, S.; Frank, H. A. Excited State Conformational Dynamics in Carotenoids: Dark Intermediates and Excitation Energy Transfer. *Arch. Biochem. Biophys.* **2015**, *572*, 175–183.

(11)   Weerd, F. L. De; Stokkum, I. H. M. Van; Grondelle, R. Van. Subpicosecond Dynamics in the Excited State Absorption of All- Trans - B - Carotene. **2002**, *354* (March), 38–43.

(12)   Billsten, H. H.; Zigmantas, D.; Sundström, V.; Polívka, T. Dynamics of Vibrational Relaxation in the S1 State of Carotenoids Having 11 Conjugated C=C Bonds. *Chem. Phys. Lett.* **2002**, *355* (5–6), 465–470.

(13)   Niedzwiedzki, D.; Koscielecki, J. F.; Cong, H.; Sullivan, J. O.; Gibson, G. N.; Birge, R. R.; Frank, H. a. Ultrafast Dynamics and Excited State Spectra of Open-Chain Carotenoids at Room and Low Temperatures. *J. Phys. Chem. B* **2007**, *111* (21), 5984–5998.

(14)   Tavan, P.; Schulten, K. Electronic Excitations in Finite and Infinite Polyenes. *Physical Review B*. **1987**, *36*, 4337–4358.

(15)   Schulten, K.; Karplus, M. On the Origin of a Low-Lying Forbidden Transition in Polyenes and Related Molecules. *Chem. Phys. Lett.* **1972**, *14* (3), 305–309.

(16)   Koyama, Y.; Rondonuwu, F. S.; Fujii, R.; Watanabe, Y. Light-Harvesting Function of Carotenoids in Photo-Synthesis: The Roles of the Newly Found 11Bu- State. *Biopolymers* **2004**, *74* (1–2), 2–18.

(17)   Gradinaru, C. C.; Kennis, J. T.; Papagiannakis, E.; van Stokkum, I. H.; Cogdell, R. J.; Fleming, G. R.; Niederman, R. a; van Grondelle, R. An Unusual Pathway of Excitation Energy Deactivation in Carotenoids: Singlet-to-Triplet Conversion on an Ultrafast Timescale in a Photosynthetic Antenna. *Proc. Natl. Acad. Sci. U. S. A.* **2001**, *98* (5), 2364–2369.

(18)   P. Chábera, P.; Fuciman, M.; Hríbek, ; Polívka, T. Effect of carotenoid structure on excited-state dynamics of carbonyl carotenoids. *Phys. Chem. Chem. Phys.*, **2009**, *11*, 8795–803.

(19)   Polívka, T.; Sundström, V. Dark Excited States of Carotenoids: Consensus and Controversy. *Chem. Phys. Lett.* **2009**, *477* (1–3), 1–11.

(20)   Lukeš, V.; Christensson, N.; Milota, F.; Kauffmann, H. F.; Hauer, J. Electronic Ground State Conformers of β-Carotene and Their Role in Ultrafast Spectroscopy. *Chem. Phys. Lett.* **2011**, *506* (1–3), 122–127.

(21)   Hauer, J.; Maiuri, M.; Viola, D.; Lukes, V.; Henry, S.; Carey, a. M.; Cogdell, R. J.; Cerullo, G.; Polli, D. Explaining the Temperature Dependence of Spirilloxanthin's S* Signal by an Inhomogeneous Ground State Model. *J. Phys. Chem. A* **2013**, *117* (29), 6303–6310.

(22)   Kloz, M.; Weissenborn, J.; Polívka, T.; Frank, H. A.; Kennis, J. T. M. Spectral Watermarking in Femtosecond Stimulated Raman Spectroscopy: Resolving the Nature of the Carotenoid S* State. *Phys. Chem. Chem. Phys.* **2016**, *18* (21), 14619–14628.

(23)   Lenzer, T.; Ehlers, F.; Scholz, M.; Oswald, R.; Oum, K. Assignment of Carotene S* State Features to the Vibrationally Hot Ground Electronic Statew. *Phys. Chem. Chem. Phys.* **2010**, *12*, 8832–8839.

(24)   Ghosh, S.; Bishop, M. M.; Roscioli, J. D.; Mueller, J. J.; Shepherd, N. C.; LaFountain, A. M.; Frank, H. A.; Beck, W. F. Femtosecond Heterodyne Transient-Grating Studies of Nonradiative Decay of the S2 (1 1Bu+) State of β-Carotene: Contributions from Dark Intermediates and Double-Quantum Coherences. *J. Phys. Chem. B* **2015**, *119* (47), 14905–14924.

(25)   Staleva, H.; Zeeshan, M.; Chábera, P.; Partali, V.; Sliwka, H. R.; Polívka, T. Ultrafast Dynamics of Long Homologues of Carotenoid Zeaxanthin. *J. Phys. Chem. A* **2015**, *119* (46), 11304–11312.

(26)   Nakamura, R.; Wang, P.; Fujii, R.; Koyama, Y.; Hashimoto, H.; Kanematsu, Y. Vibrational Relaxation Pathways in the Electronic Excited State of Carotenoid. *J. Lumin.* **2006**, *119–120*, 442–447.

(27)   Zuo, P.; Sutresno, A.; Li, C.; Koyama, Y.; Nagae, H. Vibrational Relaxation on the Mixed Vibronic Levels of the View the MathML Source and View the MathML Source States in All-Trans-Neurosporene as Revealed by Subpicosecond Time-Resolved, Stimulated Emission and Transient Absorption Spectroscopy. *Chem. Phys. Lett.* **2007**, *440* (4–6), 360–366.

(28)   Billsten, H. H.; Pan, J.; Sinha, S.; Pascher, T.; Sundstrom, V.; Polívka, T. Excited-State Processes in the Carotenoid Zeaxanthin after Excess

Energy Excitation. *J. Phys. Chem. A* **2005**, *109* (31), 6852–6859.

(29)   Cogdell, R. J.; Land, E. J.; Truscott, T. G. The Triplet Extinction Coefficients of Some Bacterial Carotenoids. *Photochem. Photobiol.* **1983**, *38* (6), 723–725.

(30)   Niedzwiedzki, D. M.; Sullivan, J. O.; Polívka, T.; Birge, R. R.; Frank, H. a. Femtosecond Time-Resolved Transient Absorption Spectroscopy of Xanthophylls. *J. Phys. Chem. B* **2006**, *110* (45), 22872–22885.

(31)   Niedzwiedzki, D. M.; Enriquez, M. M.; Lafountain, A. M.; Frank, H. A. Ultrafast Time-Resolved Absorption Spectroscopy of Geometric Isomers of Xanthophylls. *Chem. Phys.* **2010**, *373* (1–2), 80–89.

(32)   Balevičius, V.; Abramavicius, D.; Polívka, T.; Galestian Pour, A.; Hauer, J. A Unified Picture of S* in Carotenoids. *J. Phys. Chem. Lett.* **2016**, *1* (August), 3347–3352.

(33)   Fujii, R.; Inaba, T.; Watanabe, Y.; Koyama, Y.; Zhang, J.-P. Two Different Pathways of Internal Conversion in Carotenoids Depending on the Length of the Conjugated Chain. *Chem. Phys. Lett.* **2003**, *369* (1–2), 165–172.

(34)   Polívka, T.; Zigmantas, D.; Frank, H. A.; Bautista, J. A.; Herek, J. L.; Koyama, Y.; Ritsuko Fujii, A.; Villy Sundström; Sundström, V. Near-Infrared Time-Resolved Study of the S 1 State Dynamics of the Carotenoid Spheroidene. **2001**, 1072–1080.

(35)   Hashimoto, H.; Koyama, Y. The C=C Stretching Raman Lines of β-Carotene Isomers in the S1 State as Detected by Pump-Probe Resonance Raman Spectroscopy. *Chem. Phys. Lett.* **1989**, *154* (4), 321–325.

(36)   Hashimoto, H.; Koyama, Y. Raman Spectra of All-Trans-β-Carotene in the S1 and T1 States Produced by Direct Photoexcitation. *Chem. Phys. Lett.* **1989**, *163* (2), 251–256.

(37)   Miki, T.; Buckup, T.; Krause, M. S.; Southall, J.; Cogdell, R. J.; Motzkus, M. Vibronic Coupling in the Excited-States of Carotenoids. *Phys. Chem. Chem. Phys.* **2016**, *18*, 11443–11453.

(38)   Quick, M.; Kasper, M.-A.; Richter, C.; Mahrwald, R.; Dobryakov, A. L.; Kovalenko, S. A.; Ernsting, N. P. β-Carotene Revisited by Transient Absorption and Stimulated Raman Spectroscopy. *ChemPhysChem* **2015**, *16* (18),

3824–3835.

(39)   Papagiannakis, E.; Van Stokkum, I. H. M.; Vengris, M.; Cogdell, R. J.; Van Grondelle, R.; Larsen, D. S. Excited-State Dynamics of Carotenoids in Light-Harvesting Complexes. 1. Exploring the Relationship between the S 1and S* States. *J. Phys. Chem. B* **2006**, *110* (11), 5727–5736.

(40)   Ehlers, F.; Scholz, M.; Schimpfhauser, J.; Bienert, J.; Oum, K.; Lenzer, T. Collisional Relaxation of Apocarotenals: Identifying the S* State with Vibrationally Excited Molecules in the Ground Electronic State S(0)*. *Phys. Chem. Chem. Phys.* **2015**, *17* (16), 10478–10488.

(41)   Larsen, D. S.; Papagiannakis, E.; Van Stokkum, I. H. M.; Vengris, M.; Kennis, J. T. M.; Van Grondelle, R. Excited State Dynamics of β-Carotene Explored with Dispersed Multi-Pulse Transient Absorption. *Chem. Phys. Lett.* **2003**, *381* (5–6), 733–742.

(42)   Ostroumov, E. E.; Reus, M. G. M. M.; Holzwarth, A. R.; Holzwarth, A. R. On the Nature of the "Dark S*" Excited State of β-Carotene. *J. Phys. Chem. A* **2011**, *115* (16), 3698–3712.

Supporting Information

Global and Target analysis

The spectro-temporal data sets collected by the detection system were fitted globally using the DAFit software package (Pascher Instruments, Lund, Sweden). This approach allows a determination of the time constants of the excited state processes and, more importantly, an assignment of spectral profiles of the intermediate excited state species.[1] The data were fit to a sum of exponentials, including a numerical deconvolution of the FWHM of the response function, and a fourth-degree polynomial describing the chirp. The fitting procedure involved a general linear regression for the amplitudes of the exponentials and the Nelder-Mead simplex method for the rate constants, FWHM, and chirp polynomial. To visualize the excited state dynamics, we assumed a sequential, irreversible scheme A → B, B → C, C → D… representing increasingly slower, mono-exponential processes with time constants corresponding to the lifetimes of the species A, B, C, D… The spectral profiles of these species are called an evolution-associated difference spectra (EADS), and although they may not correspond to pure spectra of the individual excited states, they provide valuable information about the time evolution of the whole system.[1] For complicated systems involving branching relaxation schemes, target analysis, providing the species associated difference spectra (SADS), is often used. Here, we used software package Glotaran (Vrije Universiteit Amsterdam) to run target analysis on the data measured for spheroidene.

The global fitting analyses on the transient absorption data of neurosporene (Figure S5-1) and lycopene (Figure S5-3) provide good fits with three components. The EADS, with their lifetimes, correspond to the S_2, hot S_1, and relaxed S_1 states. A similar result with three EADS was also obtained for spheroidene when excited into the 0-0 vibrational band of the S_2 state at 488 nm (Figure S5-2a), but when excited into the 0-1 and 0-2 vibrational levels of the S_2 state, a three-component fit did not succeed in reproducing the data. Instead, a fourth component having the lifetime of 19 ps (0-1 excitation) and 54 ps (0-2 excitation) was needed to fit the data (Figure S5-2 b-e). Consequently, for

spheroidene excited into higher vibrational levels we used either branchinmg model (target analysis, SADS, Figure S5-2 c,e) or sequential model (EADS, Figure S5-2 b,d). Both models give comparable results, showing a low-amplitude EADS/SADS corresponding to a band having a maximum blue-shifted from the main S_1-S_n band, even though the bleaching bands are comparable to those observed in the S_1 spectrum, a behavior typical for the S^* signal.
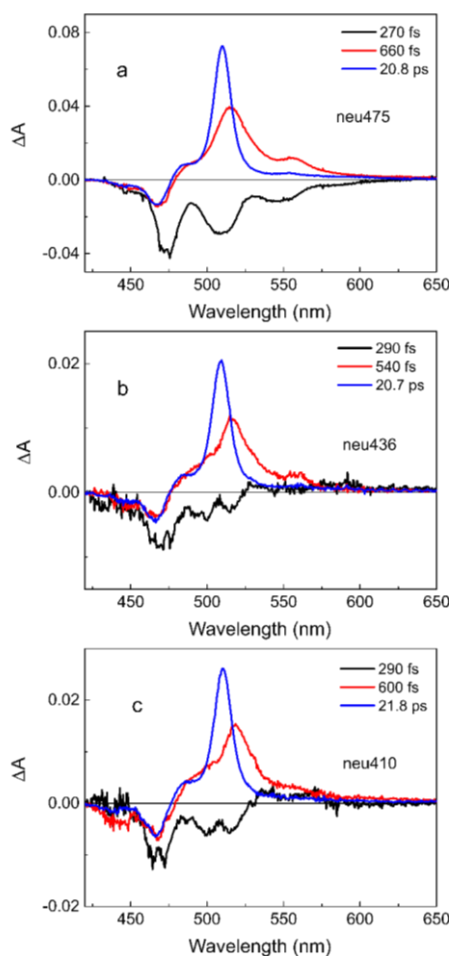

Figure S5-1. EADS obtained from global analysis of data measured for neurosporene in n-hexane after excitation to the 0-0 (a), 0-1 (b), and 0-2 (c) vibrational levels of the S_2 state.
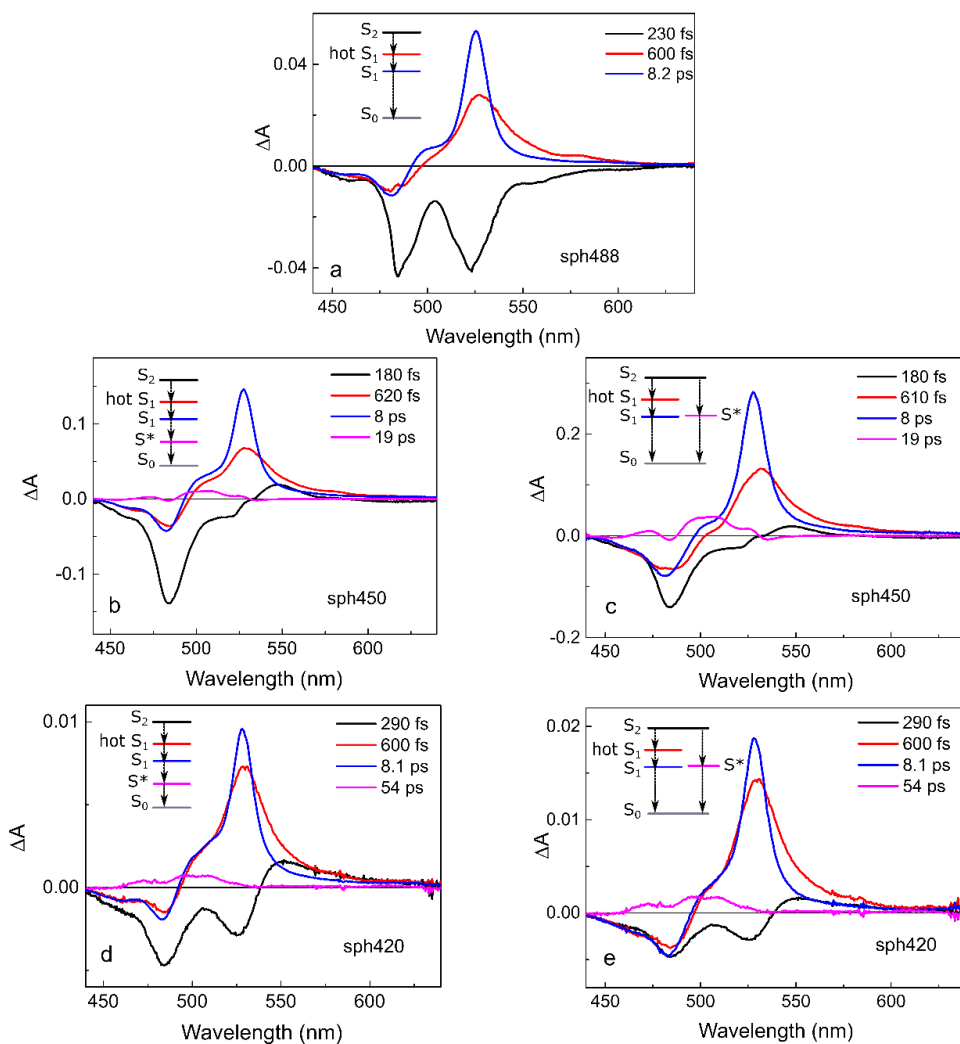
Figure S5-2. EADS (a,b,d) and SADS (c,e) resulting from global and target analysis of data recorded for spheroidene in *n*-hexane after excitation to the 0-0 (a), 0-1 (b,c), and 0-2 (d,e) vibrational levels of the S_2 state. The insets show the relaxation schemes used for fitting.
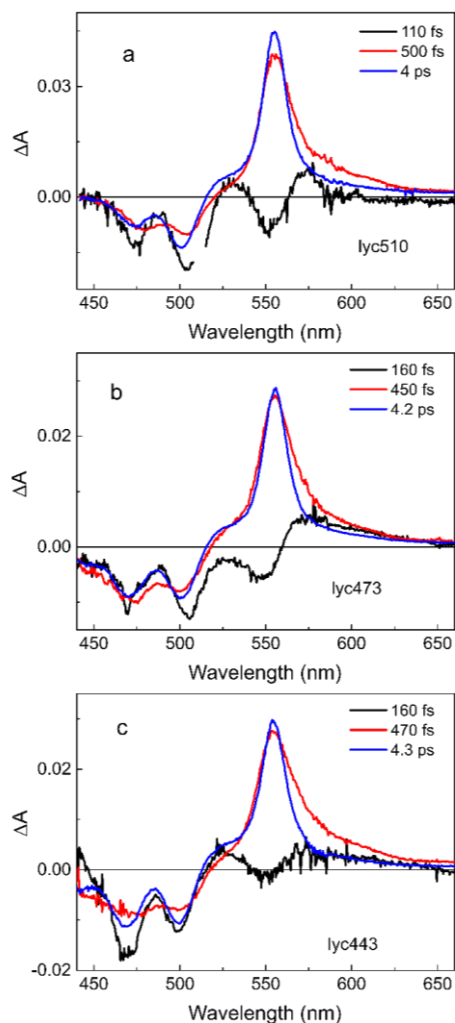
Figure S5-3. EADS obtained from global analysis of data measured for lycopene in *n*-hexane after excitation to the 0-0 (a), 0-1 (b), and 0-2 (c) vibrational levels of the S_2 state.

Reference

(1)   Van Stokkum, I. H. M; Larsen, D.S.; Van Grondelle, R. Global and target analysis of time-resolved spectra, *Biochim. Biophys. Acta,* **2004,** *1657*, 82-104.

6. Ultrafast spectroscopy tracks carotenoid configurations in the Orange and Red Carotenoid Proteins from cyanobacteria

This chapter is based on Paper IV.:

Abstract

A quenching mechanism mediated by the Orange Carotenoid Protein (OCP) is one of the ways cyanobacteria protect themselves against photooxidative stress. Here we present a femtosecond spectroscopic study comparing OCP and RCP (red carotenoid protein) samples binding different carotenoids. We confirmed significant changes in carotenoid configuration upon OCP activation reported by Leverenz et al.[1] by comparing the transient spectra of OCP and RCP. The most important marker of these changes was the magnitude of the transient signal associated with the carotenoid intramolecular charge-transfer (ICT) state. While OCP with canthaxanthin exhibited a weak ICT signal, it increased significantly for canthaxanthin bound to RCP. On the contrary, a strong ICT signal was recorded in OCP binding echinenone excited at the red edge of the absorption spectrum. Because the carbonyl oxygen responsible for the appearance of the ICT signal is located at the end-rings of both carotenoids, the magnitude of the ICT signal can be used to estimate the torsion angles of the end rings. Application of two different excitation wavelengths to study OCP demonstrated that the OCP

sample contains two spectroscopically distinct populations, none of which corresponding to the photoactivated product of OCP.

6.1. Introduction

Oxygen-dependent photosynthetic organisms such as plants, algae and cyanobacteria must protect themselves against photooxidative stress. Key players in this process are carotenoids. They quench both the reactive oxygen species such as singlet oxygen, but also prevent those species from being generated by quenching excited states of "parent" molecules, i.e. chlorophylls or phycobilins. When the parent molecules are in the singlet excited state, the process of their assisted deexcitation is called non-photochemical quenching (NPQ), which is manifested as a decrease of their fluorescence.[2]

Cyanobacteria utilize three specific types of NPQ: one is based on the iron stress-induced isiA protein,[3,4] another operates in the recently described HliD protein, which is an ancestor of antennas from LHC superfamily,[5] and, finally, the last type of quenching is associated with the Orange Carotenoid Protein (OCP), which is in the focus of this study. This water-soluble, carotenoid-binding protein was first identified in 1981.[6] It is responsible for quenching of phycobilisome fluorescence.[7,8] The crystal structure of the *Arthrospira maxima* OCP with the carotenoid 3'-hydroxyechinenone was resolved (2.1 Å) in 2003[9] and that of *Synechocystis* PCC6803 with echinenone (1.65 Å) in 2010.[10] Only recently, another X-ray structure of OCP from *Synechocystis* PCC6803 (produced in *E. coli*) binding the carotenoid canthaxanthin was obtained, with resolution of 1.9 Å.[1]

OCP consists of two domains: an α-helical N-terminal domain, which is unique to cyanobacteria, and an α-helix/β-sheet C-terminal domain which is a member of the NTF2 (nuclear transport factor 2) superfamily that can be found in a wide range of organisms.[9,10] The carotenoid spans both domains, thus contributing to stabilization of both parts of the protein. There are also other ways the overall protein conformation is stabilized: a flexible linker about 25 residues long between the C- and N-terminal domain; the first 19 amino acids of the N-terminal domain interacting with the surface of the C-terminal domain; a salt bridge between two charged amino acids, each located in another domain.

The relationship between OCP presence/absence and phycobilisome fluorescence quenching induced by blue-green light was identified ten years ago by mutational studies.[7] It was shown that fluorescence quenching was inhibited and the photoinhibition was faster in mutants lacking the OCP. Only later it was realized that OCP is a photoactive protein.[11] Upon illumination with blue-green light, it undergoes a transition from an inactive orange form (OCPo) to an active red form (OCPr), the latter being an effector in fluorescence quenching. Spectrally, the two forms of OCP not only differ in the red-shift of OCPr with respect to OCPo, but the activation is also accompanied by the loss of carotenoid vibrational structure, suggesting diminished binding constraints of the carotenoid in OCPr.

OCP from *Synechocystis* is able to bind 3'-hydroxyechinenone, echinenone, canthaxanthin, and zeaxanthin (Figure 6-1). OCP with all the mentioned carotenoids except zeaxanthin can be activated by blue-green light.[12,13] Consequently, no quenching is induced by OCP binding zeaxanthin.[12] The presence of a carbonyl group is, thus, essential for the activation because zeaxanthin is a non-carbonyl carotenoid. The importance of the carbonyl group is supported by the fact that it forms a hydrogen-bond to two neighbouring residues, Tyr201 and Trp288.[9,10] When these residues were mutated, the specificity for binding the carbonyl carotenoid was diminished. Additionally, neither photoactivation, nor fluorescence quenching were observed in these mutants.[14]

Carbonyl carotenoids are known for their specific polarity-dependent behavior. Their spectroscopic properties in non-polar solvents are comparable to their non-carbonyl counterparts. The excitation promotes the carotenoid from the ground state, S_0, to the second excited state, S_2. The carotenoid then relaxes to the first excited state, S_1, on the timescale of hundreds of femtoseconds. The spectrum of the S_1 state is then easily obtained by means of standard transient absorption spectroscopy. It is typically dominated by a strong absorption band in the visible region, associated with the transition from the S_1 to a higher excited state, denoted as S_n. The S_1 state then decays to the ground state with lifetime on the order of units to tens of picoseconds, depending on the conjugation length.[15]

The behavior of carbonyl carotenoids in polar solvents is, however, markedly different. The spectrum after the relaxation of the S_2 state is more complex, as it may contain an additional red-shifted band, which is usually assigned to a transition from the intramolecular charge-transfer (ICT) state.[16,17] The ICT nature and relation to the S_1 state are still a matter of discussion.[18–23] The decay of the S_1 and ICT states in polar solvents is typically faster than that of the S_1 state in the non-polar solvent. Whether or not these phenomena come to play depends on the structural context of the carbonyl group (part of the lactone ring or the end rings, one or two symmetrically positioned carbonyl groups in the molecule, etc.). In the specific case of a protein-bound carotenoid, one can observe a strong ICT band even for a carbonyl carotenoid having no such band in solution.[24]

Carbonyl carotenoids bound to proteins are typically known for their involvement in energy transfer to (bacterio)chlorophylls ((B)Chls), with efficiencies even approaching unity.[25–27] Carotenoids in OCP have, however, the photoprotective function in the process of NPQ. Currently, there are three models explaining how carotenoids are directly involved in NPQ: 1) energy transfer between the quenched molecule and the carotenoid,[5,28] 2) charge transfer between these molecules,[29] and 3) excitonic interaction between these molecules.[30] There is no clear evidence for any of these mechanisms in OCP-mediated quenching, and both mechanisms #1 and #2 were suggested to play a role in OCP.[31–33]

It has recently been shown that the N-terminal domain of OCP is the active part responsible for quenching, which binds to the phycobilisomes.[1,34] It is called the Red Carotenoid Protein (RCP). The C-terminal part is the regulator of the quenching activity.[34,35] Although only OCPr is physiologically relevant, absorption and Raman spectra of OCPr and RCP shared substantial similarities, demonstrating that the immediate environments of the carotenoids are very similar in both proteins.[34] Thus information about RCP can help reveal the properties of OCPr *in vivo*. Results of transient absorption spectroscopy on RCP showed that the carotenoid lifetime is close to that in solution. It was therefore concluded that a part of the carotenoid containing the carbonyl group is exposed to the buffer.[36]

The recent X-ray structure of RCP, though with a different carotenoid (canthaxanthin) than that studied in Chábera et al.[36] (3'-hydroxyechinenone), did not confirm a substantial solvent exposure of the carotenoid with the exception of the end-rings.[1] Instead, it revealed large differences between the position of the carotenoid in OCPo and RCP. This means that upon photoactivation the carotenoid must undergo a substantial translocation – while in OCPo the two halves of the carotenoid molecule are shared between the two OCP domains, in RCP the carotenoid penetrates deep into the interior of the N-terminal domain, most likely leaving the carotenoid-free C-subunit attached only by the linker.[1] The N-subunit is so activated for the quenching function. This model with detachment of the subunits held together by the linker, forming an elongated structure, was confirmed by a recent study employing various methods including small-angle X-ray scattering.[37]

Here, we present a femtosecond time-resolved study of OCP containing various carotenoids (echinenone, canthaxanthin, and zeaxanthin) and of RCP with canthaxanthin. The recently published study[1] enables us to associate molecular structure with spectroscopic measurements for the OCP-RCP pair with the carotenoid canthaxanthin. Comparisons with OCP binding different carotenoids proved very helpful in addressing the spectral heterogeneity of OCP samples described earlier.[33,38]

6.2. Materials and Methods

6.2.1. Sample Preparation

OCP-Ana-can (OCP from *Anabaena* sp. with the carotenoid canthaxanthin, hereafter called "OCP-can"), OCP-Syn-ecn (OCP from *Synechocystis* PCC6803 with the carotenoid echinenone, hereafter called "OCP-ecn") and RCP-Syn-can (RCP from *Synechocystis* PCC6803 with the carotenoid canthaxanthin, hereafter called "RCP-can") were isolated from *E.coli* cells carrying three plasmids containing all the genes necessary for the synthesis of

canthaxanthin or echinenone and the *ocp* or *rcp* genes. The production and isolation of these proteins are described in ref. 13 and ref. 1. OCP-Syn-zea (hereafter called "OCP-zea") was isolated from a *Synechocystis* mutant lacking echinenone and 3'-hydroxyechinenone and overexpressing the *ocp* gene. The construction of the *Synechocystis* mutant and the isolation of OCP-zea are described in ref. 12.
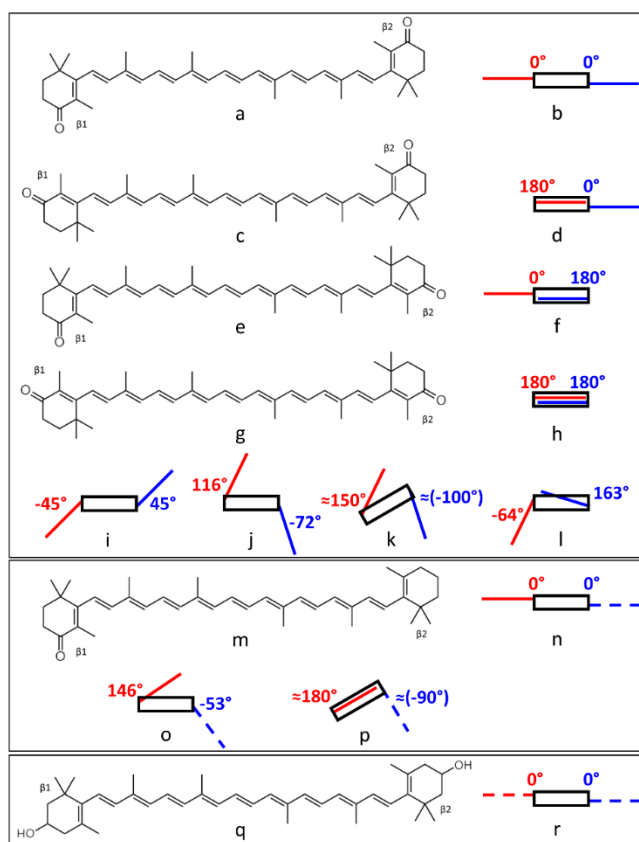

Figure 6-1. Molecular structures of carotenoids relevant to this study together with their schematic side-view representations. In the schematic representation: black rectangle – conjugated backbone; red line – *β*1 ring, blue line – *β*2 ring; solid line – a conjugated carbonyl on the ring, dashed line – no conjugated carbonyl on the ring; torsion angles indicated. Carotenoid structures: canthaxanthin (a,b: s-*cis* – s-*cis*; c,d: s-*trans* – s-*cis*; e,f: s-*cis* – s-*trans* ; g,h: s-*trans* – s-*trans*), echinenone (m,n: s-*cis* – s-*cis*), zeaxanthin (q,r: s-*cis* – s-*cis*). Schematic structure of carotenoids in solution, shown on canthaxanthin (i).Schematic structures of carotenoids in proteins: main form of OCPo-can (j, ref. 1), putative configuration in the red form of OCPo-can (k), RCP-can (l, ref. 1), main form of OCPo-ecn (o, ref. 10), putative configuration in the red form of OCPo-ecn (p).

6.2.2. Spectroscopy

Femtosecond pump-probe measurements were carried out with pulses derived from the modular laser system based on the Spitfire Ace-100F ultrafast Ti-sapphire regenerative amplifier (Spectra-Physics) seeded with the Mai Tai SP oscillator (Spectra-Physics) and pumped with Empower 30 laser (Spectra-Physics). The output from the oscillator consists of pulses with 800 nm central wavelength, ~100 fs pulse width delivered at 1 kHz repetition rate. The output beam is split into two separate beams. The pump beam is tuned by an optical parametric amplifier (TOPAS, Light Conversion), to reach the desired excitation wavelength (470 nm and 540 nm for purposes of this study). The excitation intensity of pump pulses was kept below $2 \cdot 10^{14}$ photons.pulse^{-1}.cm^{-2}. The probe beam is the white-light continuum generated by a 2-mm sapphire plate. The respective polarization between pump and probe pulses is set to the magic angle (54.7°). A detailed description of the experimental setup can be found in ref. 39.

All samples were dissolved in 40mM Tris-HCl buffer with pH 8. The absorbance of all samples were adjusted to ~0.7 OD at 470 nm, which corresponds to <0.2 OD at 540 nm (measured in a 2 mm cuvette). A rectangular 2 mm quartz cuvette with vertical magnetic stirring was used for pump-probe measurements. All measurements were performed at 12°C using a temperature-controlled cuvette holder (Flash 300, Quantum Northwest).

6.3.   Results

6.3.1. Steady-State Absorption Spectroscopy

Figure 6-2 shows steady-state absorption spectra of all studied samples. From the general point of view, OCP-can and OCP-ecn spectra are rather similar. OCP-zea differs in being blue-shifted with respect to the other two OCP samples and also exhibits a well-resolved vibrational structure. The RCP-can spectrum is red-shifted and has essentially no vibrational structure. The 0-0 bands of OCP-can, OCP-ecn and OCP-zea are 500, 497, and 493 nm, respectively. For all OCP samples, the 0-0 band is of similar strength as the 0-1 band that peaks at 477 nm

(OCP-can), 472 nm (OCP-ecn), and 463 nm (OCP-zea). This feature is rather unusual for carotenoids because the 0-1 vibrational band is typically the strongest. The increase of the 0-0 band intensity in OCP has been attributed to either OCPr partially contributing to the red tail of the carotenoid absorption band[33] or to presence of more carotenoid configurations in OCPo.[38] To confirm the presence of another band contributing to the red tail of absorption spectra, we deconvoluted the absorption spectra into Gaussian bands (Supporting Information Figures S6-1 and S6-2). The presence of the "red" band was confirmed in all OCP samples; the other bands summed together resulted in the standard carotenoid spectrum with the strongest 0-1 vibrational band, confirming that all the OCP samples exhibit spectral heterogeneity. To study this, the transient measurements on OCP were conducted with two excitation wavelengths, 470 nm and 540 nm, to address respective subpopulations in the samples.
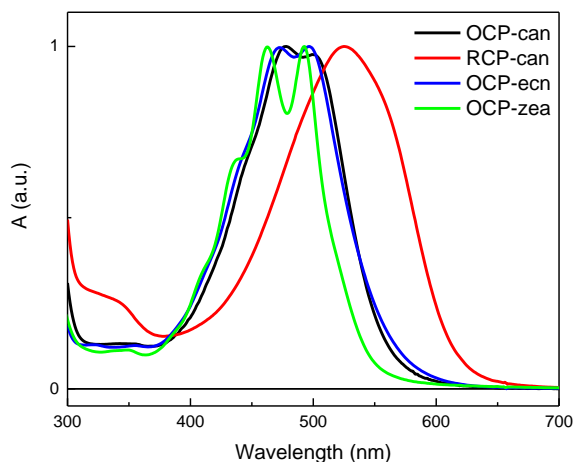
Figure 6-2. Steady-state absorption spectra of studied samples. The spectra are normalized to their maxima.

The maximum of the RCP-can absorption spectrum is largely red-shifted to 525 nm. This can point to high polarizability of the protein environment and/or longer effective conjugation length of the carotenoid molecule.[38] The essentially lost vibrational structure suggests an increased conformational disorder. This heterogeneity is, however, of a different nature than in OCP samples. Presumably, in OCP there exist two well-defined populations of carotenoid molecules (two

different carotenoid configurations), resulting in a maintained vibrational structure. In RCP, however, the vibrational structure is lost, which may mean that there exists a distribution of configurations with slightly altered structures, nonetheless, belonging to a single carotenoid configuration. The configurational homogeneity of OCPr (whose part containing the carotenoid is RCP) was confirmed by resonance Raman data.[38]

6.3.2. Transient absorption spectroscopy

a) Transient absorption spectra

Figure 6-3 shows transient absorption spectra of all studied samples at times best representing the S_1-S_n signal, with emphasized differences between excitations at 470 and 540 nm. After 540 nm compared to 470 nm excitation of OCP-can (Figure 6-3a), there is a slight red shift both in the ground-state bleaching (GSB; 512 vs. 505 nm) and excited-state absorption (ESA; 607 vs. 600 nm). The RCP sample differs in many aspects. The GSB is red-shifted, broad and unresolved as expected based on the absorption spectrum. The shoulder, seen in OCP-can around 600 nm, is not present in RCP. The maximum of S_1-S_n transition is red-shifted to ~685 nm. Most importantly, another broad and red-shifted band is present (~740 nm). Such red-shifted bands are indicative of a transition from the ICT state.[24,32,40] We will denote the ~740 nm band as an 'ICT band' in the following text. From this perspective, one can distinguish also the contribution of the ICT signal to the transient spectra of OCP-can whereby the ICT signal contribution is stronger for the 540 than for the 470 nm excitation. More details about the ICT band assignment will be mentioned in the Discussion.

Apart from the red-most part of their transient absorption spectra, OCP-ecn (Figure 6- 3b) data for the two excitations (470 and 540 nm) exhibit similar differences as OCP-can. The GSB moves from 500 to 510 nm and the S_1-S_n ESA from 661 to 675 nm. However, the signal around 740 nm is much stronger for the latter excitation, suggesting a strong contribution of the ICT signal.

Transient absorption spectra of OCP-zea (Figure 6-3c) are qualitatively very different from the others. Generally speaking, this is caused by the fact that

zeaxanthin is a non-carbonyl carotenoid. Moreover, significant differences also appear between transient absorption spectra of OCP-zea after the two excitations. The GSB minimum is shifted from 493 nm (470 nm excitation) to 507 nm (540 nm excitation). The S_1-S_n maximum is shifted even more, from 558 to 594 nm. The S_1-S_n band after the longer-wavelength excitation is somewhat "cleaner", but 470 nm excitation generates a transient spectrum containing an additional shoulder on the low-energy slope. These observations point to the fact that while the 540 nm excitation addresses only one subpopulation of OCP, 470 nm excites both subpopulations.

b) Evolution-associated difference spectra

Figure 6-4 shows evolution-associated difference spectra (EADS), which result from global fitting of transient absorption spectra of OCP-can excited at 470 nm (Figure 6-4a) and 540 nm (Figure 6-4b). The dynamics are, generally, very similar after both excitations. The black spectrum is associated with the carotenoid S2 state, but is rather unreliable given the lifetime is close to the time resolution of our setup. The black EADS is replaced within the duration of the pump pulse by the red EADS. This EADS consists of GSB in the blue-most part and a broad ESA arising from the S1-Sn transition of the carotenoid. The red EADS then decays in ~3 ps to the blue, rather weak EADS. This EADS may belong to the S_1-S_n spectrum of some carotenoid subpopulation with a slower (~6-7 ps) decay.

EADS of RCP-can are shown in Figure 6-4c. The spectra are obviously rather distinct from those of OCP-can binding the same carotenoid. Most importantly, the red EADS, which appears in less than 100 fs, contains a strong signal red-shifted from the S_1-S_n band. This is the signal from the ICT state. The 0.4 ps time constant is almost exclusively related to the decay of the ICT band. The blue EADS with the lifetime of 3.6 ps then represents mainly the signal associated with the S_1-S_n transition. Mostly, because of the missing slow component, the overall dynamics of RCP-can is faster than in OCP-can.
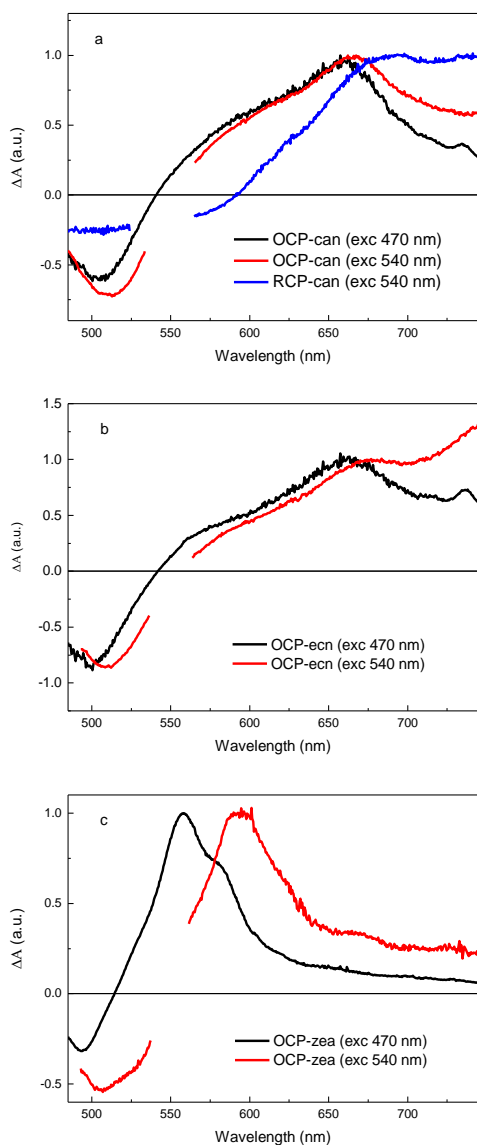
Figure 6-3. Transient absorption spectra normalized to the maximum of the S_1-S_n transition: a) OCP-can excited at 470 nm taken at 0.45 ps (black) and 540 nm taken at 0.45 ps (red), RCP-can excited at 540 nm taken at 0.2 ps (blue); b) OCP-ecn excited at 470 nm taken at 0.3 ps (black) and excited at 540 nm taken at 0.2 ps (red); c) OCP-zea excited at 470 nm taken at 0.9 ps (black) and 540 nm taken at 0.7 ps (red)

Figure 6-5 shows EADS of OCP-ecn after 470 (Figure 6-5a) and 540 nm (Figure 6-5b) excitation. Both datasets differ mainly in the reddest part of the spectra. As mentioned above, these differences are ascribed to a stronger ICT signal after 540 nm excitation. As in the case of OCP-can, three time constants were needed to obtain good fits. The first EADS (black) decay faster than the

temporal resolution of our setup. The following, red EADS bear signatures of signals from the S_1 and ICT states, the latter being stronger after 540 nm excitation. The ICT signal is associated with a shorter lifetime (0.9 vs. 0.5 ps for 470 and 540 excitation, respectively), which is also confirmed by other studies.[16,17,41] It is remarkable how different the spectral response can be for caro-
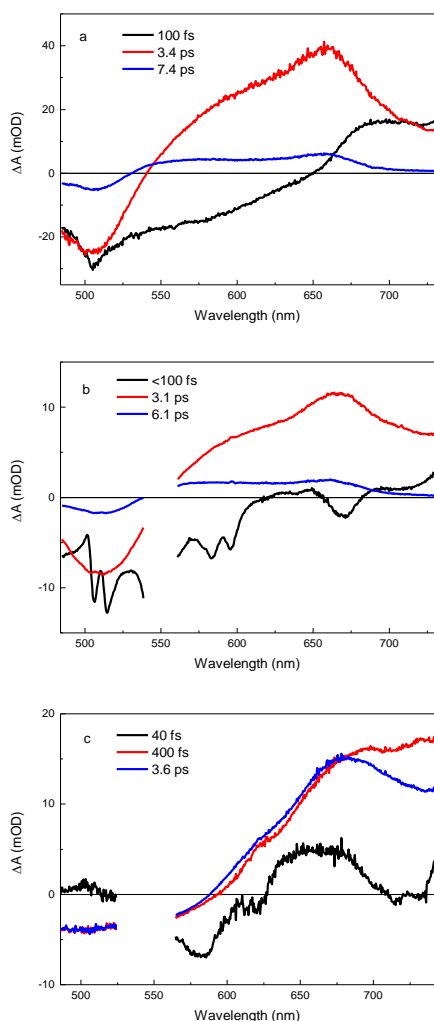

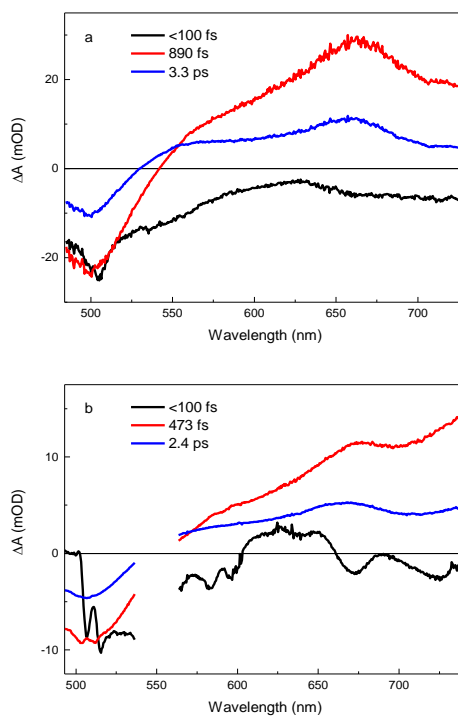Figure 6-4. EADS of OCP-can sample excited at 470 nm (a) and 540 nm (b), RCP-can excited at 540 nm (c)

Figure 6-5. EADS of OCP-ecn sample excited at 470 nm (a) and 540 nm (b)

tenoids with such similar structures as canthaxanthin and echinenone. The only difference between the two molecules is that canthaxanthin contains carbonyl groups on both end rings, while in echinenone one is missing (Figure 6-1m). The last EADS with lifetimes 3.3 ps (470 nm excitation) and 2.4 ps (540 nm excitation) are somewhat stronger than in OCP-can. The overall dynamics of OCP-ecn are faster after 540 nm excitation.
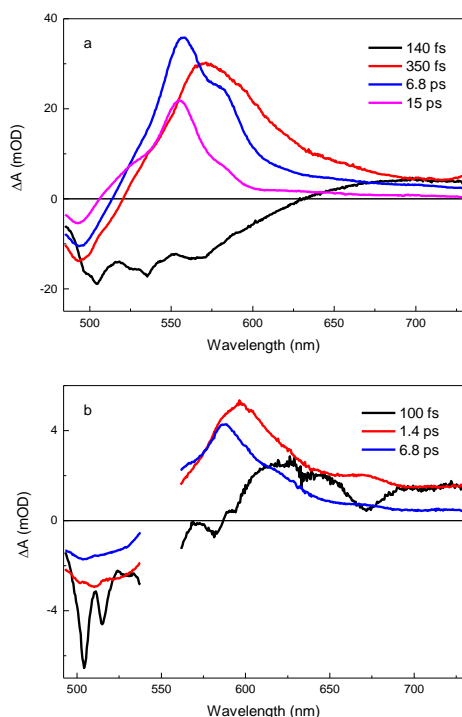
Figure 6-6. EADS of OCP-zea sample excited at 470 nm (a) and 540 nm (b)

Figure 6-6 shows EADS of OCP-zea. We will start with the description of EADS resulting from data after 540 nm excitation. They are "cleaner" in because just one subensemble of molecules was excited, which is seen both in simpler dynamics with fewer time constants and higher spectral homogeneity. With the decay of the black EADS appears the red EADS with the lifetime of 1.4 ps. This EADS (red) is spectrally broader than the next one (blue). This finding suggests that the red EADS refers to the transition from the hot S_1 state. This implies that

vibrational relaxation of zeaxanthin in OCP-zea is much slower than in solution,[42] but a comparable effect was reported earlier for another zeaxanthin-binding protein.[43] The blue EADS, thus, corresponds mainly to the S_1-S_n transition. The ~7 ps S_1 lifetime is shorter compared to the ~9 ps value reported for zeaxanthin in solution.[15] At the same time, the S_1-S_n maximum is red-shifted to 587 nm. The red-shift is in agreement with the shorter lifetime, suggesting that the carotenoid configuration preferentially excited by 540 nm has longer effective conjugation than that in solution. It must be noted, however, that there is another source of red-shift in OCP, i.e. the polarizability of the protein environment.[44]

Table 6-1. Time constants extracted from the global fitting analysis

OCP-can excited at 470 nm	OCP-can excited at 540 nm	RCP-can excited at 540 nm	OCP-ecn excited at 470 nm	OCP-ecn excited at 540 nm	OCP-zea excited at 470 nm	OCP-zea excited at 540 nm
100 fs	<100 fs	<100 fs	<100 fs	<100 fs	140 fs	100 fs
-	-	400 fs	890 fs	470 fs	350 fs	1.4 ps
3.4 ps	3.1 ps	3.6 ps	3.3 ps	2.4 ps	6.8 ps	6.8 ps
7.4 ps	6.1 ps	-	-	-	15 ps	-

The EADS after 470 nm excitation are more complex. To fit the data, four time constants were needed. The red spectrum associated with vibrational relaxation in the S_1 state decays much faster (0.35 ps) than after the 540 nm excitation. The blue spectrum then contains a shoulder on the longer-wavelength slope. Because the next EADS (magenta) differs from the blue one mainly by the absence of this shoulder, the blue EADS can, therefore, be coupled with the decay of that shoulder. Both the spectral position of the shoulder and the lifetime of 6.8 ps correspond with the S_1-S_n decay after 540 nm excitation (blue EADS in Figure 6-6b). Due to this observation, we can confirm that both subpopulations in OCP-zea are excited at 470 nm. The last, magenta EADS corresponds to the signal from the S_1 state of the "blue" subpopulation of OCP-zea, giving the S_1 lifetime of this zeaxanthin ~15 ps. Results of the global fitting are summarized in Table 6-1.

c) Kinetics

Figure 6-7 supports the statements on the general dynamics mentioned above by showing kinetics at S_1-S_n maxima for all studied samples and excitation wavelengths. The transient spectra of OCP-can for the two excitations are not markedly different (Figure 6-3a); so, the dynamics are rather similar (Figure 6-7a). The RCP-can dynamics also does not differ much, but is still faster than that of OCP-can. OCP-ecn transient absorption spectra differ mainly in the reddest part due to the presence of the strong ICT band (Figure 6-3b). Consequently, the faster ICT dynamics for the 540 nm excitation results in faster overall dynamics at the S_1-S_n maximum than for the 470 nm excitation.

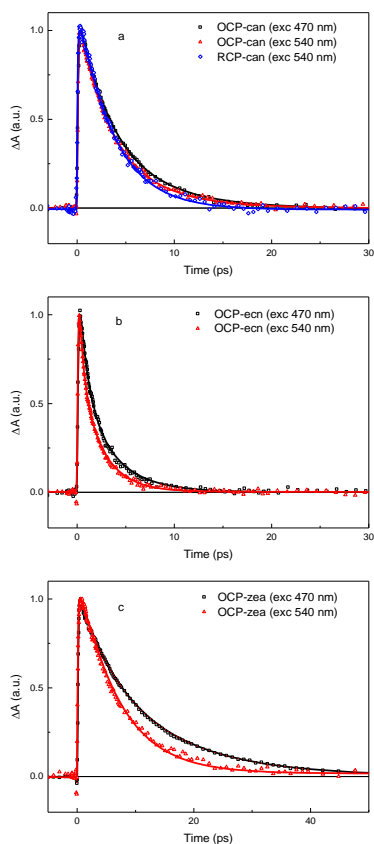Figure 6-7. Normalized kinetic traces taken at maxima of S_1-S_n transitions. Solid lines represent the fitted curves. a) OCP-can excited at 470 nm (probe at 660 nm, black) and 540 nm (at 668 nm, red), RCP-can excited at 540 nm (at 675 nm, blue); b) OCP-ecn excited at 470 nm (at 660 nm, black) and 540 nm (at 673 nm, red); c) OCP-zea excited at 470 nm (at 580 nm, black) and 540 nm (at 587 nm, red).

OCP-zea exhibits largest differences among the three OCP samples when the kinetics after the two excitations are compared (Figure 6-7c). The kinetics after 540 nm excitation are markedly faster than after 470 nm excitation. This observation is in line with the red-shifted transient absorption maximum of OCP-zea excited at 540 nm (Figure 6-3c), suggesting that a population of zeaxanthin with larger conjugation length is selected by this excitation wavelength.

6.4.   Discussion

6.4.1. What is an ICT signal, and what is not?

In the above text, we state that the ICT band is the red-most signal in the recorded spectra of RCP-can and OCP-ecn after 540 nm excitation (Figures 6-3a, 6-3b). This, however, contradicts an earlier published work on OCP-hecn (OCP with 3'-hydroxyechinenone), where the ~660 nm band in transient absorption spectra was considered to be the ICT band. Such an assignment was based on the large difference between transient absorption spectra of 3'-hydroxyechinenone in solution and in OCP.[45] In this study, however, we were able to extend our measurements more to the near-IR spectral region with the result of recording a strong signal above ~730 nm. Consequently, the band at ~660 nm is considered as the S_1-S_n signal here (Figures 6-3a, 6-3b), but the one above ~730 nm is considered as the ICT-related signal (Figure 6-3a, 6-3b), in agreement with more recent studies.[24,32,40] To support this statement, one can compare transient spectra of OCP-can (Figure 6-3a) with those of canthaxanthin in solution.[46] Given the overall symmetry of canthaxanthin, unequivocally unperturbed in solution, no features in the transient spectra were associated with the ICT signal.[46] Based on the similarity of transient spectra/EADS of canthaxanthin in solution with those of OCP-can, we assume the signal at ~660 nm (Figure 6-3a) is not related to a transition from the ICT but rather from the S_1 state. The same is true for OCP-ecn, where the transient spectra of OCP-ecn excited at 470 nm resemble those of echinenone in solution, where no ICT signal was identified due to the s-*cis* configuration of the ring containing the carbonyl group.[46] Therefore, only the signal above ~730 nm, clearly

observed in OCP-ecn excited at 540 nm (Figure 6-3b), is considered here as the ICT signal.

6.4.2. Spectroscopy-structure relationships in OCP and RCP

Recently published X-ray structures of OCP-Syn-can and RCP-Syn-can[1] enable the correlation between structural differences of these two pigment proteins and our spectroscopic results. The OCP and RCP proteins studied here contain the carotenoid canthaxanthin with a conjugated carbonyl group, which is known to have dramatic effect on transient absorption spectra through the ICT state.[17,24,47] Whether or not the ICT state-related signal is recorded for a carbonyl carotenoid depends on polarity of the environment and the symmetry of the molecule. Strong ICT signal and S_1 lifetime shortening were obtained in polar.[16,17] However, in case of symmetrically positioned carbonyl groups (e.g. in crocetindial, canthaxanthin), no ICT-related signal is detected even in a polar solvent.[46,47] On the other hand, a strong ICT signal is recorded if just one of the carbonyls is reduced to a hydroxyl as in 8,8'-diapocartotene-8'-ol-8-al.[47] But even asymmetry of the conjugated carbonyl cannot guarantee presence of the ICT band in solution as evidenced by echinenone.[46] Its single conjugated carbonyl group is located on a terminal ring, which should be twisted in solution by about 45° in respect to the main conjugated chain, as evidenced for other carotenoids with terminal rings.[48–50] In such an arrangement the effect of the conjugated carbonyl is apparently too small to induce an ICT signal, confirming that the torsion around the single bond adjacent to the terminal ring (Figure 6-1) determines how much the conjugated bonds on the rings contribute to spectroscopic properties.[50] It is thus likely that the ICT activity will be significant for a configuration close to s-*trans* (Figure 6-1c, 6-1e), as proposed earlier.[17,24]

Given the symmetric position of carbonyls in canthaxanthin (Figure 6-1a), no ICT-related signal might be expected in OCP or RCP. However, the protein can force the molecule into a configuration, which is unstable in solution[24] as it is the case of canthaxanthin in OCP/RCP[1] (Figure 6-1j, 6-1l). In both cases, the carotenoid molecule is highly non-symmetric, mainly in terms of the orientation of the end-rings with respect to the rest of the conjugated backbone. In OCP, the

orientation of both rings is very much of an out-of-plane character, even more than in solution: the $\beta 1$ ring torsion is 116° and for $\beta 2$ it is 72° (Figure 6-1j). The respective dihedral angles in RCP are 64° and 163° (Figure 6-1l).

Based on above-mentioned information, one can propose the following hypotheses:

1)   Given the significant off-plane torsion of the terminal rings in OCP-can, the conjugated bonds at the rings (and thus also the carbonyls) will be virtually isolated from the conjugated backbone (Figure 6-1j), leading to weak/no ICT state-related phenomena in transient signal of OCP-can.

2)   Because of the loss of symmetry in the position of the carbonyls and the nearly s-*trans* orientation of the $\beta 2$ ring in RCP-can (Figure 6-1l), we expect the ICT state be active and give rise to the typical signal in transient absorption spectra.

It is clear from Figure 6-3a that both hypotheses are confirmed. Although there is a non-zero signal in the ICT region in OCP mainly after the 540 nm excitation, the difference between OCP-can and RCP-can is obvious. The OCP structure can even give us a clue why there is some ICT signal recorded in OCP-can. Although the best condition for the ICT to be observed is the s-*trans* position of the carbonyl group, one can imagine a gradually lower ICT activity as the distortion from the s-*trans* configuration becomes larger. At the same time, the position of the two rings is non-symmetric (Figure 6-1j). Thus, both conditions for recording the ICT signal are at least partially met in OCP-can leading to a weak ICT signal.

Our data also shed new light on the results obtained for RCP from *Arthrospira maxima*.[36] In that case, no ICT signal was recorded and the lifetime of RCP-hecn was close to that of 3'-hydroxyechinenone in solution. It was therefore concluded that the part of carotenoid, which resides in the C-terminus of OCP, is exposed to the solvent. However, Leverenz et al.[1] suggest that there is a significant movement of the carotenoid during the transition from OCPo to OCPr (demonstrated on RCP). Therefore, the carotenoid would be embraced by the protein also in RCP. If we assume the configuration of 3'-hydroxyechinenone is similar to that of canthaxanthin in RCP, the lack of the ICT signal is not surprising.

The β1 ring, the only ring containing the conjugated carbonyl in 3'-hydroxyechinenone, is significantly distorted from the s-*trans* configuration (Figure 6-1l), thereby preventing observation of an ICT state-related signal. Although the β2 ring in configuration close to s-*trans* is crucial for the ICT activity in RCP-can, the same configuration in RCP-hecn does not lead to ICT band observation because the β2 ring does not contain the carbonyl group. The red-shift of RCP absorption spectra, explained in Chábera et al.[36] by aggregation, probably has different reasons. First, RCP with respect to the OCP population excited at 470 nm has longer conjugation mainly because the β2 ring assumes the configuration close to s-*trans*. However, no significant lifetime shortening associated with longer conjugation is observed in either RCP-can, presented here (see Figure 6-7a), or in RCP-hecn reported earlier.[36] Thus, another reason for the red-shift may be the same as proposed for the red-shift of carotenoids in OCP compared to solution, i.e. an increase of the polarizability of the environment.[44]

6.4.3. Heterogeneity of OCP

The data presented here clearly imply that the OCP sample is spectrally heterogeneous. This conclusion follows both from the absorption spectra (Figure 6-2 and Supporting Information, Figure S6-1 and Figure S6-2) as well as differences between transient absorption spectra measured after 470- and 540-nm excitations (Figure 6-3). Two hypotheses, attempting to explain this heterogeneity, were proposed. The first assumes, based on spectral deconvolution of absorption spectra, that the red wing of the OCP spectrum corresponds to the activated OCP (OCPr), which is supposedly present in the sample exposed to ambient light.[33] The second hypothesis relies on results of resonance Raman spectroscopy, showing that even the Raman spectrum of OCP excited at the red edge of absorption spectrum differs from that of the fully activated OCPr.[38] These authors conclude that the red part of the OCP spectrum still arises from the inactive OCPo yet with different spectral properties than the main form.

To test these hypotheses, we performed a study on OCP-zea (Figure 6-2, green), which does not undergo any light-induced activation.[12] Thus, any sign of spectral heterogeneity cannot be ascribed to presence of active OCPr, but it must

be a consequence of heterogeneity of the inactive OCPo itself. The steady-state absorption spectrum suggests that some heterogeneity in carotenoid binding is present (Figure 6-2) because the 0-1 transition typically dominates the absorption spectrum of zeaxanthin. Yet in OCP-zea the 0-0 and 0-1 transitions are of similar magnitude, indicating the presence of an extra absorption band at the red edge of absorption spectrum. However, in contrast to OCP-can and OCP-ecn, adding a single red-shifted band does not provide good fit of the OCP-zea absorption spectrum. Instead, fitting the OCP-zea spectrum as a sum of two full carotenoid spectra results in a reasonable fit (Supporting Information, Figure S6-2).

The heterogeneity of OCP-zea is further confirmed by transient absorption spectroscopy. Two excitation wavelengths were applied: one to select, preferentially, the putative red-shifted OCP-zea (540 nm) and the other with stronger contribution of the other form of OCP-zea (470 nm). The results presented in Figure 6-3c and global fits in Figure 6-6 confirm beyond doubt that the sample is largely heterogeneous. OCP-zea must be able to accommodate carotenoid molecules with two significantly different configurations. The red-shift is in agreement with the shorter lifetime, suggesting that the carotenoid configuration excited preferentially by 540 nm has longer effective conjugation than that excited by 470 nm. Interestingly, however, the red-shifted zeaxanthin has less-resolved vibrational bands (Supporting Information, Figure S6-2) suggesting that it is rather loose in its binding site. Thus, we can conclude that the spectral heterogeneity indeed arises from OCPo itself and not from an activated OCPr superimposed on the spectrum of OCPo. We denote the OCPo subpopulation excited by 470 nm pulses as the "main form" (based on the larger total contribution to the steady-state spectrum – Supporting Information, Figure S6-2) and the subpopulation excited by 540 nm pulses as the "red-shifted form".

Assuming the crystal structures of OCP[1,9] refer to the main form excited at 470 nm pulses, we can ask what is the carotenoid configuration in the red-shifted OCPo excited at 540 nm. The main form of OCPo-ecn (Figure 6-3b) has a rather weak ICT signal. This is a consequence of the partial out-of-plane torsion of the □1 ring containing the carbonyl group with respect to the conjugated backbone, which is 146° (ref. 10, Figure 6-1o). However, echinenone in the red form of

OCPo-ecn should have the ring closer to s-*trans* configuration because of the stronger ICT signal (Figure 6-3b). Due to the hydrogen bonding of the $\beta1$ ring to neighboring amino acids and quite tight packing around the other ring, one can assume that the rings cannot move much. On the other hand, the conjugated chain may have some room to move.[38] While the $\beta1$ ring assumes a configuration close to s-*trans* through ~30° rotation of the conjugated backbone (Figure 6-1p), the dihedral angle of the other ring is most probably also affected due to rigidity of the conjugated chain. In the first approximation, one can assume the torsion angle of the $\beta2$ ring changes to a similar extent, reaching 80-90° (Figure 6-1p) as compared to the value of 53° in the main form (Figure 6-1o).

One can explain the spectroscopic behavior of OCPo-can with the same model. The corresponding $\beta1$ ring torsion in the main form is 116° (Figure 6-1j). If the chain is turned to the same extent in the red form of OCPo-can, as in OCPo-ecn, the $\beta1$ ring assumes the configuration close to that of the main form of OCPo-ecn (~150°, Figure 6-1k). Interestingly, the magnitude of the ICT signal is similar for the red form of OCPo-can and the main form of OCPo-ecn (compare the red curve in Figure 6-3a and the black curve in Figure 6-3b, respectively). The $\beta2$ torsion angle in the red form of OCPo-can then becomes ~100° (Figure 6-1k), essentially isolating the $\beta2$ ring from conjugation. Within our hypothesis, the overall structure of canthaxanthin in the red form of OCPo-can is still highly non-symmetric, enabling some ICT signal to be recorded, but the $\beta1$ ring is still quite far from s-*trans* to enable the signal of similar magnitude as in the red form of OCPo-ecn.

Regarding OCP-zea, there is no structural information available. Due to the absence of the carbonyl oxygen on the ring, one can even expect quite a different configuration because no hydrogen bonds fix the structure as in case of OCP-can and OCP-ecn.[1,9,10] In any case, zeaxanthin in the main form of OCP-zea must be locked in a well-defined configuration as resolution of vibrational bands in the absorption spectrum (Figure S6-2) is clearly better than for zeaxanthin in solution.[51] One can, however, estimate the effective conjugation length of zeaxanthin in the main and red-shifted form. The S_1 lifetime of the main form is ~15 ps, while the corresponding lifetime of the red form amounts to ~7 ps (Figure

6-6). None of these values match the zeaxanthin S_1 lifetime in solution, which is ~9 ps.[15] However, the zeaxanthin effective conjugation length can be modified in the protein by turning the rings around the neighboring single bonds (Figure 6-1q). This carotenoid may, then, theoretically assume configurations with effective conjugation length from 9 (torsion angle of both rings 90°, isolation of rings from conjugation) to 11 (torsion angles 180°, conjugation extended to the rings). The corresponding lifetime interval is from ~23 to ~4 ps, respectively.[50] Both values obtained from our measurements, ~15 and ~7 ps, fit into this interval. Based on the analysis in Fuciman et al.,[50] we can estimate the effective conjugation length of the two OCP-zea populations to be ~9.4 (main form) and ~10.4 (red form).

6.5.   Conclusions

Spectroscopic results of this study confirm differences between RCP and OCP, which match those obtained from the recent X-ray structures.[1] The most important marker discriminating between possible carotenoid configurations in OCP is the presence/absence of the ICT band in transient absorption spectra. However, we do not ascribe the presence of the ICT state any physiological role for the following two reasons: 1) The decay of RCP-can with an active ICT state is not significantly faster than that of OCP-can without the ICT state activity. Moreover, given the ~3 orders of magnitude faster excited-state decay of carotenoid S_1 state compared to excited bilin in phycobilisome, essentially any carotenoid would serve the purpose with identical efficiency. 2) While RCP-can has an active ICT state, RCP-hecn[36] has not. However, both these RCPs serve as quenchers of phycobilisome fluorescence.[1,34] This suggests that the ICT state is not important in the quenching process. We, therefore, propose that the ICT state is a side-effect generated as a consequence of the fine-tuning of S_1 energy through ring rotations. The fact that the β1 ring with the carbonyl oxygen is a conserved structural feature in both photoactive RCPs (RCP-can and RCP-ecn) suggests a specific interaction between these carotenoid structures and the phycobilisome,

again pointing to the appearance of carbonyl carotenoid-related spectroscopic features as side effects.

Furthermore, an important conclusion is our confirmation that the spectral heterogeneity of OCP, visible even in absorption spectra (Figure 6-2, Figure S6-1, and Figure S6-2), is not the consequence of convoluted OCPo and OCPr absorption spectra. Instead, it appears as a result of two spectral variants of OCPo, denoted here the main and the red-shifted form of OCPo. The ultimate evidence provides OCPo-zea, which exhibits clear spectral heterogeneity, though having no photoactivity which would be necessary to form OCPr. Another line of evidence comes through the comparison of transient absorption spectra of the red-shifted OCPo with RCP, which are strikingly different (Figure 6-3a).

We also hypothesize the possible carotenoid configurations of the red-shifted OCPo-can and OCPo-ecn. We adhere to the assumption that the rings are rather immobile and the whole conjugated chain can turn, forming (at least) two configurations, which give rise to the unusual appearance of the OCP steady-state spectrum.

References

(1)   Leverenz, R. L.; Sutter, M.; Wilson, A.; Gupta, S.; Thurotte, A.; Bourcier de Carbon, C.; Petzold, C. J.; Ralston, C.; Perreau, F.; Kirilovsky, D.; et al. A 12 Å Carotenoid Translocation in a Photoswitch Associated with Cyanobacterial Photoprotection. *Science.* **2015**, *348* (6242), 1463–1466.

(2)   Niyogi, K. K.; Truong, T. B. Evolution of Flexible Non-Photochemical Quenching Mechanisms That Regulate Light Harvesting in Oxygenic Photosynthesis. *Curr. Opin. Plant Biol.* **2013**, *16* (3), 307–314.

(3)   Yeremenko, N.; Kouřil, R.; Ihalainen, J. A.; D'Haene, S.; van Oosterwijk, N.; Andrizhiyevskaya, E. G.; Keegstra, W.; Dekker, H. L.; Hagemann, M.; Boekema, E. J.; et al. Supramolecular Organization and Dual Function of the IsiA Chlorophyll-Binding Protein in Cyanobacteria. *Biochemistry* **2004**, *43* (32), 10308–10313.

(4)   Ihalainen, J. A.; D'Haene, S.; Yeremenko, N.; Roon, H. van; Arteni, A. A.; Boekema, E. J.; van Grondelle, R.; Matthijs, H. C. P.; Jan P. Dekker. Aggregates of the Chlorophyll-Binding Protein IsiA (CP43') Dissipate Energy in Cyanobacteria. *Biochemistry* **2005**, *44* (32), 10846–10853.

(5)   Staleva, H.; Komenda, J.; Shukla, M. K.; Šlouf, V.; Kaňa, R.; Polívka, T.; Sobotka, R. Mechanism of Photoprotection in the Cyanobacterial Ancestor of Plant Antenna Proteins. *Nat. Chem. Biol.* **2015**, *11* (4), 287–291.

(6)   Kay Holt, T.; Krogmann, D. W. A Carotenoid-Protein from Cyanobacteria. *Biochim. Biophys. Acta - Bioenerg.* **1981**, *637* (3), 408–414.

(7)   Wilson, A.; Ajlani, G.; Verbavatz, J.-M.; Vass, I.; Kerfeld, C. A.; Kirilovsky, D. A Soluble Carotenoid Protein Involved in Phycobilisome-Related Energy Dissipation in Cyanobacteria. *Plant Cell Online* **2006**, *18* (4), 992–1007.

(8)   Kirilovsky, D. Photoprotection in Cyanobacteria: The Orange Carotenoid Protein (OCP)-Related Non-Photochemical-Quenching Mechanism. *Photosynth. Res.* **2007**, *93* (1–3), 7–16.

(9)   Kerfeld, C. A.; Sawaya, M. R.; Brahmandam, V.; Cascio, D.; Ho, K. K.; Trevithick-Sutton, C. C.; Krogmann, D. W.; Yeates, T. O. The Crystal Structure of a Cyanobacterial Water-Soluble Carotenoid Binding Protein.

Structure **2003**, *11* (1), 55–65.

(10)   Wilson, A.; Kinney, J. N.; Zwart, P. H.; Punginelli, C.; D'Haene, S.; Perreau, F.; Klein, M. G.; Kirilovsky, D.; Kerfeld, C. A. Structural Determinants Underlying Photoprotection in the Photoactive Orange Carotenoid Protein of Cyanobacteria. *J. Biol. Chem.* **2010**, *285* (24), 18364–18375.

(11)   Wilson, A.; Punginelli, C.; Gall, A.; Bonetti, C.; Alexandre, M.; Routaboul, J.-M.; Kerfeld, C. A.; van Grondelle, R.; Robert, B.; Kennis, J. T. M.; et al. A Photoactive Carotenoid Protein Acting as Light Intensity Sensor. *Proc. Natl. Acad. Sci. U. S. A.* **2008**, *105* (33), 12075–12080.

(12)   Punginelli, C.; Wilson, A.; Routaboul, J. M.; Kirilovsky, D. Influence of Zeaxanthin and Echinenone Binding on the Activity of the Orange Carotenoid Protein. *Biochim. Biophys. Acta - Bioenerg.* **2009**, *1787* (4), 280–288.

(13)   De Carbon, C. B.; Thurotte, A.; Wilson, A.; Perreau, F.; Kirilovsky, D. Biosynthesis of Soluble Carotenoid Holoproteins in Escherichia Coli. *Sci. Rep.* **2015**, *5*, 9085.

(14)   Wilson, A.; Punginelli, C.; Couturier, M.; Perreau, F.; Kirilovsky, D. Essential Role of Two Tyrosines and Two Tryptophans on the Photoprotection Activity of the Orange Carotenoid Protein. *Biochim. Biophys. Acta - Bioenerg.* **2011**, *1807* (3), 293–301.

(15)   Polívka, T.; Sundstrom, V. Ultrafast Dynamics of Carotenoid Excited States-from Solution to Natural and Artificial Systems. *Chem. Rev.* **2004**, *104* (4), 2021–2071.

(16)   Frank, H. A.; Bautista, J. A.; Josue, J.; Pendon, Z.; Hiller, R. G.; Sharples, F. P.; Gosztola, D.; Wasielewski, M. R. Effect of the Solvent Environment on the Spectroscopic Properties and Dynamics of the Lowest Excited States of Carotenoids. *J. Phys. Chem. B* **2000**, *104* (18), 4569–4577.

(17)   Zigmantas, D.; Hiller, R. G.; Sharples, F. P.; Frank, H. A. Effect of a Conjugated Carbonyl Group on the Photophysical Properties of Carotenoids. **2004**, 3009–3016.

(18)   Zigmantas, D.; Hiller, R. G.; Sundstrom, V.; Polívka, T. Carotenoid to Chlorophyll Energy Transfer in the Peridinin-Chlorophyll-a-Protein Complex Involves an Intramolecular Charge Transfer State. *Proc. Natl. Acad. Sci.*

U. S. A. **2002**, *99* (26), 16760–16765.

(19)   Sumie Shima; Robielyn P. Ilagan; Nathan Gillespie; Brandi J. Sommer; Roger G. Hiller; Frank P. Sharples; Harry A. Frank; Robert R. Birge. Two-Photon and Fluorescence Spectroscopy and the Effect of Environment on the Photochemical Properties of Peridinin in Solution and in the Peridinin-Chlorophyll-Protein from Amphidinium Carterae. *J. Phys. Chem. A* **2003**, *107* (40), 8052–8066.

(20)   Papagiannakis, E.; Larsen, D. S.; van Stokkum, I. H. M.; Vengris, M.; Hiller, R. G.; van Grondelle, R.. Resolving the Excited State Equilibrium of Peridinin in Solution. **2004**.

(21)   Durchan, M.; Tichý, J.; Litvín, R.; Šlouf, V.; Gardian, Z.; Hříbek, P.; Vácha, F.; Polívka, T. Role of Carotenoids in Light-Harvesting Processes in an Antenna Protein from the Chromophyte Xanthonema Debile. *J. Phys. Chem. B* **2012**, *116* (30), 8880–8889.

(22)   Wagner, N. L.; Greco, J. a.; Enriquez, M. M.; Frank, H. a.; Birge, R. R. The Nature of the Intramolecular Charge Transfer State in Peridinin. *Biophys. J.* **2013**, *104* (6), 1314–1325.

(23)   Redeckas, K.; Voiciuk, V.; Vengris, M. Investigation of the S1/ICT Equilibrium in Fucoxanthin by Ultrafast Pump–dump–probe and Femtosecond Stimulated Raman Scattering Spectroscopy. *Photosynth. Res.* **2016**, *128* (2), 169–181.

(24)   Šlouf, V.; Chábera, P.; Olsen, J. D.; Martin, E. C.; Qian, P.; Hunter, C. N.; Polívka, T. Photoprotection in a Purple Phototrophic Bacterium Mediated by Oxygen-Dependent Alteration of Carotenoid Excited-State Properties. *Proc. Natl. Acad. Sci. U. S. A.* **2012**, *109* (22), 8570–8575.

(25)   Polívka, T.; van Stokkum, I. H. M.; Zigmantas, D.; van Grondelle, R.; Sundström, V.; Hiller, R. G. Energy Transfer in the Major Intrinsic Light-Harvesting Complex from Amphidinium Carterae. *Biochemistry* **2006**, *45* (28), 8516–8526.

(26)   Polívka, T.; Hiller, R. G.; Frank, H. a. Spectroscopy of the Peridinin-Chlorophyll-a Protein: Insight into Light-Harvesting Strategy of Marine Algae. *Arch. Biochem. Biophys.* **2007**, *458* (2), 111–120.

(27)	Gildenhoff, N.; Amarie, S.; Gundermann, K.; Beer, A.; Büchel, C.; Wachtveitl, J. Oligomerization and Pigmentation Dependent Excitation Energy Transfer in Fucoxanthin-Chlorophyll Proteins. *Biochim. Biophys. Acta* **2010**, *1797* (5), 543–549.

(28)	Ruban, A. V.; Berera, R.; Ilioaia, C.; van Stokkum, I. H. M.; Kennis, J. T. M.; Pascal, A. A.; van Amerongen, H.; Robert, B.; Horton, P.; van Grondelle, R. Identification of a Mechanism of Photoprotective Energy Dissipation in Higher Plants. *Nature* **2007**, *450* (7169), 575–578.

(29)	Holt, N. E.; Zigmantas, D.; Valkunas, L.; Li, X.-P.; Niyogi, K. K.; Fleming, G. R. Carotenoid Cation Formation and the Regulation of Photosynthetic Light Harvesting. *Science (80-.).* **2005**, *307* (5708), 433–436.

(30)	Bode, S.; Quentmeier, C. C.; Liao, P.-N.; Hafi, N.; Barros, T.; Wilk, L.; Bittner, F.; Walla, P. J. On the Regulation of Photosynthesis by Excitonic Interactions between Carotenoids and Chlorophylls. *Proc. Natl. Acad. Sci. U. S. A.* **2009**, *106* (30), 12311–12316.

(31)	Tian, L.; van Stokkum, I. H. M.; Koehorst, R. B. M.; Jongerius, A.; Kirilovsky, D.; van Amerongen, H. Site, Rate, and Mechanism of Photoprotective Quenching in Cyanobacteria. *J. Am. Chem. Soc.* **2011**, *133* (45), 18304–18311.

(32)	Berera, R.; Gwizdala, M.; van Stokkum, I. H. M.; Kirilovsky, D.; van Grondelle, R. Excited States of the Inactive and Active Forms of the Orange Carotenoid Protein. *J. Phys. Chem. B* **2013**, *117* (31), 9121–9128.

(33)	Polívka, T.; Chábera, P.; Kerfeld, C. a. Carotenoid-Protein Interaction Alters the S(1) Energy of Hydroxyechinenone in the Orange Carotenoid Protein. *Biochim. Biophys. Acta* **2013**, *1827* (3), 248–254.

(34)	Leverenz, R. L.; Jallet, D.; Li, M.-D.; Mathies, R. a.; Kirilovsky, D.; Kerfeld, C. a. Structural and Functional Modularity of the Orange Carotenoid Protein: Distinct Roles for the N- and C-Terminal Domains in Cyanobacterial Photoprotection. *Plant Cell* **2014**, *26* (1), 426–437.

(35)	Sutter, M.; Wilson, a; Leverenz, R. L.; Lopez-Igual, R.; Thurotte, a; Salmeen, a E.; Kirilovsky, D.; Kerfeld, C. a. Crystal Structure of the FRP and Identification of the Active Site for Modulation of OCP-Mediated Photoprotection in Cyanobacteria. *Proc Natl Acad Sci U S A* **2013**, *110* (24), 10022–10027.

(36)   Chábera, P.; Durchan, M.; Shih, P. M.; Kerfeld, C. a; Polívka, T. Excited-State Properties of the 16kDa Red Carotenoid Protein from Arthrospira Maxima. *Biochim. Biophys. Acta* **2011**, *1807* (1), 30–35.

(37)   Gupta, S.; Guttman, M.; Leverenz, R. L.; Zhumadilova, K.; Pawlowski, E. G.; Petzold, C. J.; Lee, K. K.; Ralston, C. Y.; Kerfeld, C. A. Local and Global Structural Drivers for the Photoactivation of the Orange Carotenoid Protein. *Proc. Natl. Acad. Sci. U. S. A.* **2015**, *112* (41), E5567-74.

(38)   Kish, E.; Pinto, M. M. M.; Kirilovsky, D.; Spezia, R.; Robert, B. Echinenone Vibrational Properties: From Solvents to the Orange Carotenoid Protein. *Biochim. Biophys. Acta - Bioenerg.* **2015**.

(39)   Kesan, G.; Litvin, R.; Bina, D.; Durchan, M.; Slouf, V.; Polívka, T. Efficient Light-Harvesting Using Non-Carbonyl Carotenoids: Energy Transfer Dynamics in the VCP Complex from Nannochloropsis Oceanica. *Biochim. Biophys. Acta - Bioenerg.* **2016**, *1857* (4), 370–379.

(40)   Berera, R.; Van Stokkum, I. H. M.; Gwizdala, M.; Wilson, A.; Kirilovsky, D.; Van Grondelle, R. The Photophysics of the Orange Carotenoid Protein, a Light-Powered Molecular Switch. *J. Phys. Chem. B* **2012**, *116* (8), 2568–2574.

(41)   Bautista, J. A.; Connors, R. E.; Raju, B. B.; Hiller, R. G.; Sharples, F. P.; Gosztola, D.; Wasielewski, M. R.; Frank, H. A. Excited State Properties of Peridinin: Observation of a Solvent Dependence of the Lowest Excited Singlet State Lifetime and Spectral Behavior Unique among Carotenoids. *J. Phys. Chem. B* **1999**, *103* (41), 8751–8758.

(42)   Billsten, H. H.; Pan, J.; Sinha, S.; Pascher, T.; Sundstrom, V.; Polívka, T. Excited-State Processes in the Carotenoid Zeaxanthin after Excess Energy Excitation. *J. Phys. Chem. A* **2005**, *109* (31), 6852–6859.

(43)   Billsten, H. H.; Bhosale, P.; Yemelyanov, A.; Bernstein, P. S.; Polívka, T. Photophysical Properties of Xanthophylls in Carotenoproteins from Human Retina? *Photochem. Photobiol.* **2003**, *78* (2), 138–145.

(44)   Niedzwiedzki, D. M.; Liu, H.; Blankenship, R. E. Excited State Properties of 3'-Hydroxyechinenone in Solvents and in the Orange Carotenoid Protein from Synechocystis Sp. PCC 6803. *J. Phys. Chem. B* **2014**, *118* (23),

6141–6149.

(45) Polívka, T.; Kerfeld, C. a.; Pascher, T.; Sundström, V. Spectroscopic Properties of the Carotenoid 3′-Hydroxyechinenone in the Orange Carotenoid Protein from the Cyanobacterium Arthrospira Maxima. *Biochemistry* **2005**, *44* (10), 3994–4003.

(46) Chábera, P.; Fuciman, M.; Hríbek, P.; Polívka, T. Effect of Carotenoid Structure on Excited-State Dynamics of Carbonyl Carotenoids. *Phys. Chem. Chem. Phys.* **2009**, *11* (39), 8795–8803.

(47) Enriquez, M. M.; Fuciman, M.; LaFountain, A. M.; Wagner, N. L.; Birge, R. R.; Frank, H. A. The Intramolecular Charge Transfer State in Carbonyl-Containing Polyenes and Carotenoids. *J. Phys. Chem. B* **2010**, *114* (38), 12416–12426.

(48) Young, A. J.; Phillip, D. M.; Hashimoto, H. Ring-to-Chain Conformation May Be a Determining Factor in the Ability of Xanthophylls to Bind to the Bulk Light-Harvesting Complex of Plants. *J. Mol. Struct.* **2002**, *642* (1–3), 137–145.

(49) Dreuw, A. Influence of Geometry Relaxation on the Energies of the S1 and S2 States of Violaxanthin, Zeaxanthin, and Lutein. *J. Phys. Chem. A* **2006**, *110* (13), 4592–4599.

(50) Fuciman, M.; Kesan, G.; LaFountain, A. M.; Frank, H. A.; Polívka, T. Tuning the Spectroscopic Properties of Aryl Carotenoids by Slight Changes in Structure. *J. Phys. Chem. B* **2015**, *119* (4), 1457–1467.

(51) *Carotenoids: Handbook*; Britton, G., Liaaen-Jensen, S., Pfander, H., Eds.; Birkhauser Basel: Basel, 2004.
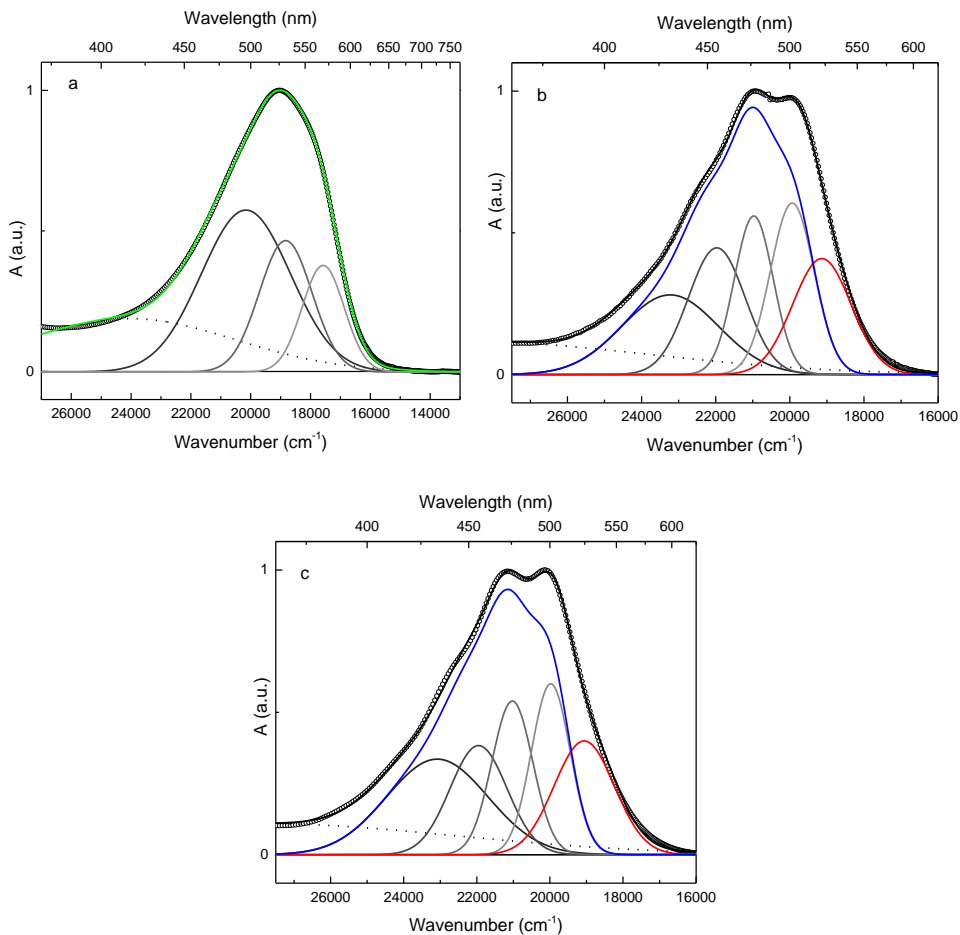
Supporting Information

Figure S6-1. Deconvolution of steady-state absorption spectra (black circles). In RCP, the green spectrum is the sum of the Gaussian bands (shades of grey and dotted line). In OCP, the red spectrum is an additional band assigned to the red form of OCPo, the blue spectrum is the sum of solid Gaussian bands and represents the main form of OCPo. a) RCP-can; b) OCP-can; c) OCP-ecn;
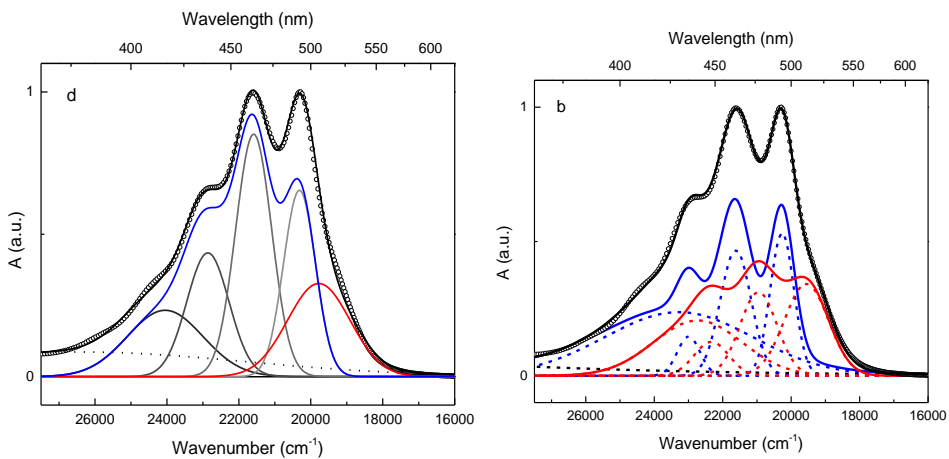
Figure S6-2. Deconvolution of absorption spectrum of OCP-zea. a) OCP-zea with a single red band; b) OCP-zea fitted as a sum of two zeaxanthin spectra (note that the blue tail of both zeaxanthins is for simplicity reproduced as one broad Gaussian band).

7. Summary and future perspectives

In this summary, I would like to give a short summary of the contributions we made to elucidate the relationship between the structure and spectroscopic properties of carotenoids both in a solution and as part of a protein.

In **Chapter 3**, we report results of ultrafast transient absorption spectroscopy of fucoxanthin stereoisomers, aiming to reveal isomerization-induced effects on excited state properties. It was demonstrated that the S_1 state lifetime of both *trans-* and *cis-*fucoxanthin are very close. This is not typical for carotenoids having symmetric conjugated backbones, which lead us to the conclusion that deviation from the C_{2h} symmetry (extension of the conjugation to the asymmetric allenic group in case of fucoxanthin) results in nearly identical S_1 state lifetimes. The characteristic for carbonyl carotenoids ICT-like band decays with the same lifetimes for both isomers, with lifetimes slightly shorter than those extracted for the respective S_1 states. These results are in agreement with the hypothesis that the S_1-like and ICT-like transitions are due to two separate yet coupled S_1 and ICT states. Since the S_1 state is unaffected by isomerization, the difference between S_1 and ICT lifetimes must be caused by alterations of ICT coupling to either the S_1 or S_0 states. Last but not least, we have observed nearly identical magnitude of the ICT band in transient absorption spectra for both isomers. The increase in the asymmetry of the conjugated chain by isomerization did not affect the magnitude of the ICT band. This clearly demonstrates that the relation between the molecular asymmetry and the ICT state formation for carbonyl carotenoids has to be studied in more details. Additional investigation of different asymmetric carbonyl carotenoids in polar solvents using multi-pulse techniques should help further elucidate this relation.

The study presented in **Chapter 4** shows the spectroscopic results of the unknown carotenoid from a newly discovered photosynthetic organism, *Chromera velia*. The major carotenoid in this organism was unidentified pigment

related to isofucoxanthin and was denoted as isofucoxanthin-like. The steady-state and ultrafast time-resolved spectroscopic results of isofucoxanthin-like, in a number of solvents, were compared with those measured for related carotenoids with known structure: fucoxanthin and isofucoxanthin. We show a solvent polarity dependence of the spectroscopic properties of isofucoxanthin-like. With increasing polarity the S_2 energy remains essentially the same, though the vibrational bands broaden resulting in the characteristic decrease of resolution of vibrational bands in polar solvents. This clearly indicates the presence of a conjugated carbonyl group in the pigment structure. The transient absorption spectral studies have also highlighted the differences between the three comprared carotenoids: isofucoxanthin-like exhibits significant spectral red-shift and shortening of the S_1/ICT lifetime compared to fucoxanthin and isofucoxanthin. This indicates that isofucoxanthin-like has longer conjugation length than that of its relatives. The specific response of isofucoxanthin-like to solvent proticity, the larger amplitude of the ICT-like band and the markedly shorter S_1/ICT lifetime in a polar aprotic solvent than in a protic one, and comparison of data with spectroscopic properties of known carotenoid structures reported earlier, shows that isofucoxanthin-like should contain a conjugated lactone ring. The experimental data were complemented by quantum chemistry calculations and classical molecular dynamics simulations that has allowed to estimate the possible structure of this unknown carotenoid. The different response to solvent proticity of fucoxanthin, isofucoxanthin, and isofucoxanthin-like is another interesting feature of carbonyl carotenoids which should be noted in future studies of any carbonyl carotenoids.

Chapter 5 presents the transient absorption spectroscopy study of three linear carotenoids with different conjugation length after excitation into higher vibrational levels of the S_2 state. We show that there is not a significant difference in the S_1 lifetimes of all three carotenoids after excitation into higher vibronic levels of the S_2 state. This result demonstrates that relaxation pathways from the S_2 potential surface always reach the same minimum at the S_1 potential surface. The excess excitation energy in the S_2 state, however, affects the vibrational

relaxation in the S_1 state. Here, we have used a band integral approach to obtain the dynamics of vibrational relaxation, and two trends were observed. First, the vibrational relaxation after excitation of the lowest energy band of the S_2 state becomes faster with the increase of conjugation length. Second, the population of the vibrational hot S_1 state, generated by internal conversion from the S_2 state, is larger and relaxes faster when the S_2 state is excited into higher vibrational levels. The transient absorption spectra of all three carotenoids contain a blue shoulder of the S_1-S_n band, referred as the S* signal. The increase of the S*signal amplitude after excess energy excitation for neurosporene and lycopene is negligible, while for spheroidene this effect is significant. This effect likely stems from the asymmetry of the spheroidene molecule which facilitates generation of specific conformations in the S_1 state that are responsible for the S* signal. These conformations are preferentially generated if the S_2 state is excited with excess vibrational energy. Future experiments using two-photon spectroscopic technique may help to address some of the questions raised in this chapter. For example, populating the S_1 state directly from the ground state should show whether the S* state can be exclusively generated from the S_2 state or not.

In **Chapter 6**, we present a femtosecond spectroscopic study comparing OCP and RCP samples binding different carotenoids. The OCP is a photoactive protein that mediates one of the non-photochemical quenching mechanisms, and the RCP represents an isolated activated N-terminal domain of OCP. The spectroscopic results together with the protein X-ray structure allow us to determine the spectroscopy-structure relationships for the OCP and RCP with the canthaxanthin. In solution the carbonyls in the canthaxanthin have a symmetric position, and the effect of the conjugated carbonyls is too small to induce an ICT signal. However, in the OCP/RCP pair carotenoid molecule is highly non-symmetric, mainly in terms of the orientation of the end rings with respect to the rest of the conjugated backbone. In this study, we demonstrated that the significant off-plane torsion of the canthaxanthin terminal rings in OCP leads to a weak ICT state signal, and the nearly *s-trans* orientation of one of the terminal rings in RCP gives rise to an ICT signal. We have applied two different excitation wavelength

to study OCP binding various carotenoids (canthaxanthin, echinenone, zeaxanthin). A strong ICT signal was recorded in OCP binding echinenone excited at the red edge of the absorption spectrum. Because the carbonyl oxygen responsible for the appearance of the ICT signal is located at the end rings of canthaxanthin and echinenone, the magnitude of the ICT signal was used to estimate the torsion angles of the end rings. Afterward, we have addressed the spectral heterogeneity of the OCP samples. We have shown that two spectral variants of the inactive orange form of OCP exist, denoted here the main and the redshifted form of inactive OCP. The ultimate evidence provides the OCP binding zeaxanthin, which exhibits clear spectral heterogeneity, though having no photoactivity. The future transient absorption experiments on this group of proteins should be performed on the active form of OCP upon illumination with blue-green light.